Heterogeneous Reactions on Salts

ARTICLE *in* CHEMICAL REVIEWS · JANUARY 2004

Impact Factor: 46.57 · DOI: 10.1021/cr020507n · Source: PubMed

1 AUTHOR:

Michel J Rossi
Paul Scherrer Institut
261 PUBLICATIONS **6,403** CITATIONS

SEE PROFILE

Heterogeneous Reactions on Salts

Michel J. Rossi

Laboratoire de Pollution Atmosphérique et Sol (LPAS), Institut des Sciences et Techniques de l'Environnement (ISTE), Ecole Polytechnique Fédérale de Lausanne (EPFL), CH-1015 Lausanne, Switzerland

Received February 3, 2003

Contents

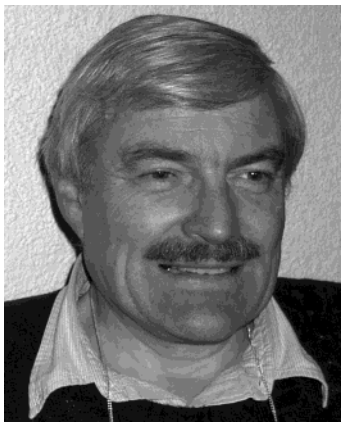

Michel J. Rossi, adjoint scientifique at the Laboratoire de Pollution Atmosphérique et Sol, Ecole Polytechnique Fédérale de Lausanne (EPFL), received a chemistry diploma (M Sc.) from the University of Basel in 1971 and a Ph D. in physical chemistry from the Institute of Physical Chemistry of the University of Basel in 1975. Subsequently he moved to Stanford Research Institute, now SRI International, in Menlo Park, CA, in order to perform research as a postdoctoral fellow on the chemical kinetics of fast gas-phase free radical reactions. He continued to work as a staff member at SRI from 1978 to 1991, when he took responsibility to set up a laboratory facility for the study of heterogeneous chemical reactions of atmospheric interest at EPFL. Currently his laboratory research group has several areas of interest: study of heterogeneous reactions on salt, soot, mineral dust, and ices; chemical kinetics of surface reactions; interfacial reactions on primary and secondary organic aerosols; interfacial reactions on materials of technological interest; aspects of heterogeneous kinetics in relation to combustion and oxidation processes; and chemical kinetic modeling of interfacial processes.

1. Introduction

1.1. Background

In contrast to homogeneous atmospheric reactions that take place in either the gas or the condensed phase, such as atmospheric cloud droplets, heterogeneous reactions involve species that are distributed in different phases or are occurring at an interface. The importance of heterogeneous atmospheric reactions has been firmly established in relation to the recurrent phenomenon of the polar stratospheric ozone losses, commonly known as Antarctic or Arctic ozone hole, as well as of the ubiquitous global stratospheric ozone loss owing to the presence of stratospheric aerosol.[1,2] The former is seasonal and occurs in the antarctic or arctic spring, whereas the latter essentially takes place continuously, independent of the seasons.[3−7] These processes take place in the stratosphere at altitudes between 12 and 30 km, depending on latitude. In addition, important heterogeneous processes also occur at lower altitudes on ice particles, mainly in the upper troposphere (UT) at altitudes of 6−15 km, rarely in the lower stratosphere (LS).[2] One of the first manifestations of the effect of heterogeneous processes on atmospheric chemistry that researchers became aware of stems

10.1021/cr020507n CCC: $44.00
Published on Web 11/18/2003

from investigations of the fate of N_2O_5 in the planetary boundary layer (PBL), as will be discussed below. It was soon realized that several heterogeneous reactions occur in the PBL as well as throughout the free troposphere (FT), which is the atmospheric layer between the PBL and the tropopause. Therefore, it now seems well established that heterogeneous reactions take place throughout the atmosphere from the PBL to the middle stratosphere.

The atmosphere contains many different kinds of particles that differ in chemical composition as well as in particle size distribution, depending on the strata considered, latitude, season, and the prevailing meteorological conditions.[8,9] Most of atmospheric particulate matter occurs as aerosol, that is, an airborne suspension of particles whose dimensions range from a few nanometers to tens of micrometers and whose atmospheric lifetime is primarily a function of its size, owing to the strong relationship between settling speed and mass.[9,10] It has recently been recognized that atmospheric aerosol particles may strongly influence the global ozone distribution through heterogeneous reactions of trace atmospheric gases, for example, on mineral dust.[11,12] Therefore, the global aerosol distribution may affect the oxidation potential of the atmosphere, depending on the extent of its heterogeneous reactions as well as on the identity of the reaction products.[13,14]

Examples of atmospheric aerosols include type I polar strospheric cloud particles (PSCs), consisting mainly of nitric acid hydrates and sulfuric acid hydrates, both of which occur in the LS. The partial list goes on with type II PSCs and Cirrus clouds, consisting of water ice laced with various amounts of contaminant trace gases and occurring in the UT/LS region, crustal materials/mineral dust encountered in the free troposphere as well as in the PBL, marine aerosols occurring in the marine boundary layer and consisting of sea salts, secondary organic aerosols (SOAs) originating from tropospheric oxidation processes of biogenic organic compounds such as terpenes and combustion aerosols originating from the combustion of fossil (oil) and nonfossil (wood) fuels, and ammonium salts over continental areas as well as others.[9,10]

Atmospheric particles mostly occur as airborne suspensions (aerosols) whose settling speed depends on particle size. Together with wash-out processes in which the aerosol particle becomes associated to a hydrometeor or raindrop, they represent the major source of loss of atmospheric particulates. Depending on the size of the atmospheric aerosol particle and other meteorological parameters, the lifetime of an aerosol particle is between 1 and 6 weeks, which is short compared to typical long-lived greenhouse gases such as CO_2, chlorofluorocarbons (CFCs), CH_4, and N_2O.[15] Nevertheless, the presence of aerosol particles has two effects, one being a factor in the chemical transformation of gases in the presence of aerosol particles (it is this feature which is the primary subject of this review), and the other being a factor in the global radiative balance affecting the global climate, commonly known as the greenhouse effect. It must be pointed out that the presence of atmospheric particles is the single largest contribution to the uncertainty in relation to predictions of climate change owing to the greenhouse effect.[1,2]

1.2. Scope of Review

This review deals with laboratory investigations of multiphase, often called heterogeneous reactions of atmospherically relevant gas-phase species on salt substrates that may be presented as solids in the form of polycrystalline grains, powders, single crystals or thin solid films, deliquescent aerosols, solutions, or frozen aqueous solutions. Laboratory investigations provide the ultimate reality check for atmospheric chemical processes that result from indications obtained during field measurement campaigns. Today, laboratory studies are seen to take on the role as mediators between field measurement campaigns and modeling efforts. Results from the field often suggest new processes, the impact of which modelers are eager to assess. However, laboratory confirmation provides the ultimate validation for novel proposed atmospheric processes.

The present synopsis will focus first and foremost on studies revealing quantitative information on the *reactivity* of the gas in the presence of the condensed phase containing the salt. Of equal importance is the *understanding* of the reaction mechanism afforded by laboratory studies. "Understanding" in this context means that the kinetics of disappearance of the reactant and the formation of the reaction products, including the corresponding branching ratios, the rate law, and the molecular identity of all products, are discovered under a range of experimental conditions so as to enable the construction of a reaction mechanism in terms of elementary chemical reactions. Validation and testing may subsequently be performed in the laboratory. This chemical kinetic aspect of the heterogeneous interaction is important in order to enable extrapolation of the reaction mechanism from experimental conditions of the laboratory to atmospherically relevant conditions that more often than not involve significantly smaller concentrations of trace species or of aerosol number densities than may be encountered in the laboratory. There are atmospheric gases that occur in the atmosphere at typical concentrations in the range 100 ppt to several tens of parts per billion that may be attained in the laboratory, for example O_3, NO_x, HNO_3, and HCl, to just name a few. For these trace gases, realistic atmospheric concentrations may be routinely attained in laboratory studies. However, for other gases, such as $BrONO_2$, HOBr, and many I-containing species, it may be difficult to attain atmospherically relevant concentrations of these gases in the laboratory, in view of their exceedingly small concentrations in the atmosphere, where their concentrations have been estimated using numerical CRT models of different complexity. We emphasize the chemical kinetic aspect of the mechanistic understanding of multiphase reactions at this point because realistic atmospheric conditions involving atmospheric particulates, such as trace gas concentrations, elapsed time, and relative humidity history, will not be attained anytime soon in the laboratory, despite assertions to the contrary.

A second crucial aspect surrounding the laboratory study of heterogeneous reactions on salt substrates, besides mechanistic understanding, is the fact that one uses surrogate substrates or proxies to real atmospheric particulates that have the same bulk composition as the atmospheric particles as far as is known from field experiments.[16−18] This aspect brings about the largest degree of uncertainty as far as reactivity with gas-phase species is concerned, because adsorbed minority or even trace components may alter the reactivity of the condensed phase substantially. Examples that may be cited are several oxidation reactions of halides by ozone interacting with either synthetic or natural sea salt substrates that have a substantially different reactivity than the majority component, NaCl.[19,20]

Most laboratory studies have used NaCl as a model for sea salt since it is the most abundant component. However, recent diffuse reflectance IR Fourier transform spectroscopy (DRIFTS) measurements suggest that NaCl may not be the component of sea salt which is most reactive with HNO_3.[21] This study indicates that HNO_3 and NO_2 appear to react preferentially with hydrate salts such as magnesium chloride hexahydrate ($MgCl_2 \cdot 6H_2O$), which is one of the constituents of natural sea salt. In addition, studies of sea salt aerosol in the presence of ozone and NO_x have shown enhanced production of atomic chlorine relative to experiments using pure NaCl aerosol.[22−26] These recent results imply that laboratory measurements of reactions 1−4 with NaCl (discussed below in more detail) may not be quantitatively extrapolated to reactions on sea salt aerosol in the troposphere. In addition, autocatalytic processes akin to chain-branching processes known from combustion chemistry may occur on the surface of salt substrates that are catalyzed by minute amounts of a reaction product whose formation necessarily remains obscure because of the small quantities involved. However, this type of surface-mediated chain reaction has also been found in the oxidation of aldehydes, whose combustion may include surface-mediated branched-chain reactions under certain experimental conditions.[27]

1.3. Atmospheric Processes Involving Salt Substrates

It is estimated[28] that the most important components of the global atmosphere are, in decreasing order of mass abundance, mineral dust aerosols [primarily from soil deflation but also with a minor component (<1%) from volcanoes (16.8 Tg or 16.8×10^{12} g)] sea salt (3.6 Tg), natural and anthropogenic sulfates (3.3 Tg), products of biomass burning excluding soot (1.8 Tg) and of industrial sources including soot (1.4), natural and anthropogenic non-methane hydrocarbons (1.3 Tg), and natural and anthropogenic oxides of nitrogen [mostly NO_x (0.6 Tg) and biological debris (0.5 Tg)]. Salt is therefore the second most abundant condensed matter suspended in the atmosphere, after dust aerosol,[8] and is the dominant aerosol species by mass above the oceans. The mechanism of marine aerosol formation involves braking of the waves, bubble formation, and extrusion of microdroplets off the surface of the ocean that will evaporate to form the marine aerosol.[8]

Moreover, halogens may be transported up to the stratosphere through violent volcanic eruptions, for which the salt content contained in the plume is extremely variable. The eruption of El Chichon in 1982 was such an example, for which the effect on the global atmosphere[29,30] has been subsequently modeled.[31,32] Halogens may also affect atmospheric processes on a local scale when considering burning oil wells that are in proximity to the marine environment, such as in Kuwait.[33−35] In this case, the interaction of hydrocarbon combustion with marine aerosols results in new chemistry.

Moreover, atmospheric particulates including salt aerosols are important light scatterers and contributors to cloud condensation nuclei, depending on their size distribution, and are therefore influencing the global radiative balance.[36] The interaction of trace gases with atmospheric particulates not only may alter the gas composition but also may lead to modifications of the optical constants and thermodynamic properties of the surface, that in turn may affect the radiative balance, leading to climate forcing. The maximum (mode) of the particle size distribution of the relatively coarse marine aerosol lies in the range of a few micrometers, such that light scattering will be inefficient (Mie scattering) owing to the mismatch between the radius of the particle and the wavelength of the light. In contrast, continental aerosol particles based on ammonium salts may be much smaller, owing to gas-to-particle conversion at the beginning of the formation process. However, the present review will put aside climate effects of salt aerosol particles and focus exclusively on the properties of salt aerosols as the seat of heterogeneous reactions that may affect the atmospheric trace gas composition.

Often, atmospheric particles consist of an internal mixture of salt, crustal, and other material of anthropogenic origin, such as soot, depending on its age, hence its size.[15,37,38] Marine aerosols rich in chlorides and bromides[8] generally undergo reactive processes with NO_x and NO_y compounds, whereas mineral dust aerosols are rarely reactive toward atmospheric trace gases as far as product formation is concerned. A notable exception is the acid−base reaction of HNO_3 and, to a lesser extent, of HCl with the $CaCO_3$ fraction of the mineral dust that leads to the formation of CO_2 and H_2O.

The interaction of alkali halide salt with atmospheric trace gases often leads to molecular, sometimes atomic halogen, release. The present review describes in detail the heterogeneous interaction leading to the volatilization of this initially locked source of molecular and atomic halogen that is initially stashed away in the form of involatile halide, which will become an agent of change for atmospheric chemical processes once its oxidation state has changed. This redox process is greatly facilitated in the presence of NO_x (NO, NO_2) or active nitrogen NO_y, which comprises NO, NO_2, HNO_3, N_2O_5, NO_3, HONO, etc., including all forms of oxidized nitrogen except N_2O. For instance, this redox process, also

called halogen activation, results in the reduction of volatile nitrate, as in N_2O_5 to NO_2 ($N(+V) \rightarrow N(+IV)$) according to reaction 1, with the concomitant oxidation of chloride ($Cl^-(-I)$) to Cl after photolysis of $ClNO_2$ into $Cl + NO_2$. The formation of $ClNO_2$ is called chlorine activation because photodissociation leads to reactive atomic chlorine. The net therefore amounts to the volatilization of Cl^- to atomic Cl, the impact of which largely depends on the atmospheric conditions such as temperature, relative humidity (rh), gas composition, and the history of the marine or continental aerosol. In what follows, we will briefly describe the role of halogen release within the marine boundary layer (MBL), both in remote locations under pristine conditions and in the polluted MBL, and the effect it has on the oxidation capacity of the atmosphere.[13,14]

Measurements of the kinetics and mechanisms of heterogeneous reactions have become increasingly important in understanding the chemistry of the troposphere.[11,12] For example, heterogeneous reactions involving sea salt aerosols rich in chlorides and bromides, dispersed into the troposphere through wind and wave action of the oceans,[39] have the potential to contribute to the tropospheric halogen budget. Reactions between sea salt aerosols and oxides of nitrogen, both NO_x and NO_y, generate inorganic halogen compounds that easily release atomic halogens upon photolysis, as briefly explained above. Examples of reactions releasing photochemically active halogen-containing compounds are reactions 1−3:[24,40−56]

$$N_2O_5 + NaCl(s) \rightarrow NaNO_3(s) + ClNO_2 \quad (1)$$

$$2NO_2 \text{ or } N_2O_4 + NaCl(s) \rightarrow NaNO_3(s) + ClNO \quad (2)$$

$$ClONO_2 + NaCl(s) \rightarrow NaNO_3(s) + Cl_2 \quad (3)$$

These reactions compete with the heterogeneous hydrolysis reactions 4−6 of N_2O_5, $ClONO_2$ (chlorine nitrate), and to a lesser extent NO_2, which generate the photochemically inert hydrochloric acid, HCl, in reaction 7:

$$N_2O_5 + H_2O \rightarrow 2HNO_3 \quad (4)$$

$$ClONO_2 + H_2O \rightarrow HNO_3 + HOCl \quad (5)$$

$$2NO_2 \text{ or } N_2O_4 \rightarrow HNO_3 + HONO \quad (6)$$

$$HNO_3 + NaCl(s) \rightarrow NaNO_3(s) + HCl \quad (7)$$

Gaseous HCl is the most abundant form of chlorine in the marine environment and reacts with OH free radicals to generate atomic chlorine according to reaction 8:

$$OH + HCl \rightarrow H_2O + Cl \quad (8)$$

However, its rate constant is fairly low[57,58] and is therefore in competition with efficient deposition, either on the ground or in aqueous aerosol particles or fog and cloud droplets, which limits the formation potential for free atomic chlorine by reactions 7 and 8. Since atomic chlorine is more reactive toward organics than OH free radicals, the existence of an atomic chlorine source may prove significant for initiating atmospheric oxidation of organics, especially at high solar zenith angle, that is, at sunrise.[59,60] The reason for this is that the UV absorption cross section of most chlorine precursors in the actinic range is significantly larger than that for ozone, which is responsible for photochemical OH free radical generation. Although direct field measurements of atomic chlorine and its precursors, such as Cl_2, $ClNO_2$, $ClONO_2$, and HOCl, are extremely difficult, Cl_2 has recently been detected and measured in the marine boundary layer.[61] This is, indeed, surprising in view of the fact that Cl_2 is both reactive and photochemically unstable. This, in turn, must mean that the as-yet unknown Cl_2 source rate is balanced by the fast Cl_2 photolysis rate, which is expected to be the most important loss term under atmospheric conditions. In addition, indirect field detection of chlorine compounds other than HCl using mist chambers,[62,63] photochemical techniques,[64,65] and the analysis of hydrocarbon concentration ratios to determine the relative atomic Cl- and OH free radical-initiated oxidation rates [66−68] has been used to estimate atomic chlorine concentrations. Estimates of peak chlorine concentrations at sunrise in the marine boundary layer range from 10^3 to 10^5 cm^{-3},[59,61−68] although the global levels averaged over the whole troposphere are smaller.[69,70]

A bold manifestation of the presence of chemically reactive halogen atoms other than chlorine is the recurrent polar sunrise chemistry or "bromine explosion" event in the lower polar troposphere that is thought to be caused primarily by the presence of active bromine, although the role of chlorine is uncertain at this point.[71−77] As briefly pointed out above, the chain-propagating step leads to a branched-chain reaction. It is heterogeneous in nature and may be represented by the following simple reactions:

$$BrX + NaY \rightarrow BrY + NaX, \quad X = OH, ONO_2, Y \text{ (halide)} = Cl, Br \quad (9)$$

$$BrY + h\nu \rightarrow Br + Y \quad (10)$$

In reaction 9, as well as in the specific all-chlorine analogue, reaction 3, the halide Y^- is activated by halide displacement and is transformed into the active volatile compound BrY that undergoes fast photodissociation (reaction 10). This leads to *two* reactive halogen atoms, namely Br, with which we started, and Y, that both regenerate BrX or some other active halogen compound. Taking atomic Br as an example, we arrive at the following halogen cycling reactions, in which Br is converted into an active halogen compound, BrX (HOBr), that is ready to undergo another activation cycle, such as reaction 9:

$$Br + O_3 \rightarrow BrO + O_2 \quad (11)$$

$$BrO + HO_2 \rightarrow HOBr + O_2 \quad (12)$$

In this way, one active halogen atom (Br) activates an additional halide Y^- (reaction 9) by turning into HOBr (reaction 12), which is either a photolytic precursor to two free radicals in the gas phase, OH and Br, or the precursor to two halogen atoms after photodissociation (reaction 10). It is evident that, after *n* cycles, the number of reactive chain carriers increases as 2^n, barring any significant losses of Br or Y. It seems that the process is selective for Y = Br, but the branched-chain concept holds without loss of generality[78−80] also for Y = Cl. The only exception to this reaction scheme is the apparent lack of reactivity of HOCl interacting on solid NaCl, which will be discussed below. However, HOCl reacts readily with deliquescent (liquid) salt aerosols.

In addition, iodine compounds such as IO have been observed in different locations in proximity to the marine environment[81−89] and are expected all the way up to the stratosphere, according to numerical simulations, where they are thought to play a significant role also in stratospheric ozone depletion. Recently, the connection between marine boundary layer halogen chemistry, including bromine- and iodine-containing precursors, with global tropospheric processes has been exposed using model calculations.[89,90]

In the absence of any chemical transformation of the constituent ions of an aqueous marine aerosol droplet, its relative composition is expected to be identical to the one for seawater from which it was generated. However, it has been conclusively shown over the years that sea salt aerosols may display a large deficit in chloride content compared to the original composition of seawater.[62,67,68,91−99] Since the mechanisms producing these aerosols, namely wave-breaking and bubble ejection,[8] should not affect their composition, the observed deficit was generally attributed to the displacement of alkali halides by strong inorganic acids, such as HNO_3 and H_2SO_4, owing to reactive uptake by aqueous aerosol following reactions 7 and 13.[94,95]

$$NaCl + H_2SO_4 \rightarrow NaHSO_4 + HCl(g) \quad (13a)$$

$$NaCl + NaHSO_4 \rightarrow Na_2SO_4 + HCl(g) \quad (13b)$$

$$2NaCl + H_2SO_4 \rightarrow Na_2SO_4 + 2HCl(g) \quad (13)$$

In some cases, the observed chloride deficit may reach up to 90% of the original chloride content. As noted by Keene et al.,[96] such a deficit cannot be explained by acid displacement alone. They postulated that other reactions are involved in which stable ions are transformed into volatile halogenated radical precursors. Accordingly, they performed field measurements of inorganic chlorides that exhibited concentrations of active chloride HCl* (that is, the sum of the HCl + $ClNO_2$ abundance) and of active chlorine Cl_2* (that is, the sum of the Cl_2 + HOCl abundance), reaching up to 250 ppt with a strong diurnal variation.[62] The latter strongly suggested a night-time buildup of Cl precursors and a subsequent rapid photolysis at dawn. These measured concentrations would correspond to an atomic Cl concentration in the range 10^4−10^5 cm^{-3}, which would imply a significant enhancement of the oxidation rate of non-methane hydrocarbons (NMHCs) RH, initiated by H abstraction in RH according to reaction 14:

$$Cl + RH \rightarrow HCl + R \quad (14)$$

Such an enhancement of the oxidation rate was, indeed, observed in Lagrangian-type field experiments, where it was shown that oxidation by OH free radical alone was unable to account for the measured NMHC decay, the latter being consistent with a Cl atom concentration of approximately 6×10^4 cm^{-3} at noon.[67] The presence of atomic Cl has been inferred from NMHC reactivity patterns in polluted air masses over the North Atlantic[67] and in the remote central Pacific.[68] The calculated concentration of Cl atoms that are formed from reactive chlorine precursors, despite being 1−2 orders of magnitude lower than the peak OH concentrations, is often sufficient to contribute significantly to the oxidation of many trace gases, especially NMHC. Sea spray constitutes the largest reservoir of chlorine in the atmosphere, but the mechanism by which it may be released from the aqueous aerosol into the gas phase is not clear yet. Acid displacement, whereby strong inorganic acids such as HNO_3 or H_2SO_4 may liberate chlorine in the form of HCl, according to reactions 7 and 13, can result in a chloride deficit of up to 90% only in polluted air masses.[94] However, this does not explain the presence of high concentrations of reactive chlorine released into the gas phase, as the HCl formed is only slowly converted to Cl atoms via reaction with OH, according to reaction 8. Other mechanisms have been proposed that involve heterogeneous reactions of members of the NO_x/NO_y families with sea salt aerosol in which photolabile chlorine-containing species are generated, most of which will be discussed in detail below.

Heterogeneous reactions involving bromides have been suggested to play an important role in ozone depletion in the Arctic troposphere, as briefly discussed above. Field studies show that ground-level ozone concentrations decrease dramatically in a period ranging from a few hours to a few days.[71−77] The smoking gun evidence for the role of bromine is the strong correlation between ozone destruction and filterable bromine, which corresponds to the sum of Br adsorbed on particles as well as gaseous species such as HBr, all of which may be measured by filtration on a combined Teflon/Nylon filter device followed by ion-chromatographic analysis.

The source of bromine in relation to the arctic tropospheric ozone depletion, the "bromine" explosion, is not obvious. Various sources of bromine atoms have been suggested, such as photolysis of $CHBr_3$ and other brominated methanes,[74] heterogeneous reactions of nitrogen oxides with sea salt aerosols,[100−102] photochemical oxidation in sea salt aerosol,[103−105] autocatalytic heterogeneous cycling of inorganic bromine species,[106,107] or free radical reactions in aqueous aerosols.[109] It seems clear that heterogeneous processing by aerosol particles, on the ice or on the snowpack, is necessary both to release bromine and to maintain a high gas-phase concentration of atomic bromine precursors that may undergo rapid photoly-

sis.[103,106,108,109] This issue is far from settled and will require careful investigation of the reaction mechanism of halogen activation. At the moment, it seems likely that a chain reaction involving heterogeneous bromine activation of bromide-containing sea salt crystals, such as reactions 9 and 10, may take place initially. However, the chain initiation processes, as well as the role of chlorine, are not clear at the moment. Atomic Br concentrations of up to 10^7 cm^{-3} have been inferred from measured NMHC depeletion rates,[110,111] and the BrO radical has been measured directly at concentrations of up to 30 pptv in the marine boundary layer, which is an order of magnitude larger than that in the stratosphere.[112−114] In contrast, ClO does not seem to be correlated with relevant trace gases However, measurements of light NMHCs have confirmed the presence of atomic bromine and indicated that atomic Cl concentrations are also elevated during low-ozone periods.[111] Recent measurements have confirmed the existence of tens of ppt of atomic Br and Cl precursors such as Br_2,[64,115] BrCl,[115] HOBr, Cl_2, and HOCl[64] during episodes of O_3 destruction.

Iodine in the troposphere is thought to arise from photolysis of alkyl halides emitted from marine macroalgae and phytoplankton, which may be found in coastal areas as well as in the open ocean. IO (from I + ozone) has been found in different locations in the remote boundary layer.[84,85] Recent measurements of IO at mixing ratios greater than 6 pptv within the marine boundary layer at Mace Head, Ireland,[84] greater than 3.5 pptv at Tenerife, and above 2.0 pptv in Tasmania 85 have been reported, which has triggered renewed interest in tropospheric iodine chemistry.[81−83,86−88] Of major interest in this regard is the potential for inorganic iodine species to initiate chlorine and bromine release from aqueous sea salt aerosols at mid-latitudes, using polar tropospheric chemistry as a guide in the search for an efficient heterogeneous reaction mechanism.

1.4. Some Properties of Atmospheric Aerosols Important to Laboratory Studies

Atmospheric particles most often occur as aerosols and contain many different salts, either as *external* or as *internal mixtures*. The former is a mixture of particles, each of distinctly different chemical composition within an air mass, whereas the latter consists of identical particles, each being a mixture of different salts, akin to a fluid or solid solution within an atmospheric particle. The differences between internal and external mixtures may significantly affect the optical properties and radiative efficiency of the atmospheric aerosol and its ability to act as cloud condensation nuclei (CCN) in cloud formation processes. It may also have important thermodynamic consequences in terms of the stability and rate of phase transitions of the aerosol, because in the case of internal mixtures, concentrated mixtures of salt solutions result upon dissolution, whereas in the case of external mixtures, aerosol droplets of uniform chemical composition will result. In contrast to the latter, mixtures of concentrated aqueous salt solutions present their own difficulties regarding proper thermodynamic description. Buseck and coworkers have presented convincing arguments, according to which atmospheric aerosols are almost always occurring as external mixtures on a global scale.[15] This includes the association of soluble salts with insoluble materials such as soot and mineral dust. For example, 90% of all atmospheric particles collected in the free troposphere above Tasmania contained sea salt, which of course says nothing about its aggregation mechanism.[38]

Moreover, the effect of external and internal mixtures has received increased attention[36] in conjunction with the climate change debate, as important differences of opinon exist. Some authors indicate that scattering calculations for mixed aerosols are not significantly affected by assumptions regarding internal or external mixing,[116,117] whereas others reach the opposite conclusion for internal mixtures of sulfate and soot.[118,119]

The chemical composition of salt aerosols differs considerably, depending on whether it is marine aerosol or an aerosol of continental origin. In the former case, the aerosol mainly consists of the salt constituents of seawater, such as alkali and earth alkali salts,[8] with NaCl being the major component. The number and mode of sea salt particles has been measured in numerous field experiments,[16−18] and, as mentioned above, the chloride deficiency in marine aerosols provided the driving force to investigate the various heterogeneous chemical reactions involving marine aerosols.[62−70,91−99] However, it was also noted above that sea salt sometimes has different properties, as far as chemical reactivity is concerned, compared to model or surrogate salt substrates, which represents an additional complicating factor in using a major component such as NaCl as a sea salt surrogate in laboratory studies.[24,26,120,121] For instance, the reactivity of NO_2 toward surrogate and natural sea salt is identical, whereas it is different for O_3−salt reactions. This underlines the need for fundamental understanding of the heterogeneous chemical kinetics of such reactions, component for component. In laboratory studies, NaCl is often used as a surrogate for marine aerosols in addition to natural and synthetic sea salt. The properties of marine aerosols certainly serve as a guide in laboratory studies, but realistic atmospheric conditions are a long way from being reproduced in the laboratory, as will be explained in more detail below.

In continental salt aerosols, sulfates and nitrates of ammonium predominate, such as $(NH_4)_2SO_4$, NH_4HSO_4, and NH_4NO_3, with NH_4Cl being a minor component. However, the total continental aerosol mass is also determined, to a variable extent, by the insoluble mass fraction of crustal components such as mineral dust as well as by soot. Owing to the surface-bound source of NH_3, which essentially originates from the decomposition of urine, together with other minor sources, ammonium salts have a characteristic altitude profile. At low altitude, the most common ammonium salt is $(NH_4)_2SO_4$, turning over to the more acidic NH_4HSO_4 at higher altitude. Finally, the NH_3 concentration in the upper troposphere and lower stratosphere is vanishing, so that

H_2SO_4 is not neutralized any more and therefore occurs as sulfuric acid droplets.[10] Similarly, NH_4NO_3 is found close to the planetary boundary layer, with HNO_3 expected to be present in the free troposphere (FT), although ammonium nitrate has been found there. In laboratory studies, ammonium salts are therefore taken as proxies for the study of continental-type atmospheric aerosols.

Deliquescence is a key property of salt aerosols and is associated with the solid/liquid phase transition once the relative humidity (rh) exceeds a threshold value proper to each salt.[9,10,122] This threshold value is given by the vapor pressure of the saturated salt solution whose thermodynamic stability is controlled by the aqueous solubility of the salt in question. Simply stated, the originally solid salt aerosol particle is more stable as a concentrated salt solution at high values of rh. Conversely, if one reduces the value of rh from the liquid solution (deliquescence) stability region in order to induce the reverse liquid/solid phase transition, one finds that one has to reduce the rh value much beyond the deliquescence rh, which is now called the efflorescence point. This hysteresis behavior has been observed for many pure salts and, in itself, suggests that kinetic processes may be important when establishing thermodynamic equilibrium in the atmosphere. In fact, in an interesting development, Ewing and co-workers have established, for the first time, that deliquescence is a nucleated phenomenon on single-crystal NaCl (001) faces, in that it occurs only after the rh exceeds the value found over a saturated aqueous solution by at least 5%[123] and therefore does not occur at the specific single value of rh given by the saturated salt solution, because it depends on the nature of the solid. This landmark study contradicts scores of other studies[122] that were performed using state-of-the-art single-particle levitation experiments, but most often on perhaps ill-defined polycrystalline salt substrates,[124] and may highlight the role that defect structures play in the kinetics of dissolution processes. However, it has been known for a long time that NH_4HSO_4 (ammonium bisulfate) breaks the mold in relation to the deliquescence behavior of pure salts, in that it does not show a distinct phase transition upon increasing rh beyond the deliquescence point.[125−127] This complicated phase behavior of salt aerosols goes to show that the rh or the partial pressure of H_2O needs to be carefully controlled in laboratory studies in order to address a defined state of the salt aerosol in laboratory experiments. The hygroscopic properties of laboratory-generated aerosols are examined in tandem hygroscopicity differential mobility analyzers (tandem-DMAs), where the first DMA size-selects a particular size fraction that subsequently passes a region of defined rh. The second DMA establishes the growth of the chosen size fraction, depending on its hygroscopic properties, which usually amounts to a few percent of its initial radius. Lately, a field-worthy version of this useful but complex piece of equipment has been developed and deployed.[128,129]

The value of rh at which a salt deliquesces is a measure of the qualitative property of *hygroscopicity*. In summary, the lower the deliquescence rh, the larger is its hygroscopicity or tendency to form concentrated salt solutions. In a seminal study, Buseck and co-workers critically compared the dimensions of sampled atmospheric particulates recorded by both transmission electron microscopy (TEM) and atomic force microscopy (AFM). They came to the conclusion that the high vacuum required for the TEM measurements led to significantly smaller particle dimensions observed by TEM compared to AFM.[37] By comparing the volumes of hydrated and dry $(NH_4)_2SO_4$ particles collected over the North Atlantic Ocean, they concluded that the volumes were larger by up to 4 times, owing to evaporation in the high vacuum of the TEM environment. The conclusion is that one needs to exercize due care when interpreting the volumes of atmospheric particles using electron-beam methods such as secondary electron microscopy (SEM) or TEM, even when certain instruments allow measurements of vapor pressures as high as a few millibar, such as in environmental SEM instruments (ESEMs).

Furthermore, large values of particle volumes measured at low partial pressure of H_2O led to the further conclusion that an amorphous organic coating was responsible for particle hydration where one expected a dry salt particle, owing to processing of the particle at rh values below the efflorescence point.[37] Although difficult to observe using the arsenal of surface investigation techniques, amorphous organic coatings, presumably consisting of surface-active polar organics, have repeatedly been proposed in the literature to exist on aged atmospheric particles.[130,131] Since these molecules have both a hydrophilic and a hydophobic part, much like an organice surfactant (soap), their orientations determine whether they increase or decrease the hygroscopicity of the coated aerosol particle.[132,133] Such coatings may influence the hygroscopicity behavior of particles by both a kinetic and a thermodynamic effect, the latter of which has been discussed as a baffling change in Henry's law constant or an anomaly in hygroscopic behavior for atmospheric particles.[132,133] The kinetic effect of an organic coating on an inorganic particle may lead to a barrier to evaporation, resulting in a decrease of the rate of evaporation[130,134] and perhaps condensation as well. However, it has to be stressed that quantitative information on condensation and evaporation rates are lacking altogether. The thermodynamic effect may lead to a change in the stability (equilibrium) constant for H_2O uptake into the organic film, depending on its orientation, as it may lead to either an increase or a decrease of hygroscopicity.[135] In conclusion, salt aerosols and salt substrates in general have a proven but variable trend toward adsorption of H_2O onto their surface and are thus distinctly different from soot and mineral dust particles, which usually do not show this tendency to the same extent. As discussed above, the reason for this environmentally important property that enables a variety of heterogeneous chemical reactions on the surface is the aqueous solubility of these particles, leading to formation of stable concentrated solutions at sometimes small rh values.

This may seem a sweeping statement, but to oversee the solubility aspect of the salts in relation to their water-binding ability would be a severe shortcoming in the fundamental understanding of heterogeneous reactivity on salts. This difference is true notwithstanding the fact that all inorganic and many organic atmospheric particles are terminated by hydrophilic groups such as OH,[136−139] as expected, which makes them hydrophilic to some extent, in clear distinction to being hygroscopic.

NaCl has been often used as a surrogate for laboratory studies of the physicochemical properties of salts, owing to its ease of growing single crystals, producing thin films, and polycrystalline materials of defined size, and the simplicity of many of its characterization techniques. It therefore has become the ideal training ground for "salt" studies. As an example, NaCl is a nonporous crystalline solid at ambient temperature, which has been proven by the fact that the calculated external surface area of a resonably monodisperse sample agreed, within experimental error, with the surface area measured using the BET technique.[140,141] Salt substrates are definitely nonporous solids, despite occasional assertions to the contrary. Lately, the H_2O adsorbing capabilities of NaCl have been placed under renewed scrutiny.[142,143] In an illuminating paper, Ewing and co-workers established that the adsorption isotherm of H_2O significantly depended on the nature of the NaCl substrate by carefully measuring and interpreting, by molecular modeling, the adsorption behavior of water on the (001) face of single-crystal NaCl using FTIR absorption measurements of the OH symmetric (ν_3) and antisymmetric (ν_1) stretching frequencies.[143]

The difference in water adsorption behavior on polycrystalline vs single-crystal faces of NaCl may be rationalized by the abundance of surface defects on the former surfaces of the crystallites, in essential agreement with the results obtained by Cox and coworkers, who arrived at their conclusions by using a mass monitor.[142] Briefly, Ewing and co-workers distinguished four characteristic adsorption regions of H_2O on NaCl single-crystal faces. The low-coverage (θ) region spans the range $0 < \theta < 0.5$ and consists of the formation of isolated islands of adsorbed water held together by hydrogen bonds. This results from a delicate balance between the interaction of H_2O molecules with the salt substrate as well as with other adsorbed H_2O molecules (lateral interactions). In the transition region, for values of $0.5 < \theta < 2.5$, a sharp rise in coverage with water partial pressure indicates the coexistence of isolated islands and multilayer thin-film regions, whereas at high coverage, for θ between 2.5 and 3.5, multilayer thin-film growth is gradually taking place, beyond which θ is taking a sharp upturn, indicating the onset of the NaCl presolution region, leading to brine formation. This goes to show that, for such a seemingly simple physicochemical system at ambient temperature, the limits between monolayer and multilayer H_2O adsorption are floating, which has been shown for the most simple case of a single-crystal face. It is very probable that the situation is even more complex in the case of polycrystalline samples incorporating various crystal defects that may have a higher affinitiy toward H_2O adsorption. This largely remains to be explored. Monte Carlo calculations have been of great help in interpreting water adsorption isotherms on single-crystal faces[143] and will likely continue to do so in the case of atmospherically relevant salt substrates at ambient temperatures, where classical surface studies cease to be of use.

In the recent past, heterogeneous reactions have been studied in aerosol flow tubes, where the condensed phase is presented as an aerosol. While this technique is closer to the reality of the atmospheric occurrence of particulate matter compared to flow reactor studies, it is fraught with numerous experimental difficulties, not the least of which is the necessity to keep the aerosol number concentration high, typically in the 10^5-10^7 cm^{-3} range, in order to enable adequate analytical detection of the gas phase. Therefore, model experiments have been performed that have the advantage of rapidly gauging the heterogeneous reactivity of the condensed phase without the need to suspend it in the form of an aerosol. Examples of experimental techniques where the aerosol phase has been replaced by bulk solids of the same chemical composition, usually powders of known or estimated particle size distribution, are laminar flow and Knudsen flow reactors, which will be discussed below in more detail. However, this sample presentation usually results in larger values of the uptake coefficients compared to those obtained with thin-film, single-crystal, or aerosol studies, because the gas may penetrate into the powdered bulk substrate during the characteristic residence time of the experiment and so, in fact, increase the gas−substrate collision frequency ω compared to the geometrical surface area A_s of the sample that is just the projection of the real surface onto the substrate plane. In this way, ω is singificantly underestimated, which leads to large values of γ.

The use of ω based on A_s yields an upper limit to the true uptake coefficient γ, defined as the fractional efficiency of the removal of the gas species M under consideration on a per-collision basis; that is, $\gamma = k_{het}/\omega$, where k_{het} is the measured rate coefficient for the gas-phase removal of M. On the other hand, the use of the total external and internal surface area of the sample as a basis to compute ω leads to a lower limit of γ if the numerical value is so small that M has time to access the total sample surface during the gas residence time of M. However, this limit is only rarely attained in practice, so the pore diffusion model is used to correct the measured values of γ for the condition that $\gamma < 5 \times 10^{-2}$. In general, the corrected values of γ will lie between the two limiting values discussed above. If γ exceeds the value of 5×10^{-2}, the rapid rate of the interfacial reaction will effectively preclude diffusion of M into the sample, which will then not be competitive with interfacial reaction.

To take gas penetration into the powdered sample substrate quantitatively into account, the pore diffusion model that is well-known within the chemical

engineering community[144−146] has been applied to heterogeneous reactivity studies.[147−152] The model or corrected uptake coefficient γ_{pd} is related to the measured or apparent value γ, derived using the geometrical surface area in eq 15:

$$\gamma = \gamma_{pd}\rho_b S_{het}(h_e + \eta h_i) \quad (15)$$

where ρ_b, S_{het}, h_e, h_i, and η are the bulk density, the specifice surface area (such as the Brunauer−Emmett−Teller (BET) surface area), the height of the first grain layer, the height of all the internal layers calculated from the total mass m of the sample ($h_i + h_e = m/A_s\rho_b$), and the effectiveness factor that is related to the well-known Thiele modulus, respectively. If the particle size distribution function is relatively well defined, this will, in turn, lead to a similarly uniform pore size distribution so that the effective number of grain layers of the sample N_{layer} may be given by $m/A_s\rho_b d$, with d being the average size of the particle. The effectiveness factor of a porous solid, to which the sample powder is approximated, primarily depends on the relative rates of surface reaction and gas-phase diffusion; it is defined as the ratio of the observed diffusion-limited reaction rate to the rate that would be observed if diffusion into the bulk of the powder were extremely fast. The effectiveness may also be thought of as the fraction of internal surface which takes part in the heterogeneous reaction. In addition, the Thiele modulus also depends on the tortuosity factor τ, which takes into account the fact that, in porous solids, the actual mass transfer is slower than predicted because, within these materials, diffusion does not occur in straight-line paths nor in pores of uniform cross section. In practice, one fits the measured values of γ as a function of γ_{pd} and τ, which is treated as an adjustable parameter, because most powders or porous solids are not characterized well enough to calculate an accurate value of τ. However, on theoretical grounds, τ may not exceed much the value of 3, and is usually found to lie between 1 and 3 for most porous solids.[153−155]

2. Experimental Techniques

A detailed overview of most of the experimental techniques used in the determination of kinetic parameters in heterogeneous chemical kinetics of atmospheric relevance has been given some years ago,[156] such that only a very brief account will be given here. Most experimental techniques used in the measurement of multiphase kinetics are inspired from gas-phase kinetics studies. Historically, the measurement of the kinetics of heterogeneous reactions began with the investigation of elementary reactions at high temperature, which were used to interpret complex combustion processes in which free radicals were involved as chain carriers. Wall deactivation or decomposition reactions of free radicals were at the origin of efforts to design and apply techniques at measuring these heterogeneous wall deactivation processes because they affected the measurement and interpretation of the reactions of interest to a significant extent. Heterogeneous reactions of atmospheric interest most often involve labile halogen reservoir molecules rather than open-shell systems, such as in combustion, because the atmospheric lifetime of free radicals is controlled by gas-phase rather than heterogeneous reactions. Exceptions are free radicals that are less reactive, such as ClO, BrO, HO_2, NO_3, and NO_2, which need to be considered in potential heterogeneous reactions. Reactive free radicals for which heterogeneous reactions are less important are the atomic halogens, H, OH, O, and all alkyl and alkoxy free radicals, with the possible exception of alkylperoxy radicals, to list just a few. One area that needs improvement in the future would be the development of multidiagnostic experimental methods that investigate both involved phases at the same time and under identical experimental conditions, and therefore really address the multiphase aspect of the kinetics, as has recently been done for thin ice films.[157,158] The multiphase system may be fully described only when information about kinetic processes in both phases is collected and mass balance is achieved. Examples abound in which either phase alone is examined, whereas there are only a handful of studies investigating both phases at the same time and under the same conditions. This multiphase aspect necessarily leads to redesigning most experimental apparatus used so far, and much progress is expected in the next few years from multidiagnostic experiments that monitor all relevant phases, hopefully leading to redundant data sets that overdetermine the kinetic system.

Flow tube techniques have been used for many decades to measure rate constants, products, and branching ratios in homogeneous gas-phase kinetics. The fast-flow or laminar flow tube technique, pushed to perfection as a technique for measuring the kinetics of fast radical reactions by Kaufman in the 1950s and 1960s, examines homogeneous gas-phase reaction rates at variable reaction times that are given by the spatial extent of the reaction zone.[159,160] The reaction time t is calculated using the relation $t = s/v$, where s is the length of the reaction zone in the laminar flow tube and v is the linear flow velocity of the carrier gas. Usually, a fixed-point detector is used downstream of the reaction zone at a few millibar He total pressure in order to enable fast mixing and diffusion. At "plug flow" conditions, the extraction of kinetic results becomes especially simple when radial diffusion is fast, and axial diffusion may be neglected, which should lead to an approximately square radial flow profile. This well-established technique has been adapted to the measurement of heterogeneous reaction rates by coating the walls of the reaction zone with the condensed-phase material of interest, such as salts, soot, and ices.[161−163] Surrogate materials are used as wall coatings for practical reasons when atmospheric aerosol reactions are studied.

Special care has to be exercized when relative humidity effects in the presence of salts and ices are to be addressed as a fraction of the total pressure, consisting mainly of He, as it is now being replaced with H_2O vapor that has a very different (lower) diffusion coefficient compared to that of the He carrier gas. Because the reaction is taking place at

the walls of the tube, consideration has to be given to the relationship between gas-phase diffusion of the average molecule toward the walls and the heterogeneous rate of disappearance, which is usually the process of interest. Practically speaking, the usefulness of this technique ceases at uptake coefficients $\gamma > 0.1$, as the diffusion corrections become unduly large and sensitive to the transport properties of the gas mixture. In this case, the measurement of the rate of disappearance of the reactant addresses the gas-phase diffusion rate of the reactant toward the walls rather than the heterogeneous rate process at the walls.

A useful variant of the flow tube technique for the measurement of heterogeneous reactions taking place at the surface of liquids, such as aqueous solutions, is the *wetted wall flow tube* (WWFT) technique pioneered by Ravishankara and co-workers.[163] This vertically mounted flow tube has a laminar flow of the liquid of interest, forming a thin flowing film running down the walls of the flow tube in order to renew the substrate surface and to prevent saturation of gas uptake. This technique comes in two flavors, one where the total pressure is in the Torr range (up to 10−12 Torr, mostly He) and the other where the total pressure is 1 atm. The former variant corresponds to the fast-flow or laminar flow tube discussed above and puts severe constraints on the vapor pressure of the liquid, which means that the temperature of the liquid has to be kept usually in the neighborhood of 273 K for aqueous solutions in order to limit the partial pressure of H_2O.[164] The latter variant is a flowing gas experiment under slow flow or stirred flow conditions that enables the measurement of slow rates of uptake or γ values in the range $10^{-4}-10^{-6}$, owing to slow atmospheric gas diffusion in ambient pressure.[165]

The *Knudsen cell flow reactor* technique has also been adapted from gas-phase kinetics studies, in that the condensed-phase substrate is housed in a sample compartment that may be isolated from the gas flow and may be opened in situ in order to expose the substrate of interest to the gas flow.[166,167] It is a versatile technique operating under molecular flow conditions, enabling the measurement of very fast uptake rates with γ approaching unity, without apparent limitations from gas-phase diffusion. However, even under molecular flow conditions, which correspond to the fastest possible mixing rates nature can offer, one has to carefully take into consideration pressure gradients within the flow reactor under certain experimental configurations.[50] Owing to fast molecular diffusional mixing, γ values ranging from essentially unity to $<10^{-7}$ have been measured.[166] However, this wide dynamic measurement range comes at the price of severe vapor pressure constraints that exclude uptake studies on most liquids and ices at higher temperatures. In practice, total pressures of 20 mTorr may be tolerated in most geometrical reactor configurations. As a balance to the vapor pressure limitation, one may point out an additional advantage resulting from the ease of interpretation of interfacial kinetic studies, as every element of the substrate surface has undergone the same number of collisions by the gas-phase reactant. Each surface element experiences saturation effects, which are, after all, the hallmark of interfacial reactions, to the same degree, in contrast to flow tube methods, where sample surface elements close to the reactant injector experience a higher number of gas−surface collisions than surface elements farther downstream. This effect has not yet been quantitatively explored as it should be, and it is expected that it may become important in cases where substrate surfaces readily saturate.

Atmospheric pressure flow tubes may be operated with *aerosols* slowly flowing across the flow tube.[126,168,169] This represents a step closer to the atmospheric reality but involves an increased degree of experimental complexity. Aerosols may be either polydisperse or monodisperse after passage across a differential mobility analyzer (DMA). In either case, the aerosol density or surface-to-volume ratio is higher than that in the atmosphere by several orders of magnitude, especially in the case of polydisperse aerosols. However, the limitation of rate-limiting gas-phase diffusion is mitigated when dealing with submicrometer-size aerosols, so that sizable γ values may be measured using this technique. The fact that the aerosols must be embedded in an atmosphere of air presents a particular challenge to gas-phase monitoring using mass spectrometry, as either atmospheric pressure ionization (API) methods have to be used or some other method of total pressure reduction, for instance through differential pumping.

For the measurement of fast heterogeneous reactions taking place on the surface of the liquid phase, the *droplet train apparatus* is frequently used.[170,171] A fast-firing nozzle generates a droplet train that is flowing down the cylindrical axis of a laminar flow tube at total pressures of a few Torr. These droplets, emitted from a piezoelectrically actuated inkjet-type nozzle, have a diameter of between 20 and 150 μm and correspond to liquid bulk phase rather than to an aerosol. It necessitates careful control of the total pressure and the transport properties of the gas phase. In one variant, the gas phase in the presence of the droplet train is investigated using optical (long-path IR) or mass spectrometric methods,[170] whereas the other variant makes use of the investigation of the condensed phase after collection of the droplet train and subsequent ion chromatography.[172] It is a pity that no study has yet been performed in which both the gas phase and the condensed phase have been investigated. Owing to stringent H_2O vapor pressure constraints, dictated by the tight control of the gas diffusion properties of the gas mixture, a fairly narrow temperature range is usually sampled which centers around 273 K but occasionally reaches down to 263 K into the supercooled regime of water. This narrow temperature range renders the resulting kinetic parameters highly uncertain.

The most realistic experimental format for the measurement of heterogeneous chemical reactions on atmospheric particulate available today is the measurement of the change in the gas phase in the presence of atmospheric aerosol surrogate particulate

within a *large static aerosol chamber*.[173−175] Traditionally, the use of these large aerosol chambers was severely limited by the restricted residence time of the atmospheric aerosol particulates that were depositing on the walls and were thus making the walls reactive to the reactant gas. Due to the progress in experimentation and the appropriate choice of materials such as FEP or PFA Teflon materials, aerosol residence times from tens of hours up to several days can now routinely be achieved. These aerosol reactors offer numerous possibilities for on-line and batch analytical techniques, covering both the gas and the aerosol phase. Examples of such techniques are optical (UV/Vis) and FTIR folded path spectroscopies across the aerosol chamber, aerosol metrology, such as differential mobility analysis (DMA) and optical particle spectroscopy (PMS) based on Mie scattering, light attenuation, and extinction measurements, but also traditional wet techniques in a batch mode, such as various chromatographic methods. This type of instrumentation certainly yields the most complete set of information but is difficult to apply in view of the long duration of experimental runs, often extending up to 1 week or more.

The most recent and informative laboratory experiments have focused on kinetic studies where the condensed phase was presented as an aerosol whose interaction with trace gases was studied either in an atmospheric pressure flow tube or in a static aerosol chamber. Compared to laboratory experiments performed in laminar flow tubes or Knudsen flow reactors and using a bulk condensed phase, the aerosol experiments approach atmospheric conditions to a higher degree, especially when the size distribution of the laboratory-generated aerosol is known. Conversely, aerosol studies, although more realistic, are experimentally demanding and present their share of experimental difficulties. The most important experimental constraint in most of these flow reactor studies is the rather restricted range of relative humidities, which is lifted in aerosol studies at atmospheric pressure. Therefore, atmospheric model aerosols both below and beyond the deliquescence rh may be investigated, which is important, as the chemical reactivity toward trace gases may abruptly change with the phase transition from dry (solid) to deliquescent aerosol.

Another decisive advantage in working with aerosols is the fact that the diffusion limitation of the trace gas species diffusing toward the substrate surface is relaxed if one works with small-size aerosols, from a few hundred nanometers to the submicrometer range. When working with a macroscopic bulk substrate, molecular diffusion at atmospheric pressure is often the rate-limiting step, in comparison with surface reactivity, which is the primary parameter of interest. At a given mass density m (g cm^{-3}) of the aerosol at a bulk density ρ (g cm^{-3}), the total aerosol volume v per volume element (cm^3) is simply given by m/ρ. The particle number density n (cm^{-3}) and the total aerosol surface s per unit volume are given by eq 16, using a spherical model for the aerosol particle of radius r. It leads to a surface-to-volume ratio (s/v) given in eq 17:

$$n = (m/\rho)(3/r^3\pi) \qquad s = (m/\rho)(3/r) \tag{16}$$

$$s/v = 3/r \tag{17}$$

Equation 17 shows that s/v increases with $1/r$, which means that, with decreasing radius of the aerosol particle, the volume decreases faster than the surface at a given mass density. The first-order heterogeneous rate constant k_{het} for interfacial reaction of a molecule of average molecular speed $\langle c \rangle$ is given by eq 18:

$$k_{het} = (\gamma\langle c \rangle/4)(s/v) = 3\gamma\langle c \rangle/4r \tag{18}$$

where γ is the measured uptake coefficient, defined as the ratio k_{het}/ω, with ω being the gas−wall collision frequency of the average molecule, determined by elementary gas kinetics. It represents the fraction of collisions leading to irreversible removal of the molecule from the gas phase on the characteristic time scale of the experiment. Depending on the characteristic particle size r, an aerosol particle embedded in a fluid, such as the atmosphere, experiences gas−wall collisions as individual events if r is smaller than the mean free path λ (Knudsen number $r/\lambda \ll 1$), whereas it behaves like an object in a fluid continuum if r is much larger than λ ($r/\lambda \gg 1$). The Knudsen number r/λ, therefore, determines the importance of the molecular flow regime of gas−substrate collisions ($r/\lambda \ll 1$) compared to the viscous flow regime ($r/\lambda \gg 1$). There are a number of expressions in the literature for the gas−substrate flux, depending on the pressure and the radius of the particle that describe intermediate cases for r/λ in the vicinity of 1, among them the Fuchs−Sutugin formula.[9,10] However, we will content ourselves here with a simple, albeit approximate expression relating the first-order mass-transfer coefficient k_{mt} to the heterogeneous rate constant for chemical conversion, k_{het}, according to eq 19, in order to determine which rate process, mass transfer or heterogeneous reaction, will be rate-limiting under the given conditions.[176] The sequential rate processes are displayed schematically in eq 19, assuming that k_{-1} is small: In eq 20, D is the diffusion coefficient (in cm^2 s^{-1}) of

$$\mathrm{M(g)} \rightleftarrows \mathrm{M(ads)} \rightarrow \text{products} \qquad (k_{mt}, k_{-1}, k_{het}) \tag{19}$$

$$k_{mt} = 4r\pi Dn \tag{20}$$

molecule M at pressure and n is the particle number density (cm^{-3}) given in eq 16. If one uses n from eq 16, the expression displayed in eq 21 is obtained:

$$k_{mt} = 3D(m/\rho)(1/r^2) \tag{21}$$

which may be combined with k_{het} of eq 18 to yield k_{tot} using the well-known approximate reciprocal relationship (resistor model)[156] given in eq 22:

$$1/k_{tot} = 1/k_{mt} + 1/k_{het} \tag{22}$$

Equations 21 and 22 unambiguously show that k_{mt} increases faster than k_{het} with decreasing r, owing

to the different r-dependence of the two terms, that is, $1/r^2$ vs $1/r$, respectively. For sufficiently small aerosol particles, the heterogeneous chemistry rate is therefore going to be rate-limiting, owing to the large values of the mass-transfer rate, even at atmospheric pressure. These are good reasons for performing aerosol experiments at atmospheric pressure in order to learn more about the rates of interfacial reactions on aerosols. However, this increased level of insight in aerosol experiments comes at the price of experimental complications, not the least of which is the separation of undesirable rate processes taking place at the walls of the aerosol flow reactor from the rate process of interest taking place on the aerosol surface. An often-encountered difficulty is the deposition of aerosols on the flow reactor walls, that usually represent a significantly larger surface area compared to the aerosol surface area, which leads, especially in the case of N_2O_5, to fast wall processes that may mask the process of interest.[168,171]

3. Heterogeneous Reactions

3.1. N_2O_5

3.1.1. Reactions of N_2O_5

Dinitrogen pentoxide, N_2O_5, is part of the family of active nitrogen, NO_y, because of its equilibrium with NO_2 and NO_3 according to eq 23, which releases photochemically active (NO_3) and reactive free radicals.

$$N_2O_5 \rightleftarrows NO_2 + NO_3 \qquad (23)$$

Owing to the fairly low N−O bond strength of 22.85 kcal/mol[57] in N_2O_5, its lifetime under atmospheric conditions and 298 K is 21 s and is a strong function of temperature.[57,58] Like no other atmospherically relevant compound, its presence has introduced the concept and emphasized the subsequent importance of heterogeneous reactions in the atmospheric planetary boundary layer (PBL). The observation of the buildup of the concentration of nitric acid, HNO_3, in the PBL during the night could only be explained by the heterogeneous conversion of N_2O_5 to HNO_3 according to reaction 24, because all other likely reactions leading to HNO_3 are too slow, namely the corresponding homogeneous reaction 24, for which only an upper limit may be given,[178−182] as well as the gas-phase reaction 25.

$$N_2O_5 + H_2O \rightarrow 2HNO_3 \qquad (24)$$

$$OH + NO_2 \rightarrow HNO_3 \qquad (25)$$

This latter reaction comes to a virtual standstill at night because of the low OH free radical concentration, provided that OH is generated from the photolysis of O_3. The substrate for the heterogeneous reaction 24 is thought to be urban H_2O-containing aerosols or humid surfaces, whose purpose is to make available adsorbed H_2O to enable reaction 24.[183,184]

In the aftermath of the observation of ozone depletion at polar latitudes, as well as in the background stratosphere, the importance of heterogeneous reactions in the atmosphere was recognized. Finlayson-Pitts and co-workers were among the first to experimentally examine the potential importance of heterogeneous reactions in the chemistry of the MBL in the presence of marine aerosol particulates.[44] They performed laboratory studies of atmospherically relevant species on surrogates of solid marine aerosol particles on alkali chlorides, such as NaCl and alkali bromides, and came to the conclusion that the reaction of N_2O_5 with NaCl could have a significant influence on the oxidative capacity of the MBL. The relevant chemistry is given in reactions 26 and 27,

$$N_2O_5 + NaCl \rightarrow ClNO_2 + NaNO_3 \qquad (26)$$

$$ClNO_2 + h\nu \rightarrow Cl + NO_2 \qquad (27)$$

where reaction 26 corresponds to the volatilization of inorganic chlorine by the heterogeneous interaction of reactive nitrogen, to yield the photochemically active intermediate nitryl chloride, $ClNO_2$, which undergoes a fast photolytic reaction, resulting in the release of a Cl atom, corresponding to an atmospheric lifetime of approximately 1 h at low zenith angle (noon). Free Cl atoms have a reactivity toward H-abstraction from hydrocarbons that is many times larger than the corresponding reaction of OH free radical, depending on the type of hydrocarbon. Therefore, the replacement of OH by Cl, that reacts only slowly with OH, changes the rate of initiation of hydrocarbon oxidation, which has an impact on the oxidative capacity of the troposphere and overall atmospheric chemistry.[4,52−55,185,186] This chemistry, based on Cl-initiated hydrocarbon oxidation with $ClNO_2$ as a precursor, will be especially important at northern mid- to high latitudes for three reasons: (a) high concentrations of NO_2 from anthropogenic sources, (b) high concentrations of sea spray aerosols owing to favorable wind patterns, and (c) high values of N_2O_5 concentrations because low temperatures shift equilibrium 23 to the left.[165]

The experimental results of the heterogeneous reactions of N_2O_5 on salts are presented in Table 1 and will be discussed in pertinent detail in the following. Livingston and Finlayson-Pitts studied reaction 26 in a static salt-packed cylindrical cell, whose content was monitored by long-path FTIR absorption spectroscopy at 1 atm of air[177] at a typical initial concentration of N_2O_5 of 5.5×10^{13} molecules cm^{-3}. The fractional yield of $ClNO_2$ relative to N_2O_5 was in the range 60−100% and was independent of the mass and of the thermal pretreatment of the used polycrystalline NaCl. A conservative lower limit of the uptake coefficient was inferred from the fractional yield of NO_2Cl relative to N_2O_5, the estimated gas-phase residence time of N_2O_5, and the total external surface area of the salt. Small amounts of water vapor, presumably adsorbed on the salt, affected neither the kinetics nor the relative yield of NO_2Cl. However, in addition to NO_2Cl, important amounts of HNO_3 ($HNO_3/N_2O_5 = 0.55 \pm 0.16$) were detected. HNO_3 is thought to originate from the heterogeneous reaction of N_2O_5 with residual water adsorbed on the internal surfaces of the apparatus,

Table 1. N_2O_5 + NaCl (KBr) → $ClNO_2$ ($BrNO_2$) + $NaNO_3$ (KNO_3), and N_2O_5 + H_2O in the Presence of NH_4HSO_4, $(NH_4)_2SO_4$, $NaNO_3$, Na_2SO_4, and $NaHSO_4$ → $2HNO_3$

symbol	uptake coefficient	substrate	temp/K	reference
γ_{ss}	$(4.9 \pm 0.7) \times 10^{-2}$	NH_4HSO_4 aerosol, 45−75% rh	293	Mozurkewich and Calvert, 1988[126]
	$(8.5 \pm 1.9) \times 10^{-2}$	NH_4HSO_4 aerosol, 55−75% rh	274	
γ	$\leq 2.5 \times 10^{-3}$	polycrystalline NaCl	300	Livingston and Finlayson-Pitts, 1991[177]
γ_{ss}	$(3.2 \pm 0.3) \times 10^{-2}$	NaCl aerosol, 71−92% rh	292	Zetzsch and Behnke, 1992[191,192]
γ_{ss}	$(3.9 \pm 1.3) \times 10^{-2}$	NaCl aqueous solution droplet	263	George et al., 1994[171]
	$(1.4 \pm 0.8) \times 10^{-2}$	NaCl aqueous solution droplet	278	
γ	1.5×10^{-2}	5% NaCl aqueous soln, high rh	300	Msibi et al., 1994[195]
	5×10^{-3}	5% NH_4HSO_4 soln, high rh		
	1×10^{-3}	solid NaCl, 45−96% rh		
γ_{ss}	$<1.0 \times 10^{-4}$	NaCl grain, baked	296	Leu et al., 1995[148]
	4.5×10^{-4}	NaCl, 1 h pumping		
	$<1.0 \times 10^{-4}$	NaCl grain, baked	223	
	2.4×10^{-4}	NaCl grain, 1 h pumping		
γ_{ss}	9×10^{-4} (3.5×10^{-3})	NaCl (KBr) powder, 35−160 μm	298	Fenter, Caloz, and Rossi, 1996[188]
	2×10^{-3} (4×10^{-3})	NaCl (KBr) grain, 200−400 μm	298	
	$(5 \pm 2) \times 10^{-4}$	NaCl spray-coat, thin film	298	
	$(3 \pm 1.5) \times 10^{-3}$	KBr spray-coat, thin film		
	$(4 \pm 2) \times 10^{-4}$	NaCl single-crystal salt flat	298	
	$(4 \pm 1) \times 10^{-3}$	KBr single-crystal salt flat		
γ_{ss}	$(3.2 \pm 0.2) \times 10^{-2}$	NaCl aerosol, 77−94% rh	291	Behnke et al., 1997[165]
γ_{ss}	$(1.7 \pm 0.2) \times 10^{-2}$	20% $(NH_4)_2SO_4$ aerosol, 93.5% rh	297	Hu and Abbatt, 1997[168]
	$(2.3 \pm 0.4) \times 10^{-2}$	40% $(NH_4)_2SO_4$ aerosol, 83.0% rh		
	$(5.3 \pm 0.6) \times 10^{-2}$	60% $(NH_4)_2SO_4$ aerosol; 68.5% rh		
	$(4.4 \pm 0.8) \times 10^{-2}$	80% $(NH_4)_2SO_4$ aerosol, 50.0% rh		
γ	$(1.8 \pm 0.3) \times 10^{-2}$	H_2O droplets, up to 1 M NaCl	262−278	Schweitzer, Mirabel, and George, 1998[172]
γ	$(1.8 \pm 0.4) \times 10^{-3}$	$NaNO_3$ aerosol, 50% rh	293	Wahner et al., 1998[175]
	$(3.2 \pm 0.6) \times 10^{-3}$	$NaNO_3$ aerosol, 60% rh		
	$(2.3 \pm 0.5) \times 10^{-2}$	$NaNO_3$ aerosol, 90% rh		
γ	$3.7\ (+0.8, -1.9) \times 10^{-2}$	Na_2SO_4 aerosol, 71% rh	293	Mentel, Sohn, and Wahner, 1999[127]
	$(1.8 \pm 0.4) \times 10^{-2}$	$NaHSO_4$ aerosol, 56% rh		
	$(2.0 \pm 0.4) \times 10^{-4}$	$NaHSO_4$ aerosol, 2% rh		
γ_0	$(3 \pm 1) \times 10^{-4}$	polycrystalline NaCl film	295	Koch, van den Bergh, and Rossi, 1999[199]
	$(2.5 \pm 1) \times 10^{-3}$	polycrystalline KBr film		
γ	$(2 \pm 1) \times 10^{-2}$	$(NH_4)_2SO_4$ aerosol, 100 μm diameter, 70% rh	295 ± 1	Kane, Caloz, and Leu, 2001[169]
	$(3 \pm 1) \times 10^{-2}$	NH_4HSO_4 aerosol, 100 μm diameter, 70% rh		
γ_{ss}	$(2.9 \pm 1.7) \times 10^{-3}$	solid crystalline NaCl grain	296	Hoffman et al., 2003[190]
	$(3.4 \pm 0.8) \times 10^{-2}$	"wet" synthetic sea salt		
	$(5.8 \pm 6.6) \times 10^{-3}$	"dry" synthetic sea salt		

and resulted in the formation of equivalent amounts of HCl in the presence of the NaCl substrate, according to the secondary heterogeneous reaction A6, to be discussed in detail in section 3.2:

$$HNO_3 + NaCl \rightarrow HCl + NaNO_3 \qquad (28)$$

However, the mass balance could not be closed in these experiments owing to lack of sensitivity of the FTIR-based detection used for HCl.

Leu and co-workers performed uptake experiments of N_2O_5 at approximately 2×10^{-6} Torr on NaCl grains using a fast-flow reactor coupled to CIMS detection.[148] Because of the efficient detection scheme of N_2O_5 compared to HNO_3, that used the fast ion−molecule reaction $I^- + N_2O_5 \rightarrow NO_3^- + INO_2$, where nitrate anion was detected, the HNO_3 impurity of approximately 10% did not perturb the kinetic measurement. No reaction products are reported, and the measured γ values listed are corrected for pore diffusion of N_2O_5 across the external voids of the polycrystalline sample,[149,152,187] which reduces the observed N_2O_5 decay rate constants by approximately a factor of 5, to result in corected uptake coefficients γ_t. Unfortunately, pore diffusion theory is applied to the measured (apparent) uptake coefficients without prior validation by studying the dependence of γ on the sample mass. On "dry" NaCl salt that has been pumped for 2 h, values of $\gamma_t \leq 10^{-4}$ have been measured both at 296 and 223 K, whereas slightly larger values had been measured on salt that had previously been exposed to H_2O vapor. The authors attribute the increase in γ_t to the competing hydrolysis reaction of N_2O_5 according to reaction 24, wherein H_2O would be adsorbed on NaCl. The present work appears to be the only study of its kind that examines the uptake kinetics over a sufficiently large temperature range that would enable the kinetic results to be applied to the upper troposphere and the lower stratosphere. However, the authors are unable to establish the branching ratio between the halogen-exchange reaction 26 and the hydrolysis reaction 24 as a function of temperature because neither product, $ClNO_2$ nor HCl, had been detected.

Fenter et al.[188] investigated the heterogeneous reactions of N_2O_5 with solid NaCl and KBr in a low-pressure flow reactor with emphasis on product detection and the influence of the sample presentation on the uptake kinetics. This was the first time the uptake kinetics on a given alkali salt sample had been studied in a systematic way. The presentation was varied, with the goal to establish a truly mass-

independent γ that was invariant to sample presentation. Sample presentation included NaCl and KBr single crystals, ground powders of various average sizes, commercially available salt grains, and thin deposited salt films. The uptake rates were independent of the N_2O_5 concentration and gas-phase residence time and thus are first order. This was also checked in pulsed N_2O_5 uptake experiments on salt that led to first-order N_2O_5 decays. The results may be summarized as follows: On solid powders, N_2O_5 reacts with high uptake probability. The main product on NaCl and KBr is $ClNO_2$ and Br_2 at a yield of (60 ± 6)% and 35%, respectively. For KBr, the primary product is $BrNO_2$, following reaction 29, in agreement with previous work.[189] However, heterogeneous decomposition prevents its observation at low pressures. Instead, the fast secondary reactions 30 and 31 take place, which were monitored by the appearance of Br_2 and HONO, the latter depending on the quantity of surface-adsorbed water (SAW), whose importance will be discussed below.

$$N_2O_5 + KBr \rightarrow BrNO_2 + KNO_3 \quad (29)$$

$$BrNO_2 + KBr \rightarrow Br_2 + KNO_2 \quad (30)$$

$$KNO_2 + HNO_3\,(H_2O) \rightarrow HONO + KNO_3\,(KOH) \quad (31)$$

However, the γ values were strongly dependent on the mass of the salt sample when presented in the form of finely ground powder or monodisperse grain. Therefore, the diffusion of N_2O_5 into the salt sample had to be taken into account using the pore diffusion model,[149,152,187] leading to the "true" or more accurately corrected values of γ, displayed in Table 1. The uncertainty of the fitted results is difficult to assess in the absence of a structurally well-defined crystalline substrate whose structural parameters are used in the model. Discrepancies of up to a factor of 4 have been noted when one compares the fitted results of γ for NaCl grains with measured values for single crystals (Table 1), whereas for KBr this gap is much smaller for reasons unknown. The authors have therefore preferred to report the measured values of γ from sample presentations that do not require correction by the pore diffusion model, such as γ values for uptake on spray-coated samples and depolished (that is, mechanically roughened) single-crystal salt windows. This leads to γ values for NaCl and KBr of $(5.0 \pm 2.0) \times 10^{-4}$ and $(4 \pm 1) \times 10^{-3}$, respectively. These values correspond to sample presentations that avoid diffusion of N_2O_5 into the bulk of the sample and correspond to the geometric surface area of the sample. On the other hand, one may have to allow a significant change of the chemical properties of the substrate when presented as a thin spray-coated salt film compared to ground powder samples. It is possible that different sample presentations may lead to intrinsically different uptake kinetics, owing, for instance, to different amounts of reactive defect sites that preferentially accumulate SAW. The γ value for single-crystal surfaces of NaCl and KBr that were previously wet-etched by rinsing with water is significantly smaller than the average, namely $<1 \times 10^{-4}$. This result points to the importance of reactive sites on solid alkali salts that may be identified with crystal defect sites or lattice imperfections that also accumulate adsorbed water, thus enabling the halogen-exchange reactions 26 and 29. During the wet-etching of the single crystal salts, reactive surface sites may preferentially be lost, which leads to a dramatic lowering of the reactivity of these processed single crystals toward N_2O_5 from $\gamma = 4 \times 10^{-4}$ to $\leq 10^{-4}$, and from 3×10^{-3} to $\leq 10^{-4}$ for NaCl and KBr, respectively. In general, added water vapor did not have a measurable effect on the rate of uptake of N_2O_5 up to a H_2O partial pressure of 100 mTorr.

Hoffman et al.[190] have reinvestigated the heterogeneous reaction using the same experimental technique as Fenter et al.[188] but have put the emphasis on measuring the uptake of N_2O_5 on polycrystalline NaCl in sublayer quantities in order to free themselves from the need to correct the measured value of γ using the pore diffusion theory. They realized that the results of experiments using multilayer quantities of NaCl led to large scatter in the corrected γ values, in view of the lack of reliable structural parameters characterizing the samples in question. They monitored the reaction products from reactions 26, 24, and 28, namely $ClNO_2$, HNO_3, and HCl, in order to establish the branching ratio of $ClNO_2$, BR^{ClNO_2}, measured as 0.73 ± 0.28, independent of sample mass. In addition, the γ values obtained in sublayer experiments were independent of the conditioning of the salt substrates and are estimated to be within a factor of 3 of the true uptake probabilities.

By going to sublayer quantities of polycrystalline NaCl, Finlayson-Pitts and co-workers are exchanging the pore diffusion model for another model based on the $\cos\theta$ directional distribution of desorbing N_2O_5 and interception of the trajectory by the crystal faces of the surrounding crystallites. The model results are quite sensitive to the estmated average geometrical arrangement of the NaCl crystallites. In conclusion, the authors have exchanged the moderately well validated pore diffusion model for a new one whose validation has not been performed on an extensive basis. Moreover, owing to the small sample mass required for sublayer coverage, the raw MS uptake signals are much weaker than in the case of multilayer samples, where the experimental signature is much more robust. Table 1 also displays results on synthetic sea salt (SSS) obtained by Hoffman et al.[190] in multilayer experiments, indicating a unity branching ratio (0.98 ± 0.12) for the formation of $ClNO_2$ and uptake kinetics that is significantly faster, by roughly an order of magnitude. Sublayer experiments were not performed because of the hygroscopic properties and difficulties in handling the SSS sample. However, it was estimated that, owing to the large quantities of surface-adsorbed water (SAW) contained in the SSS sample, the probe gas could not diffuse into the interior of the sample and that, therefore, the measured γ value corresponded to interaction of the gas with the geometric surface area of the substrate, thus $\gamma = \gamma_t$. The larger value of BR^{ClNO_2} for SSS compared to solid NaCl, namely 73

vs 100%, is somewhat counterintuitive, as a higher quantity of SAW present in SSS would normally lead to the predominance of the hydrolysis pathway (reaction 24). Hoffman et al. explain this by stating that reaction 26 is enabled by the reorganization of the substrate surface, which is faster the higher the ion mobility, and hence the SAW content, is. The ion mobility scales with the amount of SAW and is thought to be the rate-limiting step for the heterogeneous reaction 26. Both the fact that it occurs faster, as indicated by its higher value of γ_{ss}, and the fact that BR^{ClNO_2} increases with increasing amounts of SAW will be explained in more detail in section 3.1.3.

Zetzsch and Behnke[191,192] performed N_2O_5 uptake experiments in an aerosol chamber fitted with a FEP bag in which a reaction between a mixture of hydrocarbons, NO_x, and O_3 took place in the presence of a well-characterized NaCl aerosol with a known size distribution at relative humidities (rh) of 71−92% (292 K). The extent of the reaction was followed by monitoring the concentration of hydrocarbons, O_3, HCl, and NO_2 as a function of time. The amount of N_2O_5 taken up was assessed using the NO_x mass balance, and $ClNO_2$ was derived from the hydrocarbon consumption with time in the presence of light, which generates free Cl atoms according to reaction 27. The uptake coefficient γ, based on the disappearance of N_2O_5 and corrected for wall losses on the Teflon walls, is displayed in Table 1, and drops from 0.05 at 92% to 0.024 at 71% rh. The derived $ClNO_2$ yields were 61, 56, 42, and 31% for 71, 74, 83, and 92% rh. They are thus proportional to chloride ion concentration, whereas the branching ratio BR^{ClNO_2} decreases from 0.61 to 0.31 over the same relative humidity range, because the pathway leading to HNO_3, according to reaction 24, gains in importance for a more dilute aerosol. Chemical kinetic simulations using the known homogeneous chemistry lead to the same results for the $ClNO_2$ yields. In comparison, recent results[165] obtained using the same experimental methodology point toward a constant $ClNO_2$ yield of approximately 65%, independent of the extent of N_2O_5 uptake, corresponding to an inferred branching ratio BR^{ClNO_2} of 70%, independent of the rh between 77.3 and 94%, which corresponds to [NaCl] between 5.1 and 1.7 M in the aerosol. The uncertainty in the $ClNO_2$ yields of the older aerosol smog experiments,[191,192] compared to the more recent ones,[165] could not be attributed to a specific reason. However, it was found that N_2O_5 underwent rapid hydrolysis (reaction 24) on the Teflon walls at high rh. The following compounds have been found as stable reaction products in the aerosol chamber: 1,1-dichloroacetone, chloroacetone, and phosgene ($COCl_2$), which may result from the homogeneous interaction of free atomic chlorine with the hydrocarbons.

In more recent aerosol chamber measurements on the interaction of N_2O_5 with wet submicrometer-sized NaCl aerosol, Behnke et al.[165] measured both the uptake coefficient and the absolute yield of $ClNO_2$ (Table 1) at relative humidities between 77.3 and 93.9%, corresponding to aqueous NaCl concentrations between 5.1 and 1.7 M, respectively. They subsequently compared their results with those of a model experiment using a wetted wall flow tube (WWFT). The yield of $ClNO_2$ from the aerosol reaction was measured indirectly after photolysis by measuring the decrease of the concentration of added test hydrocarbons using GC analysis, whereas it was monitored using FTIR in the WWFT experiments. The average yield of $ClNO_2$ from the aerosol experiment, approximately 65%, was independent of rh and of the extent of N_2O_5 uptake. The $ClNO_2$ yield obtained in the WWFT experiments increased steeply in the range from 0 to 2 M NaCl and leveled off at approximately 90% thereafter up to 5 M, similar to the $ClNO_2$ yields from the aerosol experiment, whose absolute values were systematically lower, however. This difference may be explained by secondary uptake of $ClNO_2$ on the walls of the aerosol smog chamber, as will be discussed in section 3.5. As displayed in Table 1, the uptake coefficient of 0.032 obtained in the aerosol chamber experiment is independent of rh and is an order of magnitude larger than γ obtained for N_2O_5 interaction with solid NaCl (Table 1). This is an illustrative example of the fact that model experiments such as the one discussed above on solid alkali halide salts do not always yield identical answers compared to experiments carried out under more realistic conditions. However, the former provide a quick guide to the processes and mechanisms that may be expected under environmental conditions.

On the basis of their results obtained both in an aerosol chamber and in a WWFT experiment, Behnke et al.[165] advance a complex reaction mechanism of N_2O_5 uptake on NaCl aerosol beyond the deliquescence point. It involves autoionization of N_2O_5 (reaction 32), as well as reversible ionic dissociation of $ClNO_2$. This mechanism will be discussed in more detail below. The authors propose the key competition of the nitronium ion, NO_2^+, generated by the autoionization reaction of N_2O_5 (reaction 32), for chloride and H_2O according to reactions 33 and 34 both in the concentrated NaCl solutions used in the WWFT experiments and on or in wet NaCl aerosols. Although the mechanism seems plausible, it is surprising in view of the extremely short lifetime of free NO_2^+ in aqueous solution of approximately 10^{-9} s. This is an indication either of its reactivity in aqueous solution according to reaction 34,[193] or of the slowness of reaction 34, or both. This autoionization mechanism will be discussed below in more detail.

$$N_2O_5 \rightleftarrows NO_2^+ + NO_3^- \quad (32)$$

$$NO_2^+ + Cl^- \rightleftarrows NO_2Cl \quad (33)$$

$$NO_2^+ + H_2O \rightarrow HONO_2 + H^+ \quad (34)$$

A slightly different approach was taken by George et al.,[171] who studied the N_2O_5 uptake on a fast droplet train (80−150 μm diameter) of 1 M NaCl, moving inside a flow tube at a contact time of 4−16 ms. The temperature of the droplet was controlled by the metered partial pressure of H_2O in the synthetic air carrier gas and was varied between 2.8

and 8.2 mbar, corresponding to the temperature range 263−278 K. The N_2O_5 was monitored using FTIR absorption at the entry of the flow tube, and the extent of reaction was followed by measuring the NO_3^- concentration in the collected droplets using HPLC. The measured uptake coefficients were corrected for the rate-limiting gaseous diffusion of N_2O_5 to the droplet surface and the previously published NO_2Cl yield of 67 ± 7%.[192] The reactive uptake coefficients on droplets containing 1 M NaCl are displayed in Table 1, and are slightly larger than the ones for pure water, although that argument is based on just four data points spread over a very narrow temperature range. This experiment is one of the few where the condensed-phase reaction products resulting from a multiphase interaction have been monitored. It yields γ values that are commensurate with results of N_2O_5 uptake on aerosols or aqueous alkali halide salt solutions. Although the temperature range over which γ has been measured is extremely limited (263−278 K), the negative temperature dependence of the uptake rate coefficient is expected, in agreement with theoretical expectations,[194] if γ is interpreted as a mass accommodation coefficient.

Schweitzer et al.[172] undertook a careful reinvestigation of the uptake of N_2O_5 on a series of salt solutions using a fast droplet train (80−150 μm diameter) equipped with FTIR/long-path absorption and an ion-trap mass spectrometer for gas-phase detection of N_2O_5 and products. The uptake coefficients were independent of temperature in the range 262−278 K, in contrast to earlier results.[171] The numerical value of γ for salt-containing solutions, displayed in Table 1, was identical to the one for pure water and was independent of the NaCl concentration up to 1 M. In addition, it was identical for chlorides, bromides, and iodides up to a concentration of 1 M. The average yield of $ClNO_2$ was 100 ± 14%, and the detected reaction products were $BrNO_2$, Br_2, HONO, and I_2 for bromide- and iodide-containing solutions, respectively. From the fact that γ is independent of both the concentration and the nature of the alkali halide, the authors infer that the rate-limiting step in the N_2O_5 uptake is always the same, namely the autoionization of dinitrogen pentoxide into NO_2^+ and NO_3^- (reaction 32), as was discussed above.[165] Two arguments, namely the temperature independence of γ for uptake onto aqueous solutions as well as its independence of the nature of the alkali halide, strongly point toward the fact that γ is not dominated by a rate-controlling accommodation process, but is rather controlled by reversible autoionization in aqueous solution (reaction 32). This somewhat surprising mechanistic conclusion has been presented above and throws new light on the question of the stability of nitronium ion, NO_2^+, in the H_2O-containing condensed phase.

Msibi et al.[195] studied the deposition of N_2O_5 on bulk coatings made of aqueous solutions of the salts of high atmospheric abundance that were supported on the inner walls of an atmospheric pressure flow tube. The coating on the inner surface of the tube was divided into segments in order to resolve the axial deposition profile of the reaction product HNO_3, which was monitored as NO_3^- using ion chromatography. However, the high recovery rates of nitrogen for a 5% aqueous NaCl coating are inconsistent with the formation of volatile $ClNO_2$ resulting from reaction 26. Table 1 shows representative data for NaCl and NH_4HSO_4: the most striking result is the increase of γ for uptake on NaCl by a factor of 15, on going from solid NaCl at 45% rh to a 5% solution at 95% rh, which is in general agreement with literature results (Table 1). Neither reaction products nor branching ratios (BR^{ClNO_2}) were measured. In contrast, the γ value for NH_4HSO_4 solution seems approximately an order of magnitude too low when compared to the analogous reaction on NH_4HSO_4 aerosol at comparable relative humidity.[169]

Mozurkewich and Calvert[126] undertook a comprehensive series of uptake experiments of fine size-selected NH_4HSO_4 aerosol in an atmospheric pressure (0.8 bar) flow tube at laminar flow conditions. Three size classes, in the range 40−100 nm diameter, were investigated at relative humidities of 1−76%. N_2O_5 undergoes hydrolysis (reaction 24) with H_2O in the NH_4HSO_4 aerosol. The γ value is approximately 0.05 for rh = 40%, which is above the deliquescence point for NH_4HSO_4 at ambient temperature. At 274 K, γ increases to 0.09 at this rh (Table 1). However, when γ is recorded as a function of rh, it does not show the expected break (decrease) at the deliquescence point, a fact that the authors attribute to the presence of a thin H_2O-containing aqueous H_2SO_4 layer remaining after partial NH_3 evaporation, which leads to a significant value of γ_{ss} for NH_4HSO_4, even below its deliquescence point (rh ≤ 40%). This assumes that γ for N_2O_5 would be significantly larger if it reacted with an adsorbed aqueous solution compared to reaction on solid NH_4HSO_4, an assumption that is borne out by the data displayed in Table 1. Upon increasing the NH_4^+ content by 25% in order to counteract the NH_3 evaporation, γ_{ss} decreases at low and high rh, as expected, because of neutralization of the liquid H_2SO_4-containing layer to solid NH_4HSO_4 salt. No significant uptake of N_2O_5 on $(NH_4)_2SO_4$ aerosol was observed at rh = 25% at 293 K, due to the absence of a liquid layer on the aerosol surface. At 60% rh, $\gamma_{ss} = (4.3 \pm 0.5) \times 10^{-2}$ was measured, which suggests that the $(NH_4)_2SO_4$ aerosol was present in its deliquescent state. The negative temperature dependence of γ_{ss} observed throughout this work is interpreted in terms of increasing reevaporation of N_2O_5 with increasing temperature, assuming that the rate-limiting step in the N_2O_5 uptake is autoionization of N_2O_5 into NO_2^+ and NO_3^- according to reaction 32. This is also consistent with the fact that γ is effectively constant with H_2SO_4 concentration in the rh range of 1−10%.

Hu and Abbatt performed N_2O_5 uptake studies on $(NH_4)_2SO_4$ aerosol[168] using an atmospheric pressure laminar aerosol flow tube coupled to a chemical ionization mass spectrometer (CIMS) and an optical particle counter that classified the aerosol from 0.2 to 20 μm diameter into one of 31 channels. The typical aerosol distribution was bimodal, large (1−6 μm in diameter) and small (<0.3 μm in diameter), of which only the large aerosol size fraction significantly

contributed to the total aerosol surface. Typical concentrations of the large particles used for the kinetic studies were $3 \times 10^3-2 \times 10^4$ particles cm^{-3}, with the peak of the distribution centered between 2 and 4 μm in diameter. The used N_2O_5 concentration in the range $5 \times 10^{12}-1 \times 10^{14}$ molecules cm^{-3} decayed according to first-order kinetics. The first-order rate constant for the title reaction scaled linearly with the aerosol surface area, which was evaluated at the maximum of the aerosol particle distribution function established by the optical counter. HNO_3 accumulation, resulting from hydrolysis of N_2O_5 according to reaction 24, was deemed insignificant in view of the large aerosol volumes used. This study is of particular interest, as the size of the used ammonium sulfate aerosol has been characterized by an optical counter based on (Mie) scattering rather than on the mobility diameter, as is usually the case. The results on the uptake coefficient are in very good agreement with those obtained by Mozurkewich and Calvert,[126] for both H_2SO_4 and $(NH_4)_2SO_4$ aerosol, which instills confidence in the reliability of the experimental technique. Table 1 displays representative kinetic results as a function of relative humidity at ambient temperature. The kinetic data display a maximum at 68.5% rh, with a significant drop at 83 and 93.5% rh that is counterintuitive in view of the deliquescence point of ammonium sulfate at 79.5%.[181] Qualitatively similar behavior has been observed for NH_4HSO_4 aerosol by Mozurkewich and Calvert.[126] However, it must be kept in mind that no liquid−solid phase transition of the aerosol, and therefore no discontinuity of γ, is expected in the present experiments because the relative humidities were never allowed to drop below 40% in the aerosol-generating process. The efflorescence point for $(NH_4)_2SO_4$ is at 40% rh,[196] above which the aerosol stays in the form of a supersaturated aqueous solution when the relative humidity is gradually lowered from the deliquescence point, as is the case for the present experiments.

Direct experimental support for N_2O_5 autoionization as the rate-limiting step (reaction 32) in the heterogeneous interaction with a H_2O-containing condensed phase comes from a large aerosol chamber experiment performed by Wahner and co-workers,[175] in which N_2O_5 was exposed to $NaNO_3$ aerosol at three humidities, namely at approximately 50, 60, and 90% rh at 293 K. The large aerosol chamber of 256 m^3 volume was equipped with a long-path (30 m) FTIR absorption and UV spectrometer for monitoring concentrations of N_2O_5, HNO_3, and ozone, respectively, in the range of 1−2 ppm. The particulate phase was characterized by its distribution function using both a mobility analyzer and an optical particle counter, which were cross-calibrated and spanned a combined range of approximately 20 nm to 6 μm. The uptake experiments have been performed under conditions of changing aerosol number density and surface area S_{tot} with time at pseudo-first-order conditions with respect to S_{tot}. The aerosol lifetime was roughly an order of magnitude larger than the N_2O_5 lifetime in the presence of $NaNO_3$ aerosol, which amounted to 30 min, such that only small corrections to S_{tot} had to be applied during the heterogeneous reaction. The main result is that γ increases with increasing relative humidity, as displayed in Table 1. In other words, γ decreases with increasing $NaNO_3$ molality, which has been called the "nitrate effect" and has been interpreted in terms of the reversible reaction 32, whose net rate slows down with increasing NO_3^- concentration, owing to the increasing rate of the back reaction in much in the same way as the common ion effect reduces the solubility of a salt in aqueous solution that already contains a given concentration of a common ion. Over the rh range of 50−90%, the aerosol stayed in a metastable liquid state, as evidenced by FTIR absorption spectra that always showed the presence of liquid water. Therefore, the decrease of γ on going from 90 to 50% rh has been attributed solely to the common ion effect, which leads to increasing re-evaporation of N_2O_5 upon interaction with the concentrated $NaNO_3$ solution at 50% rh. Model simulations led to a fraction f of HNO_3 ranging from 23 to 39% for relative humidities in the range from 90 to 50% that was incorporated into the condensed phase as a result of reaction 24, whose dependence on rh is contrary to expectation. A value of $f = 10\%$ was expected on the basis of thermodynamic arguments.

Additional support for the nitrate effect in heterogeneous N_2O_5 hydrolysis on inorganic nitrate-containing aerosols has been obtained by Mentel et al.,[127] using a large aerosol chamber similar to that used by Wahner et al.[175] In contrast to $NaNO_3$ aerosols at 50 and 60% rh,[175] the γ values of $NaHSO_4$ and Na_2SO_4 aerosols at 60 and 70% rh (Table 1) fall in the 0.02−0.05 "window" characteristic for the interaction of N_2O_5 with most other H_2O-containing aerosols. An exception may be the results obtained on a 2% rh $NaHSO_4$ solid aerosol, which yielded a γ value lower by approximately 2 orders of magnitude, probably because of the lack of surface-adsorbed water (SAW) as an electrolyte. The authors have provided proof beyond doubt that the low values for γ obtained on $NaNO_3$ aerosols at 50 and 60% rh are not the result of a kinetic saturation effect occurring in the static aerosol chamber. Instead, they have confirmed the existence of the autoionization reaction A10a as the rate-limiting step in N_2O_5 uptake on H_2O-containing aerosols, which leads to a decrease in dissolved N_2O_5 with increasing nitrate molality, because the equilibrium given by reaction 32 and its reverse shifts toward N_2O_5 that desorbs into the gas phase.

Kane et al.[169] undertook a systematic study of the interaction of N_2O_5 with well-characterized NH_4HSO_4 and $(NH_4)_2SO_4$ aerosol as a function of relative humidity in the range 10−100% and compared the γ values with those obtained on a sulfuric acid aerosol obtained under the same experimental conditions. The experiments have been performed in an atmospheric pressure flow tube with characteristic reaction times in the range 1.5−7 s, once the aerosol was well mixed with N_2O_5. The salt aerosols have been generated using an atomizer, resulting in an aerosol whose mode was centered at 100 nm in both cases. Kane et al. obtained a monotonic increase of γ for both salts up to a limiting value at 100% rh of $\gamma =$

0.05, which was identical to the average value for the uptake of N_2O_5 on H_2O.[194] Ammonium bisulfate had a γ value that was approximately 50% higher than the one for ammonium sulfate over the whole rh range, but both γ values converged to 0.05 within experimental error ($\pm$0.025). However, this continuous increase of γ from low values at rh < 40%, which corresponds to the efflorescence point, below which the aerosol is a solid, disagrees with the work of both Mozurkewich and Calvert,[126] even when corrected downward by 15% as recommended by Fried et al.,[197] and Hu and Abbatt,[168] who observe a maximum in γ for both salts at approximately 40−60% rh. Even if $\gamma = 0.05$ is too high by a factor of 2.5 in the limit of high relative humidity, as suggested by the data evaluation panel,[58] the trends of γ with rh remain opposite when the work of Kane et al.[169] is compared to that of Mozurkewich and Calvert[126] and Hu and Abbatt,[168] respectively, at relative humidities larger than 40−60%. These differences are, at present, not understood from a mechanistic point of view and on the basis of an empirical model introduced by Robinson et al.[198] It seems clear that the reaction mechanism for N_2O_5 hydrolysis by more or less concentrated salt solutions seems to differ from the interaction on sulfuric acid aerosol, whose γ values monotonically decrease with increasing rh,[168,169] albeit to a lesser extent than for the ammonium salts.

3.1.2. Concluding Remarks

The value of γ for the uptake of N_2O_5 on solid alkali salt halides is characterized by a large variability, ranging from unmeasurable to 3×10^{-3}, depending on the specific conditions of the experiment. A large amount of surface-adsorbed water (SAW) leads to more rapid uptake kinetics, whereas extensive pumping and/or heating causes a significant decrease of γ. In addition, sample presentation in laboratory experiments also seems of paramount importance, in that observed or apparent uptake coefficients must be corrected following pore diffusion theory. Moreover, there are distinct differences between single-crystal and polycrystalline samples, the former leading to distinctly smaller values of γ in relation to salt powders or grains. In the past few years, many uptake experiments, conducted as gas−aerosol interaction using aerosol flow tubes, have led to a consistent picture as far as the dependence of γ on relative humidity, and thus the composition of the aerosol, is concerned. Uptake of N_2O_5 has been studied on well-characterized aerosols of NaCl, $NaNO_3$, Na_2SO_4, NH_4HSO_4, and $(NH_4)_2SO_4$[127,165,168,169,175,191] and has resulted in γ values lying within a band of 0.02−0.05, with the exception of $NaNO_3$,[175] whose aerosol is less active in taking up N_2O_5, owing to the nitrate effect. The older experiments show a maximum of N_2O_5 uptake at 60−70% rh with a distinct decrease beyond, whereas a more recent experiment[169] shows a monotonic increase of γ with increasing relative humidity for NH_4HSO_4 and $(NH_4)_2SO_4$ uptake, the values of which merge with the ones for N_2O_5 uptake into water droplets. This continuous increase toward a limiting value that is common also to the γ value of N_2O_5 uptake on water droplets is certainly reasonable and expected. It therefore puts the older values into doubt, perhaps because of the documented measurement artifact of N_2O_5 at high values of rh.[168,171,191] The N_2O_5 experiments on droplets, although not aerosols, yield values identical to those obtained in aerosol uptake experiments within experimental uncertainty. However, the claimed temperature dependence of γ in one of these experiments[191] is certainly insignificant in view of the exceedingly small range of temperature used. At the moment, it appears to be safest to assume the absence of a temperature dependence of γ for the uptake of N_2O_5 on solid salts and aqueous droplets as well as salt aerosols.

3.1.3. Mechanistic Considerations

The mechanism of N_2O_5 uptake on aqueous aerosols is related to the one for uptake of $ClNO_2$, which is the reason certain aspects of $ClNO_2$ uptake will also be discussed here. The early experiments, performed 15 years ago by Mozurkewich and Calvert,[126] dealing with the uptake of N_2O_5 on aqueous NH_4HSO_4 aerosols, gave rise to the proposal of the autoionization mechanism outlined below. Essential refinements to this mechanism have been contributed by the work of Zetzsch and co-workers[165,191] and Wahner and co-workers,[127,175] because of the identification of the product $ClNO_2$ and the discovery of the nitrate effect, respectively. The complete mechanism may be written as follows:

$$N_2O_5(g) \rightleftarrows N_2O_5(solv) \quad (35)$$

$$N_2O_5(solv) \rightleftarrows NO_2^+ + NO_3^- \quad (32)$$

$$NO_2^+ + Cl^- \rightleftarrows NO_2Cl \quad (33)$$

$$NO_2^+ + H_2O \rightarrow HONO_2 + H^+ \quad (34)$$

The different processes may be identified by physical solvation of N_2O_5 (reaction 35), reversible autoionization (equilibrium 32), reversible ionization of the product $ClNO_2$ (equilibrium 33), and the competition of NO_2^+ for both H_2O (reaction 34) and Cl^- (reaction 33). The arguments in favor of the above mechanism may be summarized as follows:

(i) The product yield of nitryl chloride, $ClNO_2$, from the N_2O_5 interaction with NaCl solutions or aqueous NaCl aerosols depends in a nonlinear manner on the chloride concentration. It essentially saturates at 100% at chloride concentrations exceeding 1 M.[191,192]

(ii) The branching ratio for $ClNO_2$ formation with respect to reacted N_2O_5 is independent of relative humidity for deliquescent NaCl aerosol, that is, for relative humidities exceeding 74% ranging up to 94% (A3).

(iii) The uptake of $ClNO_2$ is strongly inhibited by chloride.[191,192]

(iv) The uptake of N_2O_5 on sulfuric acid aerosol shows only a weak dependence on relative humidity, and therefore on aerosol composition.[126,169,198] The uptake coefficient decreases from 0.05 to 0.03 on going from 0 to 100% relative humidity. This clearly rules against an acid-catalyzed hydrolysis of N_2O_5, which is the preferred and expected hydrolysis mech-

anism for an acid anhydride, according to reaction 36:

$$N_2O_5 + H_3O^+ \rightarrow 2HNO_3 + H^+ \qquad (36)$$

The central tenet of the autoionization mechanism is that the spontaneous reaction 32 is the rate-limiting step. Such a reaction has previously been observed as a decomposition pathway for N_2O_5 in concentrated protic inorganic solvents, diagnosed by Raman spectroscopy.[200] The autoionization reaction is occurring akin to an S_N1 substitution reaction, resulting in spontaneous formation of nitronium ion, NO_2^+, whose lifetime in aqueous solution has been estimated to be 10^{-9} s.[193] Such an autoionization or decomposition was also observed when N_2O_5 was used in nitration reactions. In these studies, NO_2^+ was identified as the effective nitrating agent. Support for the presence of nitronium ion in the condensed phase comes from adsorption studies of N_2O_5 on ice at low temperatures, performed by Sodeau and co-workers,[201] who investigated the nature of adsorbed N_2O_5 using grazing incidence FTIR absorption. Up to 140 K, the adsorbed N_2O_5 was covalently bound as is the gas-phase species, whereas at temperatures in the range 140−170 K, a rearrangement to the ionic form $NO_2^+NO_3^-$ (nitronium nitrate) was observed. Apparently, solvation processes are enabled at higher temperatures, resulting in a relaxed ionic structure depending on the relative composition of H_2O and HNO_3. At still higher temperatures, conversion of adsorbed N_2O_5 to amorphous HNO_3 or nitric acid hydrates took place. Analytical and numerical modeling by fitting to results from aerosol experiments led to the conclusion that the rate constant for the rate-limiting step, k_{32}, was $>10^4$ [191,192] or 6×10^6 s^{-1},[127] but that it was not very sensitive to the experimental uptake kinetics. The nitronium-based reaction mechanism effortlessly explains the inhibiting effect of $ClNO_2$ uptake by chloride, thereby affecting the equilibrium 33 by shifting it to the right in the presence of significant concentrations of chloride.

Similarly, the nitrate effect, which consists of a decrease of γ of N_2O_5 on aqueous nitrate aerosol by a factor of 10, as demonstrated by Wahner and coworkers in two careful aerosol chamber studies,[127,175] may be rationalized by invoking equilibrium 32. It is shifted toward the molecular form of N_2O_5 in the presence of significant amounts of nitrate and leads to a change in the physical solubility of N_2O_5 in case an equilibrium situation has been achieved during the uptake of N_2O_5. This nitrate effect is not simply the consequence of a saturation effect like, for example, a lack of nitrate within the reacto-diffusive penetration depth of N_2O_5 in the condensed phase, because reference experiments using $NaHSO_4$ and Na_2SO_4 aerosols behave as expected. Wahner and coworkers also demonstrated the need for the existence of an aqueous solution for the mechanism to proceed as displayed, because γ of N_2O_5 for a $NaHSO_4$ aerosol at 2% relative humidity displays a value that is smaller by 2 orders of magnitude relative to the value for the same aerosol at 60% rh. This shows that there is no heterogeneous interaction, neither hydrolysis (reaction 24) nor halogen exchange (reaction 26), in the absence of electrolyte. In contrast, the data of Hanson[202] on the uptake of N_2O_5 on the ternary system $HNO_3/H_2SO_4/H_2O$, presented in the form of films and aerosols, did not show a significant nitrate effect at stratospheric temperatures.

The surprising aspect of the nitronium mechanism expressed in reactions 32−35 lies in the high nucleophilicity of chloride compared to that of water. This is the reason for the small amount of HNO_3 compared to $ClNO_2$ that is formed, despite the large excess of H_2O. The short lifetime of NO_2^+ in water leads to the constraint $k_{34}[H_2O] \approx 10^9$ s^{-1}. To explain the formation of significant quantities of $ClNO_2$ in a concentrated aqueous solution characteristic of aerosols, a rate constant ratio k_{32}/k_{34} of 836 ± 32 has been deduced from the work of Zetzsch and co-workers.[165] This ratio has to be compared with a statement by Johnson and Margerum,[203] who claimed that the nucleophilicity of Cl^- is higher by a factor of 10^5 compared to that of H_2O, using the rate constants k_{33} and k_{34} as a gauge. This discrepancy of a factor of 100 remains unexplained. In addition, Johnson and Margerum also claimed that the reaction of NO_2^+ with OH^- is more than 10 orders of magnitude faster than that with water. From the work of Zetzsch and co-workers,[165] the uptake of N_2O_5 on strongly alkaline 5 M NaCl solution at pH = 12 resulted in the conclusion that the reactivity of NO_2^+ is not significantly larger toward OH^- than toward Cl^-, both of which have rates close to the diffusion limit, but is larger toward water (reaction 34). Even with an increase of $[OH^-]$ by 7 orders of magnitude, significant amounts of $ClNO_2$ have been observed. These conclusions suggest that the data of Johnson and Margerum must be used with caution.

It is important to realize that, at the moment, the nitronium mechanism is only a semiquantitative explanation of experimental results of both N_2O_5 and $ClNO_2$ uptake on deliquescent salt aerosol particles, because too many parameters are not known with sufficient accuracy in order to make it a fully quantitative theory with predictive value. Moreover, there are indications that the mechanism may be more complex than described above. One of the difficulties with it is the fact that the theory is unable to explain the significant increase of γ for N_2O_5 interacting with NH_4HSO_4 and $(NH_4)_2SO_4$ aerosol with increasing relative humidity,[169] because the rate-limiting step (reaction 32) should be independent of H_2O concentration, akin to an S_N1 reaction. However, the reverse of reaction 32 may change and become faster with increasing concentration of the ions NO_2^+ and NO_3^- in the case of a limited supply of H_2O. In this case, the net reaction A10a will slow significantly. However, this quantitative argument will have to be checked against reliable data.

The recent experimental data[169] are more credible than the older ones, because they smoothly connect to the results pertaining to N_2O_5 uptake on water droplets, reported by van Doren et al.[194] A second difficulty arises when the reverse trend of γ with relative humidity is considered, namely for the

uptake of N_2O_5 on H_2SO_4 solutions or aqueous aerosols, for which γ decreases from 0.05 to 0.03 on going from 0 to 100% relative humidity. Some data at low rh even extend to γ values of 0.11. For this case, the empirical model proposed by Robinson et al.[198] successfully explains the trend in terms of two competing hydrolysis reactions according to reactions 36, which is identical to reaction 37 in aqueous solution, and reaction 38:

$$N_2O_5 + H_3O^+ \rightarrow 2HNO_3 + H^+ \quad (36)$$

$$N_2O_5 + H^+ \rightarrow HNO_3 + NO_2^+ \quad (37)$$

$$N_2O_5 + H_2O \rightarrow 2HNO_3 \quad (38)$$

According to Robinson et al.,[198] reaction 36 or 37 is important at high acidity, thus low rh, whereas reaction 38 would take over at high rh. In this respect, it is important to note that the N_2O_5 uptake experiments on NaCl aerosols reveal that reaction 38 may still be important, despite the incidence of reaction 32 as the rate-limiting step in the nitronium mechanism.[165]

Hoffman et al.[190] present data on the heterogeneous reaction of N_2O_5 on solid NaCl and synthetic sea salt powders and note increases both in γ by roughly an order of magnitude and in the branching ratio BR^{ClNO_2} for the formation of $ClNO_2$ (reaction 26) vs HCl (reaction 24 followed by 28). In contrast to the explanation proposed by the authors, which is based on the increasing ability of the substrate surface to "reorganize" with increasing SAW, an alternative point of view, albeit somewhat complementary, may be expressed as follows. SAW creates "pools", or regions of saturated alkali halide salt solutions, that enable reaction 26. The hydrolysis reaction 24, followed by the halogen-exchange reaction 28, occurs on sites other than the saturated halide solutions, perhaps on OH-terminated sites that preserve the integrity of the crystalline alkali halide salt. In this way, the SAW regions that form to a larger extent on synthetic sea salt compared to solid NaCl would be responsible for the increased rate of reaction 26, because of the larger physical extent of these SAW regions. Briefly, more SAW leads to a higher coverage of liquid-saturated salt pools. This increase would be balanced by a concomitant decrease of the extent of OH coverage responsible for the hydrolysis reaction 24. This increase, therefore, leads to larger values of both γ and BR^{ClNO_2}. However, this two-site model is at variance with results where γ scales with the Cl^- concentration and BR^{ClNO_2} decreases with increasing rh, corresponding to decreasing Cl^- concentration.[191,192] On the other hand, another series of experiments, performed in the same smog chamber, revealed a constant value for BR^{ClNO_2}, independent of rh in the range 77−94% rh.[165] This two-site reactivity model may also be attractive from another pont of view, in that it may explain the approximate independence of the rate of N_2O_5 hydrolysis on the acidity of H_2SO_4 aerosols.[169,198]

3.2. HNO_3

3.2.1. Reactions

Nitric acid, HNO_3, is part of reactive nitrogen, NO_y, and is a fairly inactive form of oxidized nitrogen whose primary fate in the atmosphere is wet deposition (rain-out) and photolysis. Nitric acid has come into focus in recent years as a constituent of polar stratospheric clouds (PSCs), in connection with polar ozone depletion.[1] The two main reactions that are responsible for its formation in the midlatitude atmosphere are reactions 24 and 25.

$$N_2O_5 + H_2O \rightarrow 2HNO_3 \quad (24)$$

$$OH + NO_2 \rightarrow HNO_3 \quad (25)$$

Reaction 24 is a heterogeneous reaction that takes place on H_2O-containing inorganic aerosols of both continental and marine origin, whereas reaction 25 occurs in the homogeneous gas phase. Model calculations indicate that, in wintertime, over the industrialized areas at the middle and northern latitudes, the heterogeneous conversion of N_2O_5 on aqueous aerosols may be responsible for up to 50% of diurnal HNO_3 formation.[11] This conversion has an important impact on the concentration of ozone and of other oxidants on a global scale according to these models. The heterogeneously formed HNO_3 is subject to partitioning between the gas phase and the condensed phase. Global simulations of atmospheric chemistry indicate that, when globally and seasonally averaged, this heterogeneous process accounts for approximately 50% of the total nitrogen oxide removal from the troposphere.[11,12] Concerning HNO_3, we therefore have a strong implication of heterogeneous processes, both with respect to its formation and with respect to its fate in the atmosphere. HNO_3 may contribute to the acidification of marine aerosol and thereby cause chloride deficits in sea salt particles in the marine boundary layer of polluted coastal regions. This halide deficit has been studied by several research groups over the years and is defined with respect to the expected composition of sea salt obtained by evaporative processes that should reflect the composition of seawater.[62,67,68,91−99]

The reaction of HNO_3 with solid NaCl has been the subject of many studies. In the early 1960s, Cadle and Robbins[41] reported an immeasurably fast reaction between NO_2 and NaCl in the presence of water vapor in an aerosol reactor. They attributed the observed HCl formation to the reaction of HNO_3, formed by the disproportionation of $2NO_2$ to HONO and HNO_3, with salt. Since 1955, atmospheric aerosol measurements have revealed a deficit in chloride content, as indicated above, which has been explained by the reaction of HNO_3 with NaCl. On the basis of a simple thermodynamic model, Brimblecombe and Clegg concluded that HCl should be displaced by HNO_3 in these aerosols.[204,205] Mamane and co-workers focused on the transformation of salt grains by exposure to HNO_3 and other nitrogen oxides, finding that the reaction product nitrate is located on the surface of the solid.[206−208] Livingston and Finlayson-

Table 2. HNO_3 + NaCl (NaBr, KBr) → HCl (HBr) + $NaNO_3$ (KNO_3)

symbol	uptake coefficient	substrate	temp/K	reference
γ_0	$(2.8 \pm 0.3) \times 10^{-2}$	NaCl, KBr salt powder, grains	300	Fenter, Caloz, and Rossi,1994[211]
γ_0	$(4.0 \pm 2.0) \times 10^{-4}$	(100) face of single-crystal NaCl	300	Laux, Hemminger, and Finlayson-Pitts, 1994[218]
γ_{ss}	$(1.3 \pm 0.4) \times 10^{-2}$	NaCl grains	296	Leu et al., 1995[213]
	$(8 \pm 3) \times 10^{-3}$	NaCl grains	223	
	$(2.4 \pm 0.6) \times 10^{-3}$	seven NaCl single crystals	296	
γ_0	$(2.8 \pm 0.5) \times 10^{-2}$	NaCl powder, 35−160 μm	298	Fenter, Caloz, and Rossi, 1996[188]
	$(2.2 \pm 1.0) \times 10^{-2}$	spray-coated thin NaCl film		
	$(1.3 \pm 0.6) \times 10^{-2}$	NaCl single crystal, wet-etched		
	$(5.5 \pm 2.0) \times 10^{-2}$	NaCl single crystal, coarse polish		
γ_0	$(1.4 \pm 0.6) \times 10^{-2}$	NaCl grains and powder	300	Beichert and Finlayson-Pitts, 1996[167]
γ_0	$(3.5-80) \times 10^{-2}$	synthetic sea salt	298	De Haan and Finlayson-Pitts, 1997[121]
γ_{ss}	$(1.5-35) \times 10^{-3}$	synthetic sea salt		
γ_0, γ_{ss}	0.48 ± 0.40, 0.37 ± 0.27	polycrystalline $MgCl_2 \cdot 6H_2O$		
γ_{ss}	$(2.8 \pm 0.5) \times 10^{-3}$	NaBr grains	296	Leu, Timonen, and Keyser, 1997[214]
γ_{ss}	$8 \times 10^{-5}-1.5 \times 10^{-3}$	NaCl grains, thin films	298 ± 3	Davies and Cox, 1998[212]
γ_{ss}	>0.2	NaCl aerosol, pH = 0.3, 7.2	300	Abbatt and Waschewsky, 1998[225]
γ_0	$(1.3 \pm 0.6) \times 10^{-3}$	NaCl powder, single crystal	300	Ghosal and Hemminger, 1999[219]
γ_0	$(4 \pm 1) \times 10^{-2}$	polycrystalline NaCl film	300	Koch, van den Bergh, and Rossi, 1999[199]
	$(2 \pm 1) \times 10^{-2}$	polycrystalline KBr film	300	
γ_{ss}	$(5.9 \pm 0.8) \times 10^{-2}$	recrystallized NaCl	300	Zangmeister and Pemberton, 2001[221]
γ_{ss}	$<(5 \pm 3) \times 10^{-3}$	NaCl single crystal	300	Ghosal and Hemminger, 2002[220]
γ	0.50 ± 0.20	NaCl aerosol, 70 nm diameter	300	Guimbaud et al., 2002[226]
γ_{ss}	$(6.5 \pm 4.2) \times 10^{-4}$	ground and sieved NaCl grains	298	Hoffman et al., 2003[217]
	$(4.0 \pm 1.5) \times 10^{-4}$	sieved NaCl grains		
γ_0	$(1.2 \pm 0.7) \times 10^{-3}$	NaCl grains		

Pitts[177] exposed the salt samples to N_2O_5 with an important HNO_3 impurity and observed HCl that they attributed to reaction 28.

Although reaction 28 is of interest primarily for the tropospheric boundary layer, stratospheric modelers have also expressed interest in it because of the large amounts of NaCl and other salts that can be injected into the middle atmosphere in the aftermath of certain volcanic eruptions.[31,32] Salt particles were collected from the El Chichon volcanic clouds in the lower stratosphere in the spring of 1982.[209] Their concentration attained values up to 26 particles cm^{-3}, of typically 1−2 μm in size. Simultaneous measurement of the HCl column by FTIR absorption showed approximately a 40% enhancement over the background observed prior to the eruption.[210]

In what follows, we will present laboratory results on the heterogeneous reaction of HNO_3 with salts in pertinent detail. A summary of the experimental results is displayed in Table 2. Fenter et al.[211] were the first to systematically perform uptake experiments of HNO_3 on solid alkali salt powders (NaCl, NaBr, KCl, KBr) and $NaNO_3$ in the size range from 5 to 100 μm in a two-chamber low-pressure reactor (Knudsen cell), with molecular beam sampling and phase-sensitive detection using an electron-impact quadrupole mass spectrometer. Both steady-state and transient dosing experiments using a pulsed valve, the latter corresponding to $\sim 10^{14}$ molecules/pulse and representing a few percent of a monolayer in relation to the geometric surface of the sample, were performed and showed identical results. The initial uptake coefficient γ_0 was measured in the low dose limit and was found to depend only on the external (geometric) surface, independent of the type of salt, whereas the rate of formation of HCl and HBr and the onset of partial saturation of HNO_3 uptake were found to be sensitive to several experimental parameters, such as the nature, mass, and grain size of the salt. The yields of HCl and HBr were 115 ± 25 and 80 ± 25%, respectively. It has to be stressed that the kinetic results refer to the initial uptake coefficient γ_0, whereas later work, performed by Davies and Cox,[212] report significantly smaller values for γ obtained at steady state. The estimated steady-state values of γ are a factor of 5−15 smaller than γ_0. However, this estimate represents an upper limit, because in most experiments steady state was not established.

Several experimental facts point to the importance of SAW in these experiments, despite the high-vacuum conditions of approximately 10^{-4} Torr of background pressure: (a) the uptake kinetics (Table 2) are identical regardless of the type of sample (chloride, bromide, nitrate), (b) the γ value for HCl uptake is $\sim 3 \times 10^{-2}$ on the salt samples including $NaNO_3$, and (c) there is a significant induction time for HCl and HBr appearance, during which the hydrohalic acids HX may be displaced by HNO_3. A simple chemical kinetic model could explain the main features of HNO_3 uptake on salts, in which the rate-limiting step was the adsorption of HNO_3 into a precursor state on the salt substrate.[211] The authors concluded that the observed HNO_3 adsorption (rate-limiting) occurred on the geometric surface, whereas formation of HX could well take place in the bulk powder resulting from the slow diffusion of HNO_3 on salt. Experimentally, no uptake of H_2O vapor on the salt and no synergistic effect of the HNO_3 uptake was observed in the presence of water vapor in the 10^{-3} mbar range, presumably because the sample was already saturated in H_2O. Later, the same authors[188] revisited the reaction kinetics of reaction 28, using several different salt sample presentations, such as single crystals, sprayed-on thin salt films, monodisperse salt grains, and sieved salt powders, and they reached the same conclusions. The uptake coefficient is first order in HNO_3 and independent of the sample presentation, within experimental error, as γ did not show any dependence on sample mass. The pore dif-

fusion model is commonly tested by studying the uptake coefficient as a function of the number of grain or powder layers down to one residual layer.[149,152,187] Therefore, the γ values have not been corrected by pore diffusion theory, in contrast to results obtained for N_2O_5. It was demonstrated in this study that the rate constant for heterogeneous interaction was indeed constant over the range $6 \times 10^{-7}-1.3 \times 10^{-4}$ Torr for all chloride and bromide salts investigated.[213] The value of γ averaged over the different types of samples (NaCl, KBr) corresponds to $(2.0 \pm 1.0) \times 10^{-2}$. However, the value of γ on a single crystal NaCl or KBr surface, previously wet-etched by rinsing with water, is significantly smaller than the average, namely $(1.3 \pm 0.6) \times 10^{-2}$ and $(0.5 \pm 0.3) \times 10^{-2}$ on NaCl and KBr, respectively. This trend had also been observed for the interaction of N_2O_5 with salt[188] and had been attributed to the preferred wet-etching and removal of reactive sites for N_2O_5 adsorption and reaction, leaving behind a residual crystal with a lower number of reactive defect sites, as the defect sites are preferentially dissolved. Therefore, owing to the "sticky" nature of HNO_3, Fenter et al.[188,211] did not apply the pore diffusion model to correct their γ values.

Leu et al.[213] performed uptake experiments using a fast-flow reactor coupled to a quadrupole mass spectrometer with either chemical or electron-impact ionization using partial pressures of HNO_3 in the range $6 \times 10^{-8}-2 \times 10^{-6}$ Torr. The NaCl substrate consisted of grains of average size 0.44 mm, and HCl was observed as the sole product of reaction, essentially in 100% yield. The γ values listed in Table 2 are corrected by a factor of approximately 5 using the pore diffusion model and decrease by less than a factor of 2 over the HNO_3 pressure that is considered insignificant. The γ values were found to be independent of the NaCl pretreatment (baked to 473 K, unbaked, or with added water vapor), in agreement with literature results.[188,211] However, the authors never justified the application of the pore diffusion model,[149,152,187] as the mass dependence of the observed γ value had not been demonstrated in their work.[213] One notes that the measured uptake coefficients are larger by a factor of approximately 2 in comparison with the results obtained by Fenter et al.[188,211] before correction by the pore diffusion model. The yield of HCl for uptake experiments of HNO_3 on NaCl at 223 K is greatly reduced compared to the behavior at ambient temperature, and a significant part of HNO_3 desorbs after reaction, which leads to the hypothesis that the uptake is dominated by physical uptake under those conditions. Physical adsorption of HNO_3 on $NaNO_3$ has been shown in reference experiments at 223 K, the extent of which was very similar to the reactive situation on NaCl as far as HNO_3 adsorption was concerned. The pertinent observation made by Leu et al.,[213] that γ decreases to 4×10^{-4} at HNO_3 pressures in the range $(1-3) \times 10^{-5}$ Torr, is at variance with results obtained by Fenter et al.,[188,211] whose partial pressure range overlapped with the one used by Leu et al. These workers did not see a significant decrease of γ over their range of $6 \times 10^{-7}-4 \times 10^{-4}$ Torr. It is not clear if the low γ value reported by Leu et al.[213] corresponds to the observed or to the corrected one, although one may suspect the latter to be the case.

In a related study, Leu et al. have investigated the heterogeneous interaction of HNO_3 with NaBr grains using the same technique,[214] including the reverse reaction HBr + $NaNO_3$. The measured γ values are identical to the ones obtained by Fenter et al.[188,211] and are independent of the salt pretreatment, such as baking in a vacuum and adding H_2O vapor. The HBr yield is 34%, in agreement with previous values.[188] The γ values displayed in Table 2 have been corrected by scaling down the measured uptake coefficients by a factor of 10 by applying the pore diffusion model, again without giving any justification for its application in the present case, such as by investigating the mass dependence of the measured uptake kinetics. Leu et al.[214] attribute the difference between their results and those of Fenter et al.[188,211] to surface deactivation of the salt substrate in the latter work, even though the HNO_3 partial pressure was as low as 6×10^{-7} Torr, identical to the one displayed by Leu et al.[214] It is therefore hard to see why a surface saturation effect in Fenter et al.'s work [188] should give rise to a larger value of γ compared to that obtained by Leu et al.,[214] as a smaller value of γ is usually expected on account of surface saturation. The reverse of the title reaction (reaction 39) has been studied under the same conditions and results in HNO_3 yields of 10−30%, which points, like in the case of the forward reaction, to a mechanism including physical adsorption and chemical reaction.

$$HBr + NaNO_3 \rightarrow HNO_3 + NaBr \qquad (39)$$

The average measured γ value is $(6.6 \pm 0.9) \times 10^{-2}$, whereas the corrected value is $(1.2 \pm 0.2) \times 10^{-2}$, a factor of 5 smaller, and is again independent of the salt pretreatment (dry vs unbaked salts).

Beichert and Finlayson-Pitts[167] reinvestigated the uptake of HNO_3 on solid NaCl in a halocarbon wax-coated Knudsen flow reactor at ambient temperature using modulated molecular beam electron impact MS and HNO_3 concentrations in the range $(3.0-35.1) \times 10^{12}$ molecules cm^{-3}. The salt substrates were sieved grains and finely ground NaCl powder of average dimension 0.5 mm and 4 μm, respectively. The HNO_3 uptake coefficient γ was calculated using the geometrical surface area of the sample holder (Table 2), and no dependence of γ on [HNO_3] was observed, thus confirming a first-order rate law. The product yield of HCl was 100% within experimental uncertainty. The HNO_3 rate of uptake is characterized by a fast initial process exceeding γ_{ss} given in Table 2, especially on the fine powder, followed by a slower steady-state uptake. Pretreatment of the salt by heating under vacuum to 353 K affects only the slower steady-state uptake process and leads to the differentiation of two types of SAW, namely weakly bound and strongly bound adsorbed water. The former evaporates upon heating to 353 K, whereas the latter persists and supports the slow uptake process quantified by γ_{ss}, which is independent of the salt pretreatment.

Further support for SAW comes from isotopic substitution experiments using D_2O and DNO_3 for pretreatment and uptake, respectively, which leads to a mixture of DCl and HCl. Despite extensive pumping and heating during pretreatment, some SAW apparently remains on the salt substrate because it has not been possible to completely replace HCl by DCl. The steady-state uptake of nitric acid is not saturable, which is an observation that is in agreement with literature results.[188,211,213,214] This may be explained by the fact that the product $NaNO_3$ does not form a coherent thin film on the salt sample. Instead, it crystallizes in well-defined regions on the substrate. Neither HNO_3 uptake nor HCl formation was observed on the (100) and (111) faces of NaCl single crystals, which is in agreement with the SAW hypothesis because less SAW is expected on the single-crystal faces. All results are consistent with the fact that SAW is mainly located on structural defect sites of the crystalline salt substrate. The SAW model will be presented in more detail below. It is useful to point out already at this point the equivalence of the semiquantitative conclusions of the SAW model proposed by Finlayson-Pitts and co-workers[167] with the chemical kinetic model proposed by Fenter et al.[211] The quantitative framework for the former is given by the thermodynamic models of Brimblecombe and Clegg,[205,215,216] whereas the latter makes use of ancillary kinetic data obtained at HNO_3 partial pressures that are lower by 1−2 orders of magnitude. These two points of view are complementary in that the SAW model determines the composition of the condensed phase at steady state, whereas the kinetic model obtains the time frame over which these changes occur.

In related experiments, De Haan and Finlayson-Pitts[121] examined the uptake of HNO_3 on solid synthetic sea salt and $MgCl_2 \cdot 6H_2O$ in a halocarbon wax-coated Knudsen flow reactor at ambient temperature using modulated molecular beam electron impact MS. Both as-received (coarse, 300 μm average size) ground (0.3 μm average size) samples of synthetic sea salt (SSS) were pumped for a minimum of 2 h while the Knudsen reactor was heated to 75−80 °C. However, the uptake measurements were performed at ambient temperature and led to a HCl yield of 100% within experimental uncertainty. The initial value of the uptake coefficient, γ_0, decreased to a steady-state value γ_{ss} smaller by approximately a factor of 2 on the time scale of 1 h at typical HNO_3 concentrations of 5×10^{12} molecules cm^{-3}. These concentrations are higher by 1−2 orders of magnitude compared to similar studies.[188,211,213] The absolute magnitude of both values strongly depended on the pretreatment conditions as far as the amount of physisorbed water was concerned, and it was controlled by pumping and heating in situ prior to HNO_3 uptake. Table 2 displays the range of both initial and steady-state uptake coefficients as a function of pretreatment of SSS. All reported uptake coefficients have been found to be independent of reactor geometry (two apertures were examined), geometric surface, sample mass, and average size of salt grains. Uptake of HNO_3 on $MgCl_2 \cdot 6H_2O$ (700 μm average size) was also studied, resulting in slightly higher values for both γ_0 and γ_{ss}. The authors make a case that this latter compound should be taken as a model compound to mimic the physicochemical behavior of solid marine aerosol rather than its main component, NaCl. The presence of surface-adsorbed water (SAW) on those salt substrates was highlighted with uptake experiments using DNO_3 and D_2O, whose uptake on SSS resulted in desorption of an excess HCl and H_2O/HDO, respectively, despite extensive system passivation with deuterated reagents, leading to replacement of H against D. This result is as expected and underlines the quantity of SAW that is available for isotopic exchange of the deuterated probe molecules. Specifically, the heterogeneous D_2O measurements that lead to measurable uptake of D_2O and desorption of HDO and H_2O only reflect fast isotopic exchange on the salt sample but no mass accommodation of water vapor at these low partial pressures. Mass balance experiments of H_2O uptake resulted in no net H_2O uptake, in agreement with previous experiments.[167,188] In particular, the estimate of the volume of 50 nL of SAW on 1.3 g of SSS, based on the isotopic exchange experiments with D_2O, may well result from a measurement artifact, as net uptake of H_2O could not be observed after salt pretreatment. It is not clear how an experiment addressing the replacement of H_2O with D_2O and HDO may lead to absolute amounts on the basis of the few reported isotopic exchange experiments. In view of the independence of γ on the number of grain layers and grain size, no correction to diffusion of HNO_3 into the external voids of the samples was performed.

In an attempt to further decrease the uncertainty of the measured value of the uptake coefficient of HNO_3 on NaCl, Hoffman et al.[217] reinvestigated the uptake kinetics of HNO_3 on NaCl sample masses corresponding to sublayer quantities using a Knudsen flow reactor coupled to a phase-sensitive MS detector, similar to the one used before.[121,167] Typical HNO_3 concentrations were in the range 2×10^{11}−9×10^{13} molecules cm^{-3}. Solid sieved NaCl particles in the average size range 164−428 μm, as well as mechanically ground NaCl samples of 10 μm average size, were used for comparison, the latter of which resulted in $\gamma_{ss} = (2.4 \pm 1.3) \times 10^{-2}$ for multiple NaCl layers, in agreement with previous measurements by Finlayson-Pitts and co-workers.[167] On the basis of a 100% yield of HCl per HNO_3 taken up, which is well documented in the literature,[167,188,199,213] the uptake coefficient was expressed in terms of HCl generated rather than HNO_3 lost because the results showed less scatter, especially for sublayer quantities.

Experiments on sublayer quantities have been performed for essentially two reasons: on one hand diffusion of HNO_3 into deeper layers is precluded, and on the other hand no liquid H_2O would remain adsorbed within the capillaries formed between two neighboring salt particles. In this way it was hoped to circumvent the application of the pore diffusion model in order to arrive at the corrected value of γ_{ss} without having to use uncertain or unknown structural parameters characterizing the salt sample.

However, as has been pointed out above in relation with the heterogeneous reactions of N_2O_5 on NaCl, one replaces the pore diffusion model for a multilayer sample by an interaction model for sublayer quantities whose validation is more uncertain than the original pore diffusion theory.

Table 2 displays the average γ_{ss} values for the sublayer experiments whose results are approximately a factor of 50 lower than previous results using similar experimental techniques.[121,167,188,211,213] The γ_0 value obtained by extrapolation of the uptake to the beginning is a factor of 3 larger than γ_{ss} because it accounts for the absence of the solid product $NaNO_3$ that is present on the surface to some extent during steady-state uptake, and therefore precludes the interaction of HNO_3 with some of the active sites on the NaCl surface. These results are in good agreement with results obtained on NaCl single-crystal substrates[218−220] and on solid polycrystalline NaCl films by Davies and Cox[212] in terms of quantitative agreement of the γ values. Interestingly, these new results raise questions that seemed to have been settled before when we compare the sublayer results[217] with the ones obtained previously.[121,167,188,199,211,213,221] It seems unlikely to obtain an increase in γ by a factor of 10−50 by allowing HNO_3 to diffuse into deeper layers of NaCl, especially when the NaCl sample is presented as coarse grains of 0.5 mm average size. Moreover, pulsed-dosing experiments[188] give results identical to those obtained with continuous-flow experiments, the former of which unambiguously preclude the diffusion of HNO_3 into deeper layers of the NaCl sample, owing to the short time scale of the interaction given by the gas-phase residence time of typically 1 s. In addition, the equivalence between kinetic results obtained by observing the loss of HNO_3 and the formation of HCl may not be equivalent under all experimental conditions, as Fenter et al. have observed a substantial induction time for HCl formation.[188] The work by Hoffman et al.[217] is at variance with literature results[188,211,213] regarding the properties of "wet" and "dry" multilayer NaCl samples. Even after evacuation of the sample for 1 h or more by pumping off SAW, the γ value stays high, whereas Hoffman et al. reportedly obtained a dry sample that is associated with a γ value that is smaller by an order of magnitude after a pumping time of 1 h. However, it is possible that the removal of SAW is more efficient for a sample whose mass is small, as is the current case, because multiple adsorption/desorption cycles are less probable.

Davies and Cox[212] studied the uptake rate of HNO_3 on solid NaCl grains of 500 μm average size as well as on thin salt films generated by evaporating aqueous methanolic NaCl solutions in a coated-wall laminar flow tube coupled to a differentially pumped mass spectrometer. The reported values of γ have been measured under steady-state conditions and have been found to follow a rate law that is first order in HNO_3. They depended both on the initial HNO_3 concentration, which varied between 6×10^{11} and 7×10^{13} molecules cm^{-3}, and on the H_2O partial pressure, which varied in the range 0.0002−10 mbar. HCl was observed as the sole reaction product in 100% yield. For NaCl grains, the uptake coefficient γ_{ss} decreased with $[HNO_3]$ according to a power law, namely γ_{ss} being proportional to $[HNO_3]^{-(0.5\pm0.1)}$. The value of γ_{ss} increased by approximately an order of magnitude from 4×10^{-4} to 5×10^{-3} with a change in $[H_2O]$ in the range stated above and followed quite closely the H_2O adsorption isotherm given by Barraclough and Hall.[222] The indications from the water adsorption isotherms on NaCl point quite clearly to quantities of adsorbed water up to and exceeding one formal monolayer at the upper limit of the water partial pressure of 10 mbar. This result has also been recently confirmed by Ewing and co-workers.[143] The striking similarity of the H_2O dependence of γ_{ss} to the water isotherm suggests that the rate of reactive uptake depends on the volume of adsorbed water, which is one of the essential points proposed by the SAW concept. In additional experiments, Davies and Cox exposed HCl to a NaCl sample that had been poisoned by HNO_3 previously, and they observed desorption of HNO_3, as did Fenter et al.[211] This result is proof that reaction 28 is reversible, which is an important conclusion. The dried thin films of solid NaCl were prone to surface saturation, primarily owing to a sample mass lower by a factor of 100 compared to that of the salt grains. Therefore, no steady-state rate of uptake could be measured as the rate tended to zero on the time scale of 10 min at the fairly large HNO_3 concentrations used. Nevertheless, these experiments on thin solid salt films resulted in initial uptake coefficients identical to the γ_{ss} values presented above for solid salt grains. The uptake coefficients on dried salt films decreased by a factor of approximately 4 when the aqueous solution was replaced by pure methanol for the spray application. This again highlights the important role of SAW for the reactivity of the solid salts. The most noticeable feature of this work is that the γ_{ss} values are much lower, both for solid polycrystalline NaCl and for thin sprayed NaCl films, compared to other values obtained in the laboratory,[167,188,211,213] except perhaps for the most recent results reported by Hoffman et al.[217]

The other feature reported by Davies and Cox[212] is the decrease of γ_{ss} with increasing HNO_3 concentration. It may be noted that both features show up in steady-state experiments, in contrast to experiments addressing the initial phases of HNO_3 uptake, for which these effects are not expected and, in fact, are not observed. Saturation phenomena that might give rise to complex rate laws are absent in the very first phases of HNO_3 adsorption on salts, especially at low partial pressures. Davies and Cox have therefore applied a two-site Langmuir adsorption model in order to parametrize γ_{ss} as a function of relative humidity and $[HNO_3]$. One site is the adsorption site for initial HNO_3 adsorption, the second site is the supply site for chloride (Cl^-) undergoing the ion-exchange reaction and ultimately resulting in HCl. The model successfully fits the $[H_2O]$ and $[HNO_3]$ dependence of γ_{ss} by applying the well-known rate law for Langmuir adsorption for nitric acid and a BET multilayer adsorption model for the volume

of water adsorbed as a function of relative humidity. In the range of relative humidity used by Davies and Cox, spanning 0−35% rh, the number of active sites providing chloride ions increases from 2.5 to 15% of the available surface ion-pair sites of 6.4×10^{14} cm^{-2}, which is a physically reasonable number. Water adsorption isotherms on solid NaCl correspond to the presence of the adsorption equivalent of between one and two monolayers of H_2O, depending on rh, in essential agreement with Ewing and co-workers.[143]

Another experimental approach was taken by Laux et al.,[218] who investigated the title reaction from the point of view of the buildup of the solid reaction product $NaNO_3$ resulting from HNO_3 exposure to the (100) face of single-crystal NaCl. The reaction was monitored by recording the X-ray photoelectron spectroscopic signals (XPS) for O, N, and Cl atoms as a function of time. These were calibrated in terms of the surface Cl^- and NO_3^- concentration as a function of exposure of a single-crystal NaCl sample to dry HNO_3 that was dispensed from a capillary mounted 1 mm in front of the dry salt sample under ultra-high-vacuum (UHV) conditions. The average sticking coefficient was obtained by dividing the absolute concentration of nitrate species on the surface at saturation by the collision frequency of HNO_3 on the sample integrated over time. The assumption was made that at saturation (that is, when the XPS signal due to N and O stopped changing with exposure time), the sample had acquired one monolayer of nitrate at the expense of the chloride. At saturation the Cl signal also reached a constant value, having decreased by 50% compared to the original clean NaCl sample. However, the Cl XPS signal could not be quantified because the penetration depth of the X-rays could not be unambiguously determined. This precluded the determination of the sample volume and the corresponding NaCl consumption that was probed in this experiment.

In a subsequent reevaluation and extension of their XPS data at UHV conditions, Ghosal and Hemminger[219,220] nicely demonstrated that the quantity of surface oxygen (O) that was interpreted as either being adsorbed H_2O or surface hydroxyl groups was undetectable on the (100) face of single-crystal NaCl. However, increasing amounts of SAW could be detected on NaCl particulates of 500 and 1−10 μm average size. On this account, it is not surprising that the heterogeneous reaction of HNO_3 on NaCl single crystals comes to complete saturation under UHV conditions once one to two monolayers of the solid product $NaNO_3$ have been generated by reaction. In fact, Hemminger and co-workers have interpreted the measured oxygen coverage on single-crystal NaCl as a function of HNO_3 dose in terms of a single-site Langmuir model resulting in the initial (that is, zero-coverage) uptake coefficient listed in Table 2. They showed that the two-site Langmuir adsorption model used by Davies and Cox[212] in the interpretation of results obtained in their laminar flow tube could be replaced by a single-site Langmuir model, presumably because of the extensive mobility of H^+ in the presence of SAW. The ability to saturate further adsorption of HNO_3 on a poisoned single-crystal NaCl sample is therefore attributed to the sole presence of solid nitrate at the interface. Apparently, a single-site Langmuir adsorption model is able to explain data obtained under UHV conditions that do not show the presence of SAW, as well as laminar flow tube data obtained at H_2O background pressures of 2×10^{-4} mbar. The successful reaction mechanism involves two reactions, as follows:

$$HNO_3(g) + NaCl(site) \rightleftarrows NO_3^-(ads) + HCl(g) \quad (40)$$

$$NO_3^-(ads) + H_2O(ads) \rightleftarrows NaCl(site) + NaNO_3(s) \quad (41)$$

Reaction 40 describes the occupation of a reactive site on the NaCl substrate related to the formation of the reaction products, whereas reaction 41 describes the return of the occupied sites to the pool of available reactive surface sites ready to adsorb additional gas-phase nitric acid. Reaction 41 describes the crystallization of the surface nitrate that is enabled by the ionic mobility of nitrate, depending on the quantity of SAW (= H_2O(ads)). Hemminger and co-workers have used TEM and XPS to show that the initial product of the reaction of dry HNO_3 with NaCl is a uniform, ultrathin passivating layer of $NaNO_3$ which saturates the reaction after buildup of one to two monolayers. They also showed conclusively that the presence of SAW leads to recrystallization of surface nitrate to microcrystallites on particular locations of the crystalline substrate.[218,223,224] The same conclusion has been reached by Vogt and Finlayson Pitts,[140] who used DRIFTS spectra as a function of time of exposure to polycrystalline NaCl samples. They showed that surface nitrate recrystallized in situ under the used reaction conditions to form microcrystallites that were localized over only a fraction of the available surface of the NaCl sample, thereby freeing up reactive surface sites for further reaction.

The single-site Langmuir adsorption model using the reaction mechanism described by reaction 40 and 41 is able to explain the data obtained at high relative humidites, and thus at large quantities of SAW, corresponding to the prevailing conditions of many low-pressure flow reactor experiments. In the limit of large quantities of SAW, the uptake coefficient becomes independent of the partial pressure of HNO_3. In addition, the large rate of reaction 41 prevents the complete saturation of the heterogeneous reaction, in agreement with experimental results. The overwhelming majority of experiments on NaCl particulates show a limited partial saturation of γ, turning over to a steady state which is controlled by the rate of reaction 41 because there are always sufficient reactive sites available. The work of Laux et al.[218,223,224] has therefore shown three facts: first, that the dissociative adsorption of HNO_3 on solid NaCl follows a one-site Langmuir adsorption model; second, that the initial nitrate formed on the surface blocks, in part, the subsequent heterogeneous reaction; and third, that water enhances the mobility of the nitrate, thereby opening up blocked sites for further reaction. The quantity of SAW is therefore critical to the understanding of the quantitative aspect of NaCl reactivity.

The study by Zangmeister and Pemberton[221] is one of the few studies that have focused on the surface chemistry of powdered NaCl reacting with HNO_3, where the condensed phase was monitored in order to measure the progress of the heterogeneous reaction. Raman spectroscopy was used to monitor the interfacial changes of recrystallized NaCl particles of approximately 7 μm size, in that $NaNO_3$ growth was followed as a function of HNO_3 exposure. In the absence of water vapor, the intensities of the $NaNO_3$ bands increase with HNO_3 exposure, to result in an amorphous capping layer of $NaNO_3$ which prevents subsequent HNO_3 from reacting with the underlying NaCl. The spectral intensity ratio of the in-plane ONO angle deformation and the symmetric N−O stretch in NO_3^- changes with HNO_3 exposure, although the spectral position of the nitrate bands remains unchanged. These spectral changes lead to the unambiguous identification of this amorphous layer, which is distinctly different from bulk crystalline $NaNO_3$ used as a reference. A rough estimate of the flow rate of HNO_3 across the slow-flow reactor resulted in a semiquantitative estimate of $NaNO_3$ coverage as a function of HNO_3 dose using the saturation behavior of the well-behaved symmetric NO stretch vibration of the nitrate band. The dose-dependent change of the IR band intensity as a function of HNO_3 coverage followed a single-site Langmuir adsorption model and resulted in an uptake coefficient whose value is listed in Table 2. The numerical value of $(5.9 \pm 0.8) \times 10^{-2}$ for γ is certainly the largest measured so far but also among the most uncertain ones because of the large partial pressure of HNO_3 used (63 Torr) and other experimental uncertainties, such as the role of gas diffusion and total used pressure. Exposure of the $NaNO_3$-capped amorphous layer to water results in hydration of the surface, to form an aqueous solution containing $NaNO_3$ and NaCl whose layer thickness continues to grow upon continued exposure to water vapor. It is noteworthy that the dissolution of $NaNO_3$ in this H_2O layer atop the NaCl crystal is fully reversible, with the relative humidity staying well below the NaCl deliquescence point. This is additional proof that interfacial dissolution processes occur at relative humidities significantly below the deliquescence point, in agreement with H_2O adsorption isotherms on NaCl.[142,143]

Aerosol experiments are designed to take the laboratory experiments one step closer to the reality of atmospheric conditions. Abbatt and Waschewsky[225] have performed a HNO_3 uptake experiment on deliquescent (that is, liquid) NaCl aerosol flowing down through an aerosol flow tube at atmospheric pressure and 75% relative humidity. The gas surviving the heterogeneous reaction downstream of the interaction area was analyzed using CIMS detection after passage through a pinhole into the detection chamber. The polydisperse NaCl aerosol formed in an ultrasonic nebulizer from a 4−5 M concentrated salt solution had a bimodal distribution (large average diameter, representing approximately 95% of the total aerosol surface area, 2−4 μm; small, <1 μm) with typical surface areas and particle number densities in the range of $(1-6) \times 10^{-3}$ cm^2/cm^3 and $(1-4) \times 10^4$ particles/cm^3, respectively, which was detected using an optical particle spectrometer. However, the authors believe that the evaluation of the rate constant for uptake on a polydisperse aerosol is fraught with only a small error when they use an average diameter at the maximum of the surface area distribution of approximately 3 μm. The lower limit value of $\gamma \geq 0.2$ given for pH = 0.3 and pH = 7.2, displayed in Table 2, refers to a NaCl aerosol acidified with HCl and buffered with NaH_2PO_4/Na_2HPO_4, respectively, and is obviously limited by diffusion of HNO_3 toward the aerosol surface. The uptake of HNO_3 has been found to be governed by the large solubility of nitric acid in aqueous solution and not by reactivity. The large aerosol volume used in these experiments prevents the saturation of nitric acid uptake into the condensed phase. A large background of HCl within the aerosol flow tube, which probably came from NaCl aerosol deposited at the internal walls of the flow tube, prevented the quantitative measurement of the reaction product HCl as a function of aerosol parameters.

A similar experiment using monodisperse aerosol of 70 nm average diameter has been performed by Guimbaud et al.[226] using an aerosol flow tube at approximately 55% rh and HNO_3 concentrations ranging from 2 to 575 ppb. They used radioactively labeled $H^{13}NO_3$, synthesized on-line from the ^{13}NO source, coupled with denuder technology for HNO_3 and HONO detection and particle filters for deposition of particulate matter such as NaCl aerosol contaminated with product nitrate at various concentrations. The detection occurred on-line using γ radiation detectors emitted during the radioactive decay ($\tau(^{13}N) = 862.07$ s). The NaCl aerosol has been generated by atomizing commercially available synthetic sea salt and conditioned to approximately 55% rh, as this value represents an acceptable compromise between aerosol stability and uptake of HNO_3 on the walls of the flow tube. A systematic study of the particle diameter as a function of relative humidity confirmed the liquid nature of the present aerosol. Owing to the high ionic strength of the salt solution, all HNO_3 is taken up and readily displaces HCl into the gas phase. The measured uptake coefficient given in Table 2 is likely to be equal to the mass accommodation coefficient, as it is invariant with the HNO_3 concentration, except at the highest value of 572 ppb, where γ is lower owing to Cl^- depletion of the condensed phase. All the performed experiments were sufficiently far away from equilibrium of the H_2O-HNO_3-HCl condensed phase with its vapor, which was verified using a condensed-phase equilibrium model. The model calculations imply that the equilibrium affects the rate of uptake only when the gas-phase concentration of HNO_3 significantly exceeds that of aerosol chloride. Therefore, the uptake remains limited by mass accommodation until the aerosol chloride starts to be significantly depleted. Qualitatively similar conclusions have been made by ten-Brink[227] on the basis of a smog-chamber experiment, where the ionic content of airborne particles was studied during HNO_3 uptake. As observed many

years before,[41] the presence of nitrate in the aerosol particles was accompanied by an equivalent loss of chloride. The authors found that the rate of substitution of chloride ions by nitrates is independent of the size of deliquescent NaCl particles and suggested that the rate-limiting step was the formation or the release of HCl into the gas phase, and not HNO_3 uptake by the aerosol.

3.2.2. The Role of Surface-Adsorbed Water and the Reaction Mechanism of the HNO_3–Salt Reaction

Several observations discussed in relation to the results obtained in flow reactors lead to the postulate that surface-adsorbed water (SAW) enables, facilitates, or catalyzes the title reaction. Observations range from the absence of any measurable uptake of HNO_3 on the (100) and (111) faces of NaCl single crystals[167,188] to the formation of "excess" HCl over DCl in DNO_3 uptake on NaCl[167] or on synthetic sea salt.[121] Most of these results are consistent with the existence of strongly bound SAW that survives extensive heating and/or pumping. Initially, the SAW pool is a neutral concentrated aqueous solution of Na^+ and Cl^- ions into which HNO_3 is taken up, leading to decreasing pH values and increasing nitrate concentrations. Once the SAW becomes sufficiently acidified, HCl starts to degas, subject to the constraints of the solubilities of HCl, $NaNO_3$, and HNO_3 in a concentrated aqueous solution of NaCl.[204,205]

There are various ways to describe the SAW, ranging from thermodynamic[121,167] to kinetic models.[211,212] However, all models necessarily remain crude approximations because so little quantitative information on the SAW is available. Brimblecombe and Clegg[205,215] and Tang and co-workers[216] have treated the thermodynamics of HNO_3 and HCl being taken up by concentrated aqueous salt solutions believed to exist in the marine boundary layer as marine aerosol. They have expressed the corresponding equilibrium constants for HCl and HNO_3 solubility at a chloride concentration of 6.3 molal, which is the solubility limit of NaCl at ambient temperature. The equilibrium constants lead to an estimate of pH = 1.7 within the SAW at steady-state conditions and typical HCl concentrations measured in flow reactors. The typical correlated nitrate concentration is 14.0 molal, beyond which $NaNO_3$ precipitates. This model is consistent with an induction period necessary to establish the equilibrium conditions that enables the desorption of HCl, which indeed has been observed by Fenter et al.[211]

An important question that has been raised in numerous studies is the physical location of the SAW sites on the NaCl substrate.[167,212,220,223,229] It is thought that H_2O will adsorb preferentially on surface defects, steps, edges, or other structural imperfections.[222,224,230−235] The total number of ion-pair sites, Na^+Cl^-, on a (100) NaCl crystal face is 6.4×10^{14} cm^{-2}.[236] However, not all of these sites support SAW at relative humidities below the deliquescence point. Barraclough and Hall[222] found, using IR spectroscopy, that approximately 25% of the surface NaCl is composed of "active sites" which are identified with surface impurities, surface defects, and hollows as well as planes other than (100), including corners and edges. They furthermore showed that it was necessary to heat the polycrystalline NaCl to approximately 623 K in order to completely remove SAW. Dai et al.[235] showed that approximately 20% of the surface sites on NaCl crystallites are defects, some of which are chemically reactive with water itself. At higher relative humidity, multilayer adsorption occurs, even on planar (100) NaCl surfaces, as shown by Ewing and co-workers.[143,237]

Barraclough and Hall[222] obtained adsorption isotherms for H_2O on polycrystalline NaCl at 298 K and reported that only after adsorption of the first two monolayer equivalents at the water partial pressure of 15 mbar at 298 K did the system behave as if a saturated solution of NaCl was present. Following these results and others,[238,239] Davies and Cox[212] concluded that the maximum partial pressure for water used in their experiments corresponded to an adsorbed quantity exceeding a formal monolayer. This means that there is water present in sufficient quantities to support ionic reactions well below the deliquescence point of 74% for NaCl at ambient temperature. It furthermore supports the idea that steady-state kinetics will be proportional to the volume of adsorbed water, which indeed has been used in the empirical model of Davies and Cox, who preferred a distinctly kinetic approach. The mechanism involves the following reversible steps:

$$HNO_3(g) + SS_1 \rightleftarrows HNO_3(ads) \quad (42)$$

$$HNO_3(ads) + SS_2 \rightleftarrows H_3O^+ + NO_3^- \quad (43)$$

$$H_3O^+ + Cl^- \rightleftarrows HCl(ads) \rightarrow HCl(g) \quad (44)$$

where SS_1 is the adsorption site for the initial HNO_3 adsorption and SS_2 the reactive site for ion exchange, leading to the product HCl. The latter type of reactive surface site is thought to hold the SAW and to provide the chloride ion that is supplied by the bulk of the NaCl sample and is transferred to the reaction site by aqueous diffusion. The nonvolatile product $NaNO_3$ migrates to certain sites on the NaCl surface and crystallizes in the form of small satellite crystallites that seem to be randomly distributed on the NaCl surface.[224] This diffusional transport of $NaNO_3$, which is thought to occur by ionic diffusion, is important as it prevents the passivation of the surface by a nonreactive $NaNO_3$ coating that would prevent further reaction by blocking free reactive sites. It is possible that the reaction supplying the chloride ion from the bulk sample may be rate-limiting under conditions of low water partial pressure.

An interesting feature of the mechanism summarily displayed in reactions 42−44 is the fact that the HNO_3 adsorption site does not coincide with the reactive site for ion exchange. This may be due to the presence of a large NO_3^- concentration at the SS_2 site, resulting from the ion-exchange reaction 44, preceded by reaction 43, which inhibits the further adsorption and/or dissolution of HNO_3, owing to the common ion effect that limits the solubility of HNO_3.

This effect has already been encountered in the case of N_2O_5 adsorption onto $NaNO_3$ aerosol and is known as the "nitrate effect". Therefore, HNO_3 adsorption is directed toward nitrate-free SS_1 sites rather than to SS_2 sites that may contain a high steady-state concentration of nitrate in order to maintain a substantial nitrate concentration gradient that drives nitrate diffusion out of SS_2 toward building up the observed $NaNO_3$ crystallites.

The reaction mechanism presented above is very similar to the one proposed earlier by Fenter et al.[211] in order to explain the kinetics of HNO_3 adsorption on polycrystalline NaCl in a Knudsen cell reactor. The model was constrained as much as possible by observations and implies the separation of HNO_3 adsorption and ion-exchange reaction as discussed above, which seems to be a robust feature of the nitric acid reaction system. The mechanism comprises the following steps:

$$HNO_3(g) + S_{surf} \rightleftarrows HNO_{3(surf)} \quad (45)$$

$$HNO_{3(surf)} + S_{int} \rightleftarrows HNO_{3int} \quad (46)$$

$$HNO_{3(int)} + S_{HCl} \rightleftarrows HCl(ads) + NaNO_3(s) \quad (47)$$

$$HNO_{3(int)} + HCl(ads) \rightleftarrows HCl(g) + HNO_{3(int)} + S_{HCl} \quad (48)$$

where S_{surf}, S_{int}, and S_{HCl} are adsorption sites for the external (= geometric) surface, the sites for HNO_3 adsorption located in the bulk, and reactive sites for ion exchange, respectively. The model was designed to describe HNO_3 adsorption on polycrystalline powders, which is the reason that the model distinguishes between adsorption sites S_{surf} and S_{int} located on the geometric surface and the interior of the bulk NaCl sample, respectively. The presentation of the NaCl sample notwithstanding the sum of S_{surf} and S_{int} may be identified with SS_1 and S_{HCl} with SS_2 of the Davies and Cox model,[212] where the abundance of S_{int} is approximately 25 times that of S_{HCl} in the Fenter et al. model.[211] Reaction 48 has been introduced into the mechanism because it was observed that HNO_3 displaces adsorbed HCl into the gas phase from the reservoir state HCl(ads) that is stable at ambient temperature and high-vacuum conditions. This process may be regarded as "salting out" of the chloride from a concentrated electrolyte solution by HNO_3, akin to the discussion of the thermodynamic SAW model discussed above. Moreover, the reaction mechanism given by reactions 45 to 48 accounts for the significant induction time, by which HCl formation lags the uptake of HNO_3 by first filling up the reservoir HCl(ads) in reaction 47.

In summary, there is increasing evidence from various experiments that H_2O adsorbed on defects on the surface plays a key role in the reactivity of salt substrates toward N-containing molecules and the volatilization of inorganic chloride, bromide, and even iodide in the form of active halogen. For example, the reaction of HNO_3 with single crystals of NaCl(100) in an UHV system, where there is no detectable amount of surface water, is relatively slow, with a reaction probability of $(4 \pm 2) \times 10^{-4}$.[218] On the other hand, the reaction with NaCl grains and especially ground powders is much faster (Table 2), being in the range $10^{-4}-10^{-2}$. Water apparently adsorbs on crystal defects, serving thus as the controlling factor, and is therefore the focal point for the reactivity toward gas-phase molecules. While water does not adsorb to the (100) face of single-crystal NaCl at room temperature,[231,233,240] it does in fact adsorb onto surface defects[222,230,232,235,240] and is not readily removed by pumping and heating at moderate temperatures of approximately 400 K.[228]

3.2.3. Concluding Remarks

Surface-adsorbed water (SAW) on solid alkali halide salt substrates is a crucial component for promoting heterogeneous reactions with atmospheric trace gases. SAW has two principal functions in that it dissolves HNO_3 and enables the recrystallization of the solid product $NaNO_3$, which is the reason the rate of uptake never completely saturates, even under high-vacuum conditions. It appears that the major part of SAW is strongly bound on alkali halides, as desorption seems to take place only at temperatures in excess of 550 K. HNO_3 is a "sticky" molecule on alkali halide salts, which has been quantitatively expressed by the measurement of the surface residence time τ_{res} of HNO_3 and which corresponds to the inverse of the first-order desorption rate constant k_{des} using simple Langmuir first-order desorption kinetics as a rate law.[199] A low value of k_{des} ensures that surface reactions leading to reaction products may occur competitively, which is the main reason for the high reaction probability of "sticky" molecules such as HNO_3 on a variety of substrates. Therefore, we believe that the application of the pore diffusion model for the quantitative correction of γ values is not appropriate in the present case. As an aside, it must be made perfectly clear that the decision whether to apply the pore diffusion model depends on a particular combination of gas−substrate, as the properties of the substrate as well as of the gas molecule control the magnitude of τ_{res}. This pairwise interaction concept has sometimes been overlooked in the literature. As a case in point, an interesting debate on the application of the pore diffusion model to heterogeneous reactions taking place on porous ice may be cited, where both parties completely ignore the identity of the gas-phase reactant.[150,152] In the case of the interaction of a sticky molecule such as $ClONO_2$ with water ice, no correction will be necessary, whereas in the case of the N_2O_5 interaction with ice, the application of the pore diffusion model may well be necessary. As a corollary, we may state that nitric acid interacts only with the external surface of a polycrystalline sample, at least in the first instants of its heterogeneous interaction, without exploring deeper layers of the bulk sample.

Nitric acid uptake on polycrystalline solid alkali salts is characterized by a large γ value in the percent range (10^{-2}) that is essentially controlled by the presence of SAW into which HNO_3 is dissolved. This conclusion was reached on the basis of both gas uptake experiments and spectroscopic observation of the nitrate reaction products. However, this scenario

Table 3. $ClONO_2$ + NaCl (KBr) → Cl_2 (BrCl) + Na(K)NO_3

symbol	uptake coefficient	substrate	temp/K	reference
γ_{ss}	$(4.6 \pm 3.1) \times 10^{-3}$	solid NaCl	296	Timonen et al., 1994[147]
	$(6.7 \pm 3.2) \times 10^{-3}$	solid NaCl	225	
γ_0, γ_{ss}	$(2.3 \pm 0.6) \times 10^{-1}$	solid NaCl	298	Caloz, Fenter, and Rossi, 1996[243]
	$(3.5 \pm 0.6) \times 10^{-1}$	solid KBr		
γ_0	0.1	solid polycrystalline NaCl film	298	Koch and Rossi, 1998[242]
γ_0, γ_{ss}	0.10 ± 0.05	solid NaCl	298	Aguzzi and Rossi, 1999[228]
	0.18 ± 0.07	solid KBr		
	0.27 ± 0.10	solid $NaNO_3$, Na_2SO_4		
γ_0	≥ 0.10	solid NaCl	298	Gebel and Finlayson-Pitts, 2001[229]
γ_{ss}	$(6.5 \pm 3.0) \times 10^{-3}$			
γ_0	0.42 ± 0.46	synthetic sea salt		
γ_{ss}	0.16 ± 0.20			

has been put into doubt recently following studies on nitric acid uptake on sublayer quantities of polycrystalline substrates, and future experiments may shed more light onto this aspect of the HNO_3−salt interaction. The γ value is significantly smaller for the uptake of HNO_3 on single crystals under UHV conditions whose initial values are smaller by a factor of 10−20. These uptake experiments under UHV conditions serve to illustrate the crucial role played by the SAW, as its absence has obviously a dramatic effect on the initial rate of uptake as well as on the recrystallization kinetics. Under UHV conditions, solid $NaNO_3$ forms a coherent layer which prevents further uptake of HNO_3, whereas in the presence of SAW, $NaNO_3$ recrystallization always frees up sufficient reactive halogen-exchange sites to support a steady-state rate of uptake. On aerosols the uptake of HNO_3 is fast, as expected from the foregoing discussion, and limited by the solubility of HNO_3 in the aerosol droplet. In a particular atmospheric situation, the extent of HNO_3 uptake will critically depend on the aerosol volume or liquid aerosol content. The kinetics of interaction of HNO_3 with atmospheric aerosol will therefore be controlled mostly by gas-phase diffusion and not by surface chemistry. Alkali salt halides have a strong affinity to adsorb H_2O, leading to SAW, owing to the thermodynamic stability of concentrated salt solutions, as discussed above, such that even solid aerosols below their deliquescence point will have a water adlayer under atmospheric conditions that will enable a heterogeneous reaction. In contrast, some mineral dust surfaces, as exemplified by $CaCO_3$ substrates, have much less water adsorbed at their interface, whereas aerosols derived from clays may have SAW in sufficient quantity to support a heterogeneous ion-exchange reaction, owing to their layered molecular structure.

3.3. Reactions of $ClONO_2$

Timonen et al.[147] performed uptake experiments of $ClONO_2$ in the presence of NaCl grain in a flow reactor coupled to a differentially pumped electron-impact quadrupole mass spectrometer at a total pressure of 0.4 mbar He according to reaction 49.

$$ClONO_2 + NaCl(s) \rightarrow Cl_2 + NaNO_3(s) \quad (49)$$

Both the decrease of $ClONO_2$, monitored at *m*/*e* 46, and the increase of Cl_2, monitored at *m*/*e* 70, were used to calculate the uptake coefficient and resulted in identical values within experimental uncertainty. The internal surface of the dry NaCl sample, ground to an average size of 4 mm, was determined in separate experiments and agreed with the internal surface calculated from average dimensions observed in SEM pictures. This confirms the widely held view, expressed in more detail above, that in general alkali halide salt surfaces are nonporous because the evaluated external surface obtained from inspection agrees well with measured BET surface areas.[140,141,147,148] The $ClONO_2$ partial pressure varied from 3.3×10^{-8} to 2.5×10^{-6} mbar, and the uptake coefficient was found to be independent of the $ClONO_2$ pressure, resulting in first-order uptake rate constants. The measured uptake coefficient was corrected for radial diffusion, which amounted to a few percent, and for the uptake on the external surface of deeper layers of NaCl exposed to the gas phase according to the pore diffusion model. This latter correction decreases the observed value for γ_{ss} by a factor of 7−8, with a global uncertainty of a factor of 2 associated with uncertainties in the model parameters used to reduce the raw values of γ_{ss}. The values displayed in Table 3 do not correspond to the measured uptake coefficients but reflect the results after the correction, which is why they are not comparable to the other values listed. However, Timonen et al.[147] never put the pore diffusion model to the test, as was pointed out earlier for the case of N_2O_5 interacting with NaCl. Koch and Rossi[242] concluded, on the basis of surface residence time measurements, that $ClONO_2$ reacted with NaCl faster than it diffused throughout the salt sample, such that it never penetrated into the bulk of the NaCl sample, owing to its reactive behavior. In addition, the surface residence time τ_g of $ClONO_2$ on NaCl was found to be large compared to that of a nonreactive reference substrate, which leads to the conclusion that Knudsen (molecular) diffusion of $ClONO_2$ throughout the bulk NaCl sample is slow. Another way of saying this is that reaction 49 takes place during the surface residence time of $ClONO_2$ at the interface, effectively preventing Knudsen diffusion across the polycrystalline sample.

Timonen et al.[147] found that, at ambient temperature, the $ClONO_2$ uptake reaction was never completely saturated, even after many hours of uptake, whereas it took 100 min or so to deactivate the salt surface at 225 K. The dose of $ClONO_2$ to saturation is estimated at 18 monolayers at 296 K and at just

one monolayer at 225 K. This may be explained by the fact that diffusion of $ClONO_2$ across the solid NaCl is slowed at the low temperature such that the uptake process comes to a screeching halt, owing to the accumulation of $NaNO_3$ that blocks the reactive surface sites for $ClONO_2$ uptake. The addition of H_2O vapor in the range $7.6 \times 10^{-5}-4 \times 10^{-4}$ mbar decreased γ_{ss} by approximately 10% at both temperatures. With increasing H_2O concentration, small amounts of HNO_3 and HOCl were observed, but no HCl.

Caloz et al.[243] compared the uptake of $ClONO_2$ on solid NaCl and KBr using a Knudsen flow reactor coupled to molecular-beam-modulated electron impact mass spectrometry (MS). Both steady-state and pulsed-valve experiments were performed in order to keep the extent of reaction and thus poisoning of the alkali salt substrates to a minimum. The flows of $ClONO_2$ for the steady-state experiments were in the range $1 \times 10^{13}-1.6 \times 10^{15}$ molecules s^{-1}, and the doses for the transient supersaturation experiments were in the range $1.5-4 \times 10^{14}$ molecules/pulse, corresponding to 1.5−5% of a formal monolayer of $ClONO_2$ on the salt surface. Both steady-state and transient exposure experiments resulted in identical values for γ, which was moreover independent of chlorine nitrate concentration over the range given above. Cl_2 was the only product of reaction 49, and was formed in a yield of 110 ± 15%. The uptake coefficient was independent of the substrate presentation, such as finely ground powder with a grain size between 35 and 100 μm, salt grains of approximately 350 μm, spray-deposits leading to thin films, and single-crystal optical flats. In addition, γ was independent of the mass of the sample in the range between 1 and 10 grain layers. This is a strong indication that diffusion of $ClONO_2$ into the salt is not competitive with reaction, in agreement with the results obtained by Koch and Rossi[242] using a different experimental method. Therefore, no correction of the measured γ values according to the pore diffusion model has been made. Although the product analysis is in good agreement with the work of Timonen et al.,[147] their experimentally determined rates are a factor of 7−8 smaller than those obtained by Caloz et al.[243] After correcting their data for the effects of diffusion into the interstitial spaces of their granular sample, they conclude that the "true" or corrected value of γ is about 50 times smaller that the value reported by Caloz et al. Unfortunately, Timonen et al.[147] have not performed the critically important test of the mass dependence of γ, and so the reasons for this disagreement remain unclear.

The reaction of $ClONO_2$ with solid KBr presents an interesting case of the importance of fast secondary reactions that determine the product spectrum. Caloz et al.[243] have performed all the necessary control experiments on solid KBr and observed that steady-state experiments resulted in Br_2 at first. Subsequently, BrCl and Cl_2 gained in importance at the expense of Br_2. Real-time transient dosing experiments using a pulsed solenoid valve unambiguously established that BrCl was the primary product. The following reaction sequence was established that could explain all experimental observations:

$$ClONO_2 + KBr \rightarrow BrCl + KNO_3 \quad (50)$$

$$BrCl + KBr \rightarrow Br_2 + KCl \quad (51)$$

$$ClONO_2 + KCl \rightarrow Cl_2 + KNO_3 \quad (52)$$

$$Cl_2 + KBr \rightarrow BrCl + KCl \quad (53)$$

The rate of reaction 51 is larger than that for process 50, which prevents observation of BrCl in steady-state experiments. With the buildup of KCl according to reaction 51, reaction 52 gains in importance at the later stages, whereby a part of Cl_2 is again converted into more Br_2 via reactions 53 and 51. Eventually, all the chlorine will end up as active Cl_2 in the gas phase as the sum of reactions 50 and 51 results in the following net stoichiometry:

$$ClONO_2 + 2KBr \rightarrow Br_2 + KCl + KNO_3 \quad (54)$$

This is in agreement with the observed Br_2 yield of 100 ± 15%, which pertains to the initial reaction kinetics prior to the heterogeneous reaction of KCl with $ClONO_2$ according to reaction 52. The kinetics of reaction 50 is very similar in most respects to the one for reaction 49.

In an extension of previous work using the same experimental method, Aguzzi and Rossi[228] systematically investigated the competition between halogen exchange, reactions 49, 50, and 52, hydrolysis, and heterogeneous decomposition of $ClONO_2$ at ambient temperature. The γ values are comparable to those obtained in previous work,[243] albeit a factor of 2 smaller for reasons that are not clear, with the Cl_2 yield being 103 ± 15%. The kinetic results for $ClONO_2$ interaction with KBr are in better agreement with previous work. As expected from previous work, the Br_2 yield steadily decreases, from 100% at $ClONO_2$ concentrations of 10^{11} molecules cm^{-3} to 40% at $[ClONO_2] = 4 \times 10^{12}$ molecules cm^{-3}, owing to the increasing importance of fast secondary reactions, such as 51, 52, and 53. One may note, in passing, that in contrast to gas-phase reactions, experimental heterogeneous kinetic studies performed at low partial reactant pressures do not de-emphasize secondary reactions, because the concentration of the solid reactant is unchanged. The hydrolysis of $ClONO_2$ with SAW, resulting in adsorbed HNO_3 and HOCl, does not appear to be competitive with halogen exchange, in contrast to the hydrolysis of $BrONO_2$ under the same conditions. However, on both $NaNO_3$ and Na_2SO_4, heterogeneous decomposition has been observed, with the kinetics listed in Table 3 and a Cl_2 yield of 28 ± 7% for the Na_2SO_4 substrate. The fast-uptake kinetics is controlled by the presence of SAW because no uptake is recorded on alkali halides after they have been dried in situ at temperatures of 550 K. Heterogeneous decomposition of $ClONO_2$ on nonreactive salt surfaces such as those investigated in this work may also represent a form of halogen activation that may become important on polar surfaces that represent nonreactive substrates.

Gebel and Finlayson-Pitts[229] investigated the uptake and reaction of $ClONO_2$ on NaCl and synthetic sea salt (SSS) powders at 298 K using a Knudsen cell reactor equipped with a quadrupole mass spectrometer. The raw results were similar to the ones obtained in Knudsen cell flow reactors previously.[228,243] The initial rate of uptake is large ($\gamma \geq 0.1$, see Table 3) due to the effect of SAW on the powder or grains and at first follows a $t^{-1/2}$ dependence, in agreement with the accepted flow resistance model, as would be expected when $ClONO_2$ is taken up into the liquid phase,[156] whose uptake is limited by $ClONO_2$'s aqueous solubility. However, the time over which the uptake follows the $t^{-1/2}$ dependence seems quite short, and the associated MS signal change is small, such that the resulting mechanistic conclusion must be used with caution. The uptake of $ClONO_2$ on SSS follows a similar dependence and is even larger than that on NaCl, probably because of higher quantities of available SAW. At longer reaction times, γ decreases from 0.1 for NaCl toward a steady-state value of 0.039 ± 0.018, which is markedly smaller than the γ_0 initially observed.[229] Even though γ_{ss} does not depend on the mass of NaCl, in agreement with results obtained by Caloz et al.,[243] Finlayson-Pitts and co-workers believe that it results from penetration of $ClONO_2$ into an average of two layers of salt. Experiments at single particle layers and below indicate that the "true" γ value is that indicated in Table 3, which corresponds to the interaction of $ClONO_2$ with the total calculated internal surface of the salt sample and therefore would correspond to a lower limit for γ. The main experimental evidence is the increase of the observed γ value by 50% when the number of particle layers is increased from 1 to 10. This causes the observed steady-state γ value to decrease by a factor of 6, accepting the "true" or corrected value as a lower limit. In later work, the data of Gebel and Finlayson-Pitts[229] were reanalyzed by Hoffman et al.[190] to result in significantly lower values for γ that are listed in Table 3.

For reasons that are not exactly clear, the observed γ value found by Aguzzi and Rossi[228] is a factor of 2.5 higher than that found by Gebel and Finlayson-Pitts[229] but a factor of 2.5 lower than that found by Caloz et al.[243] using the same experimental method. However, it is clear that both the initial and the steady-state γ values pertaining to SSS are significantly larger than the ones for the model NaCl substrate (see Table 3), and so one expects a fast reaction under atmospheric conditions, which may be in part responsible for the observed levels of Cl_2 at night in the marine boundary layer.[61−63]

Concluding Remarks. From the work of Aguzzi and Rossi,[228] Gebel and Finlayson-Pitts,[229] and Koch and Rossi,[242] a consensus value $\gamma = 0.1$ seems to emerge, with the assertion that this value may be even higher for SSS substrates. The γ values reported by Timonen et al.[147] are low, due in part to the application of the pore diffusion model that Koch and Rossi have shown to be inapplicable for the interacting pair $ClONO_2$/NaCl[242] because of long surface residence times of $ClONO_2$. These latter workers also agree with the consensus value of $\gamma = 0.1$, even though it is fraught with a larger uncertainty than flow reactor measurements because of the fitting procedure. The reinvestigation of the data of Gebel et al.[229] by Hoffman et al.[190] using a model for interpretation of sublayer quantities of NaCl also results in values of γ that are smaller by a factor of 4 compared to the consensus values, despite the small mass dependence of γ reported by these workers,[229] which should rule out significant corrections of the raw value. It would be prudent to await additional validation experiments of the sublayer approach, especially in view of the reduced signal-to-noise ratio in these experiments.

Table 4. $BrONO_2$ + NaCl (KBr) → BrCl (Br_2) + Na(K)NO_3

symbol	uptake coefficient	substrate	temp/K	reference
γ_0, γ_{ss}	0.31 ± 0.12	solid NaCl	300	Aguzzi and Rossi, 1999[228]
	0.33 ± 0.12	solid KBr		
	0.35 ± 0.10	solid $NaNO_3$		
	0.20 ± 0.12	solid Na_2SO_4		

3.4. Reactions of $BrONO_2$

Aguzzi and Rossi[227] have investigated the reaction of $BrONO_2$ with solid alkali halides such as NaCl and KBr, as well as with nonreactive salt substrates such as $NaNO_3$ and Na_2SO_4, in a Teflon-coated Knudsen flow reactor at ambient temperature. Both real-time pulsed and steady-state continuous-flow uptake experiments have been performed, and their results are given in Table 4. Under conditions of the presence of SAW on the solid salt substrates, no saturation of the uptake has been detected, resulting in a time-independent value for γ which was independent of sample presentation and sample mass. Therefore, no correction of γ for gas diffusion within the bulk sample using the pore diffusion model[147−152] has been performed, in agreement with the high value of γ. The rate law for $BrONO_2$ uptake was first order. For NaCl substrates, the primary product BrCl has been detected in a yield of $80 \pm 20\%$, in addition to Br_2 and HCl. For KBr, both Br_2 and HBr are observed as products according to the halogen-exchange reactions 55 and 56, as expected.

$$BrONO_2 + NaCl \rightarrow BrCl + NaNO_3 \quad (55)$$

$$BrONO_2 + KBr \rightarrow Br_2 + KNO_3 \quad (56)$$

The absolute yield of Br_2 decreases from 70 ± 10 to $45 \pm 5\%$ with increasing [$BrONO_2$] because of the increasing importance of the heterogeneous self-reaction on the surface of the salt substrate. HCl and HBr result from the secondary reaction of HNO_3 with NaCl and KBr, respectively, which is formed during the hydrolysis of $BrONO_2$. On a NaCl substrate, Br_2 stems from heterogeneous decomposition of $BrONO_2$, which also occurs on nonreactive salts. Similar to the uptake of $BrONO_2$ on reactive salts, the γ values are in the range 0.2−0.4, and a Br_2 yield of $45 \pm 5\%$ is observed on nonreactive salts, leading to a closed mass balance for Br_2. Owing to the concentration

Table 5. $ClNO_2 + X^- \rightarrow$ Products

symbol	uptake coefficient	substrate	temp/K	reference
		$ClNO_2 + 2I^- \rightarrow I_2 + Cl^- + NO_2^-$		
γ_{ss}	$(6.6 \pm 0.6) \times 10^{-3}$	0.01 M NaI	280	George et al., 1995[244]
	$(1.2 \pm 0.2) \times 10^{-3}$	0.001 M NaI	280	
	$(5.4 \pm 0.2) \times 10^{-3}$	0.01 M NaI	268	
γ_{ss}	$(3.3 \pm 0.1) \times 10^{-5}$	10^{-4} M NaBr	275−288	Schweitzer, Mirabel, and George, 1998[172]
	$(1.0 \pm 0.2) \times 10^{-3}$	10^{-3} M NaI		
	$(3.7 \pm 0.3) \times 10^{-3}$	10^{-2} M NaI		
		$ClNO_2 + Cl^- \rightarrow$ Products		
γ_{ss}	$(4.54 \pm 0.17) \times 10^{-6}$	pure water	291	Behnke et al., 1997[165]
	$(2.7 \pm 0.2) \times 10^{-7}$	4.6 M NaCl		
		$ClNO_2 + Br^- \rightarrow BrNO_2$ ($+NO_2$, Br_2, Cl^-, NO_2^-, NO_3^-)		
γ_0	$(1.4 \pm 0.2) \times 10^{-5}$	0.5 and 1 mM NaBr, HBr	275, 291	Frenzel et al., 1997[247]
	$(3.7 \pm 1.5) \times 10^{-5}$	5 mM NaBr, HBr		
γ_{ss}	$(6.7 \pm 1.3) \times 10^{-6}$	10^{-4} M NaBr	275−288	Schweitzer, Mirabel, and George, 1998[172]
	$(8.2 \pm 1.0) \times 10^{-5}$	10^{-2} M NaBr		
	$(8.8 \pm 2.6) \times 10^{-4}$	1 M NaBr		
γ_{ss}	$(1-10) \times 10^{-5}$	10^{-4}−1 M NaBr solution	274	Fickert et al., 1998[248]
γ_0	2×10^{-4}	solid polycrystalline KBr film	298	Koch and Rossi, 1998[242]
		$ClNO_2 + NO_2^- \rightarrow$ Products		
γ_{ss}	$(3.7 \pm 0.3) \times 10^{-6}$	0.5 mM $NaNO_2$	291	Frenzel et al., 1998[247]
	2×10^{-5}	0.2 M $NaNO_2$		
		$ClNO_2 + KBr \rightarrow BrNO_2 + KCl$		
γ_{ss}	1.3×10^{-4}	thin film, salt grain, salt powder	300	Caloz et al., 1998[249]
		$ClNO_2 + KNO_2 \rightarrow 2NO_2 + KCl$		
γ_{ss}	3.0×10^{-4}	thin film, salt grain, salt powder	300	Caloz et al., 1998[249]

dependence of $BrONO_2$ self-reaction, it is concluded that the reaction products must be Br_2O and N_2O_5, which undergo secondary reactions to $Br_2 + 0.5O_2$ and $2HNO_3$(ads) on the salt substrate, the latter of which undergoes secondary reactions such as reaction 28 or the reverse of reaction 39. Independent experiments using laser-induced fluorescence (LIF) detection of NO_2 within the Knudsen flow reactor pointed to the absence of NO_2, which was an expected product of the first-order Br−O bond-breaking process under the assumption of $BrONO_2$ first-order decay.

In summary, it appears that $BrONO_2$ reacts quickly on a multitude of ionic surfaces in the presence of SAW. However, it is expected that the overall reactivity of $BrONO_2$ is a superposition of heterogeneous halogen-exchange, hydrolysis, and presumably second-order decomposition reactions. In view of the small concentrations of $BrONO_2$, ranging from tens to hundreds of ppt, the latter reaction is not expected to be of any importance under atmospheric conditions.

3.5. Reactions of $ClNO_2$

Nitryl chloride, NO_2Cl, is the gas-phase product of the heterogeneous reaction of N_2O_5 with aqueous NaCl solutions (reaction 1) which was formed in surprisingly large yields compared to the expected HNO_3 reaction product (see section 3.1). Nitryl chloride, in turn, may react with aqueous salt solutions, resulting in stable ions and gas-phase products. George et al.[244] studied the uptake of $ClNO_2$ onto aqueous salt solutions using the droplet train technique, in which a stream of monodisperse droplets interacts with the gas phase within a flow tube at typically 13−40 mbar total pressure. The trace gas density was monitored at the entry of the flow tube by FTIR, while the quantity of trace gas absorbed by the droplets is derived from the Cl^- concentration in the collected droplets measured by ion chromatography. The uptake coefficient on pure water was immeasurably small ($\gamma < 10^{-5}$) but was dramatically enhanced on solutions containing 10^{-3}−10^{-2} M concentrations of iodides, as listed in Table 5. It appears that the uptake of $ClNO_2$ is controlled by chemical reaction rather than uptake into the aqueous phase, in agreement with the positive temperature dependence of γ observed in the range 268−280 K, whereas a negative T-dependence is expected for uptake into pure water, akin to a mass accommodation process.[156,170] Moreover, the concentration dependence of γ pointed to a surface-enhanced process in addition to the bulk chemical process. The surface process corresponds to an Ely−Rideal mechanism, which had also been found for uptake of SO_2 on water by Jayne et al.[245] and for $ClONO_2$ on sulfuric acid by Hanson and Ravishankara.[246]

The analysis of the droplets revealed Cl^- and NO_2^- as well as I_2, monitored by formation of the I_2−starch complex. The rate-limiting step of the uptake process is reaction 57, followed by the fast secondary reaction 58.

$$ClNO_2 + I^- \rightarrow ICl + NO_2^- \quad (57)$$

$$ICl + I^- \rightarrow I_2 + Cl^- \quad (58)$$

The NO_2^- yield is 66% with respect to Cl^-, suggesting missing nitrite, probably in the form of NO_2 resulting from a fast secondary reaction between $ClNO_2$ and NO_2^-. The authors make the point that the latter is improbable because iodide is a stronger nucleophile compared to NO_2 by a factor of 100. Another pos-

Table 6. Reaction Enthalpies (in kJ/mol)[a]

	reaction	measd uptake coefficient on solid salt	$\Delta H°_r(298)$ solid crystalline salt	$\Delta H°_r(298)$ solution at infinite dilution
(61)	$ClNO_2 + KCl \rightarrow Cl_2 + KNO_2$	no uptake	54.3	50.1
(61)	$ClNO_2 + KBr \rightarrow BrCl + KNO_2$	no uptake	26.0	19.1
(76)	$BrNO_2 + KCl \rightarrow ClNO_2 + KBr$	no uptake	4.9	7.6
(77)	$BrNO_2 + KCl \rightarrow BrCl + KNO_2$	no uptake	30.9	26.7
(65)	$ClNO_2 + KBr \rightarrow BrNO_2 + KCl$	1.3×10^{-4}	−4.9	−7.6
(66)	$BrNO_2 + KBr \rightarrow Br_2 + KNO_2$	>0.3	4.3	−2.6
(71)	$ClNO_2 + KNO_2 \rightarrow KCl + 2NO_2$	3.0×10^{-4}	−13.1	−8.9
(73), (71)	$BrNO_2 + KNO_2 \rightarrow KBr + 2NO_2$	no uptake	−8.2	−1.3
(86)	$BrNO_2 \rightarrow 0.5Br_2 + NO_2$		−2.0	

[a] Standard heats of formation in kilojoules per mole for salt in pure crystalline state and in aqueous solution at infinite dilution using $\Delta H°_f(BrNO_2)$ from Lee.[250]

sibility would be the formation and evaporation of HONO upon hydrolysis of N_2O_5 and subsequent acidification of the solution. Using an estimated diffusion coefficient of $ClNO_2$ in water at 280 K, the results lead to $H(k)^{0.5} = (6000 \pm 900)$ atm^{-1} M$^{0.5}$ s$^{-0.5}$, where H is Henry's law solubility of $ClNO_2$ and k the reaction rate constant according to the rate-limiting step (reaction 57), following the accepted resistance model introduced by Worsnop et al.[156,170] However, in light of later experimental evidence, the halogen-exchange reaction may also occur according to reactions 59 and 60,

$$ClNO_2 + I^- \rightarrow INO_2 + Cl^- \quad (59)$$

$$INO_2 + I^- \rightarrow I_2 + NO_2^- \quad (60)$$

as the formation of interhalogen compounds is generally not favored on thermodynamic grounds, as displayed in Table 6. Direct interconverions between nitrylhalogenides may be of some importance because of the differential reactivity of $ClNO_2$ with respect of the bromine and iodine analogues.

Behnke et al.[165] compared the uptake of $ClNO_2$ on pure water and on NaCl solutions up to 4.6 M in a wetted-wall flow tube reactor (WWFT). The uptake coefficient decreased by almost a factor of 10 from pure water to a 1 M NaCl aqueous solution, which was taken as evidence for reversible ionic dissociation of $ClNO_2$ into $Cl^- + NO_2^+$, because the precipitous drop in γ was not consistent with a salting-out effect of $ClNO_2$ by NaCl. The overall mechanism of $ClNO_2$ dissociation has been discussed in detail in the discussion of the N_2O_5 uptake on NaCl aqueous solution.

Schweitzer et al.[172] investigated the uptake of $ClNO_2$ on aqueous solutions containing bromide and iodide in the range $10^{-4}-1$ for bromide and $10^{-4}-10^{-2}$ for iodide using a variable-length WWFT at 1 atm of synthetic air. They detected the gas phase at the exit of the flow tube using both long-path FTIR absorption and residual gas MS. On NaBr solutions, the main gas-phase product was Br_2, but traces of $BrNO_2$ and BrCl were also observed. On NaI solutions, the main product was I_2, together with traces of ICl. Two slightly different reaction mechanisms were proposed that are each given in the pairwise equations 61/62 and 63/64, respectively.

$$ClNO_2 + NaX\ (X = Br, I) \rightarrow XCl + NaNO_2 \quad (61)$$

$$XCl + NaX \rightarrow X_2 + NaCl \quad (62)$$

$$ClNO_2 + NaX \rightarrow XNO_2 + NaCl \quad (63)$$

$$XNO_2 + NaX \rightarrow X_2 + NaNO_2 \quad (64)$$

The latter mechanism is preferred, because reaction 61 may be endothermic in the condensed phase as it certainly is endothermic in the gas phase, at least for X = Br, as shown in Table 6. In addition, flow reactor measurements using solid bromides have never resulted in any interhalogen compounds. The rate of uptake depends on the halide ion concentration and was found to follow a pseudo-first-order decay, the decay constant of which resulted in concentration-dependent uptake coefficients. Plots of $1/\gamma$ vs $[NaX]^{-1/2}$ resulted in straight lines that were interpreted using the accepted resistance model[156] and resulted in characteristic values for $Hk^{1/2}$. In contrast to the conclusion of Behnke,[165] no temperature dependence of the uptake was observed for both bromides and iodides in the narrow temperature range 275−293 K. However, there are slight indications of a surface-enhanced interaction[245,246] between $ClNO_2$ and I^-, and less so for $ClNO_2$ and Br^-, in agreement with Behnke.[165]

Frenzel et al.[247] studied the interaction of $ClNO_2$ with aqueous solutions using two WWFTs in series, one to synthesize $ClNO_2$ in situ using Cl_2 + nitrite, and the other to measure the uptake kinetics at 1 atm of synthetic air. Both the gas phase and the liquid phase were investigated using UV/vis and FTIR absorption and ion chromatography, respectively. The uptake of $ClNO_2$ on bromide is strongly enhanced compared to that on water. The decrease of $ClNO_2$ in the flow tube was of single-exponential type, and $BrNO_2$ and Br_2 were produced. Measurements on buffered and on acidic solutions showed similar results. The uptake coefficients were obtained by fitting the measured initial time/position-dependent concentration profiles in the reaction time range 0−7 s using a complex reaction mechanism, including gas-phase and liquid diffusion. The rate-limiting step is given by eq 65, followed by

the fast secondary reaction 66,

$$ClNO_2 + Br^- \rightarrow BrNO_2 + Cl^- \quad (65)$$

$$BrNO_2 + Br^- \rightarrow Br_2 + NO_2^- \quad (66)$$

the former of which retains some importance for the interconversion reaction between nitryl chloride and nitryl bromide, as both react quite differently in terms of their hydrolysis and toward chloride. $ClNO_2$ is the anhydride of HCl and HNO_3, whereas $BrNO_2$ is that of HOBr and HONO. The uptake of $ClNO_2$ into a chloride-containing solution is inhibited, owing to the common-ion effect, whereas that of $BrNO_2$ is accelerated because of reactive uptake, owing to the halogen-exchange reaction (see section 3.6). The alternative reaction path 61, leading to an interhalogen compound as discussed above, may safely be discarded on the grounds that the gas-phase reaction is significantly endothermic. Some of the kinetic results were obtained for the reaction system given by eq 67, where $ClNO_2$ subsequently reacted with excess nitrite according to reaction 68.

$$Cl_2 + NO_2^- \rightarrow ClNO_2 + Cl^- \quad (67)$$

$$ClNO_2 + NO_2^- \rightarrow Cl^- + N_2O_4 \quad (68)$$

Owing to the small solubility of N_2O_4, NO_2 desorbed into the gas phase, as detected using UV/vis absorption spectrometry. Nitrite enhances the uptake of $ClNO_2$ into the solution, as it does in the case of $BrNO_2$, but the effect is lower and the uptake showed no reaction time dependence, in contrast to the case with $BrNO_2$. Frenzel et al.[247] successfully modeled the multiphase system consisting of $ClNO_2$ interacting with an aqueous solution containing chloride, bromide, and nitrite using the rate-limiting steps given above. The numerical model seems to confirm that the halogen-exchange reaction of $ClNO_2$ with bromide seems to occur via $BrNO_2$ as an intermediate rather than the interhalogen compound BrCl, and that reaction 64 does not occur for X = Cl, both owing to their endothermicity. The model also confirms that $ClNO_2$ hydrolysis to HCl + HNO_3 is slow.

Fickert et al.[248] studied the uptake of $ClNO_2$ on pure water, NaBr, and mixed NaBr/NaCl solutions in a wetted-wall tubular flow reactor at 10−28 Torr of He as a carrier gas under laminar (that is, fast-flow) conditions at 274 K in order to keep the vapor pressure of H_2O to a minimum. The time scale of interaction was in the range 0.1−0.7 s that effectively prevented the occurrence of secondary reactions. The gas-phase reactants and products were monitored using a differentially pumped MS. The gas-phase diffusion coefficient of $ClNO_2$ was measured on 0.1−0.5 M KOH solution in order to accelerate the ractive uptake and to make accommodation rate-limiting. It resulted in a mass accommodation coefficient of $ClNO_2$ on water of $(9 \pm 4) \times 10^{-3}$, which seems rather low. The rate of uptake of $ClNO_2$ was measured on solutions of different bromide concentration in the range 10^{-4}−10^{-2} M and led to pure single-exponential decays of the reactant, except for the very first portion of the decay, which was attributed to a solvation effect. In agreement with this interpretation, no product formation during this initial uptake was observed. The value of γ_{ss} as well as the product distribution remained unchanged upon addition of 1 M NaCl to the bromide solution.

The gas-phase products were found to be Br_2, $BrNO_2$, and amounts of BrCl that were smaller by 2 orders of magnitude. Br_2 was formed in a secondary reaction, resulting from the condensed-phase reaction of $BrNO_2$ with Br^-. The reaction products were consistent with reactions 66 and 67, because the relative concentrations of the Br_2 and $BrNO_2$ products clearly shifted toward Br_2 as the Br^- content of the solution was increased and the total amount of gas-phase products substantially increased. Careful calibration and extrapolation to zero bromide concentration established that the yield of the primary reaction product, $BrNO_2$, initially was 100 ± 30%, in agreement with the proposed reaction mechanism. At finite bromide concentration, the effective yield of active bromine (that is, the sum of $BrNO_2$ and Br_2) accounted for 70 ± 18% of the lost $ClNO_2$. The fact that the addition of large amounts of chloride to bromide did not affect the $ClNO_2$ uptake kinetics is an elegant demonstration that an S_N2-type reaction mechanism is operative rather than an S_N1 reaction. Therefore, the direct reaction 65 is preferred over a reaction mechanism whose rate-limiting step is ionic dissociation of $ClNO_2$, according to reaction 69, and ensuing recombination of NO_2^+ with bromide, reaction 70. Specifically, quantitative consideration ruled out the incidence of reaction 61 or the formation of BrCl.

$$ClNO_2 \rightleftarrows Cl^- + NO_2^+ \quad (69)$$

$$NO_2^+ + Br^- \rightarrow BrNO_2 \quad (70)$$

Caloz et al.[249] performed uptake experiments in a Knudsen cell flow reactor at ambient temperature using different substrate presentations in order to evaluate the true uptake coefficient on a per-collision basis. Although no bulk H_2O is formally present in these experiments under high-vaccum conditions, sufficient SAW on the salts enables the halogen-exchange reactions, provided they are thermodynamically driven. Table 6 lists the kinetic observations as well as the reaction enthalpies for the reactions studied in this work, which also serve as a useful guide to gauge the importance of processes involving $ClNO_2$ taking place in solution. The observed uptake coefficients for $ClNO_2$ on KBr salt grain or powder are $(1.5 \pm 0.6) \times 10^{-2}$ in pulsed-valve real-time experiments and $(1.9 \pm 0.6) \times 10^{-2}$ in continuous-flow experiments. The observed mass dependence of γ necessitated the correction of the observed value of γ using the pore diffusion model, in agreement with the results of a molecular diffusion tube study by Koch and Rossi,[242] who measured an uptake coefficient of 2×10^{-4}, as well as the surface residence time of $ClNO_2$ on solid KBr. They confirmed the nonsticky nature for this particular reactant/substrate combination, in view of the short surface

residence time of 20 μs for KBr at ambient temperature, and thus justified the need to apply the pore diffusion model to correct the raw values of γ. Therefore, the corrected γ value obtained in the study of Caloz et al.[249] is 1.3×10^{-4} and pertains to reaction 65, followed by the fast secondary reaction 66. The primary product is $BrNO_2$, which is not observable because it undergoes a fast secondary reaction with KBr to result in Br_2 and KNO_2. The mean Br_2 yield is 0.55 ± 0.2, and depends on the gas-phase residence time. In contrast to continuous-flow experiments, pulsed-valve studies reveal the intermediate $BrNO_2$, whose gas-phase residence time was measured as 300 ms in the presence of solid KBr.

The primary product of $ClNO_2$ uptake on nitrite is NO_2, which has been deteced using LIF at limiting yields of 200% per reacted $ClNO_2$ at the longest gas-phase residence time of 26 s. The reaction takes place according to eq 71,

$$ClNO_2 + KNO_2 \rightarrow KCl + 2NO_2 \qquad (71)$$

with an observed γ value of $(1.7 \pm 0.2) \times 10^{-2}$, resulting in a true value of 3×10^{-4} after correction using the pore diffusion model. This small value is rather surprising in view of the significant exothermicity of the process (see Table 6). Nitryl chloride seems to have a significant activation barrier to heterogeneous reaction on solid salts. A typical example is reaction 65, which occurs with low reaction probability, given its appreciable exothermicity.

Concluding Remarks. In general, the uptake kinetics of $ClNO_2$ on dilute bromide and iodide solutions is slow and controlled by an ionic S_N2-type ionic displacement according to reaction 59 or 65. The reactive uptake coefficient of $ClNO_2$ in solution is therefore a function of the halide concentration. The primary reaction product seems to be the nitryl halide incorporating the exchanged halide rather than the interhalogen obtained from reaction 61. This follows from the calculated thermochemistry of the reactions displayed in Table 6 and explains why $ClNO_2$ is not reactive toward chloride. Moreover, the nonreactive uptake on chloride-containing solutions is inhibited because of the common ion effect akin to the "nitrate" effect discussed in section 3.1. If the condensed phase is presented as a solid alkali halide, then the uptake kinetics remains slow, on the order of $(1-2) \times 10^{-4}$, and stable molecular halogens are generated as final products that are formed in fast secondary reactions of the nitryl halide with excess alkali halide, following reactions 64 and 66, akin to the reaction in solution. The surface residence time of $ClNO_2$ on KBr is short compared to that of $ClONO_2$, which therefore makes $ClNO_2$ interacting with KBr a nonsticky molecule whose uptake kinetics has to be unraveled using the pore diffusion model.

3.6. Reactions of $BrNO_2$

Nitryl bromide, $BrNO_2$, is the primary product of the heterogeneous reaction of N_2O_5 with bromides (reaction 29), followed by the fast secondary reaction 30 under conditions of excess bromide. In the laboratory, $BrNO_2$ has been generated from the multiphase reaction of Br_2 with a nitrite solution. Frenzel et al.[247] studied the interaction of $BrNO_2$ with aqueous solutions using two WWFTs in series, one to synthesize $BrNO_2$ in situ using 700 ppm of Br_2 and 5 mM of $NaNO_2$ aqueous solution, and the other to measure the uptake kinetics at 1 atm of synthetic air. Both the gas phase and the liquid phase were investigated using UV/vis and FTIR absorption and ion chromatography, respectively. Typically, 190 ppm of $BrNO_2$ were obtained and monitored by UV/vis absorption in the range 200−400 nm. Observed reaction products included NO_2 in the gas phase and Br^- and NO_3^- in the condensed phase. On bromide solution, $BrNO_2$ shows a fast initial loss rate. The fact that the initial rate of uptake of $BrNO_2$ on a bromide solution is much faster than than on water and dependent on the bromide concentration indicates the occurrence of reaction 72.

$$BrNO_2 + Br^- \rightarrow Br_2 + NO_2^- \qquad (72)$$

Toward longer reaction times, the system reaches steady state, owing to the accumulation of the reaction products in the liquid film along the flow tube. Similar γ values are obtained on buffered solutions, whereas the loss rates are faster on acidic solutions. This reaction is very different from the analogous reaction, namely $ClNO_2 + Cl^-$, as the uptake rate is inhibited with increasing chloride concentration. The loss of $BrNO_2$ on a nitrite solution increases with reaction length and occurs in analogy to $ClNO_2 + NO_2^-$ according to reaction 73,

$$BrNO_2 + NO_2^- \rightarrow Br^- + N_2O_4 \qquad (73)$$

where the product N_2O_4 dissociates into NO_2, which is only slightly soluble in solution and desorbs into the gas phase. The initial uptake of $BrNO_2$ on a nitrite solution is slower than that on an equally concentrated bromide solution, indicating a slower reaction of $BrNO_2$ with nitrite than with bromide, as is also the case for $ClNO_2$. The uptake of $BrNO_2$ on a 0.5 M chloride solution was also enhanced in the first part of the flow tube, but subsequently an equilibrium between $ClNO_2$ and $BrNO_2$ appeared to control the kinetics, where both nitryl halides decreased at aproximately the same rate, somewhat faster than in water. Together with the reaction of $ClNO_2$ with bromide, these results describe the rapid interconversion of $ClNO_2$ and $BrNO_2$ in the presence of halide ions. The uptake coefficients were obtained by fitting the measured initial time/position-dependent concentration profiles in the range 0−4 s using a complex reaction mechanism including gas-phase and liquid diffusion. No distinct temperature dependence of γ has been detected over the given small temperature range. Noteworthy is the different reactivity of $ClNO_2$ and $BrNO_2$ toward hydrolysis and chloride solutions, which has been discussed above, and which follows eq 74 rather than reaction 75.

$$BrNO_2 + H_2O \rightarrow HOBr + HONO \qquad (74)$$

$$BrNO_2 + H_2O \rightarrow HBr + HNO_3 \qquad (75)$$

Table 7. $BrNO_2 + X^- \rightarrow$ Products

symbol	uptake coefficient	substrate	temp/K	reference
		$BrNO_2 + Br^- \rightarrow$ Products		
γ_0	$>1.2 \times 10^{-4}$	5 mM NaBr aqueous film	291	Frenzel et al., 1997[247]
	$>2.1 \times 10^{-4}$	10 mM NaBr aqueous film		
	$>6.5 \times 10^{-4}$	50 mM NaBr aqueous film		
	$>2.2 \times 10^{-5}$	1 mM HBr aqueous film		
	$>9.3 \times 10^{-4}$	10 mM HBr aqueous film		
γ_{ss}	$(1.1 \pm 0.3) \times 10^{-5}$	5×10^{-4} M NaBr aqueous film	278−293	Schweitzer, Mirabel, and George, 1998[172]
	$(6.2 \pm 3.1) \times 10^{-4}$	5×10^{-3} M NaBr aqueous film		
	$(1.4 \pm 0.4) \times 10^{-4}$	5×10^{-2} M NaBr aqueous film		
		$BrNO_2 + I^- \rightarrow$ Products		
γ_{ss}	$(4.5 \pm 0.3) \times 10^{-4}$	5×10^{-3} M NaI aqueous film	276−293	Schweitzer, Mirabel, and George, 1998[172]
	$(2.4 \pm 0.4) \times 10^{-5}$	10^{-4} M NaI aqueous film		
	$(2.5 \pm 0.7) \times 10^{-6}$	pure water		
		$BrNO_2 + NO_2^- \rightarrow$ Products		
γ_0	$<2.2 \times 10^{-5}$	5 mM $NaNO_2$ aqueous film	291	Frenzel et al., 1997[247]
		$BrNO_2 + Cl^- \rightarrow$ Products		
γ_0	$>3.8 \times 10^{-5}$	0.5 M NaCl aqueous film	291	Frenzel et al., 1998[247]
γ_{ss}	$(1.1 \pm 0.3) \times 10^{-5}$	0.5 M NaCl aqueous film	278−293	Schweitzer, Mirabel, and George, 1998[172]
		$BrNO_2 + KBr \rightarrow Br_2 + KNO_2$		
γ_{ss}	>0.3	solid KBr	300	Caloz et al., 1998[249]

However, whenever the condensed phase has been monitored, NO_3^- has always been found, which is not readily understandable on the basis of reaction 74 alone. It is most probably a secondary reaction product, as it is formed at late reaction times. Therefore, reaction 75 has also been invoked as a parallel reaction, in violation of the formal oxidation state of bromine in $BrNO_2$, namely Br(+III). In addition, the propensity for the formation of the nitryl halide (reaction 76) over the interhalogen (reaction 77) in the halogen-exchange reaction has already been pointed out in section 3.5.

$$BrNO_2 + Cl^- \rightarrow ClNO_2 + Br^- \quad (76)$$

$$BrNO_2 + Cl^- \rightarrow BrCl + NO_2^- \quad (77)$$

Schweitzer et al.[172] performed uptake experiments with $BrNO_2$ on dilute aqueous solutions of chloride, bromide, and iodide in a variable-length WWFT at 1 atm of synthetic air. The gas phase was monitored using both long-path absorption by FTIR and residual gas ion-trap MS, whereas the condensed phase was monitored by ion chromatography. $BrNO_2$ was synthesized in a 15-cm interaction length WWFT upstream of the variable interaction length kinetics flow tube by interacting 460−740 ppm of Br_2 in air with a 5 mM $NaNO_2$ aqueous solution. $BrNO_2$ was monitored by FTIR absorption in the range 600−2000 cm^{-1}. The extent of reaction, monitored as the depletion of $BrNO_2$ as a function of reaction time or interaction length, always followed single-exponential decay, in contrast to the study of Frenzel et al.,[247] where secondary reactions and saturation effects were observed. These led to halogen interconversion reactions that re-form $BrNO_2$ at long interaction times. The characteristic time scale for heterogeneous interaction was between 0.2−5 and 0.05−0.2 s for the studies performed by Frenzel et al.[247] and Schweitzer et al.,[172] respectively. The uptake coefficient was found to be a function of $BrNO_2$ concentration and was extracted from the slope of the exponential decay of $BrNO_2$ with reaction time. Table 7 lists characteristic values of γ at a few selected halide concentrations. Plots of $1/\gamma$ vs the inverse square root of the halide concentration result in characteristic values of $H(k^{II})^{1/2}$, where H is the Henry's law constant and k^{II} is the second-order rate constant for the reactive uptake of $BrNO_2$.

The uptake coefficient for $BrNO_2$ on pure water is in the 10^{-6} range, in excellent agreement with the results of Frenzel et al.[247] The uptake coefficient for $BrNO_2/H_2O$ is smaller by a factor of 2 compared to that for $ClNO_2/H_2O$, in contrast to γ for uptake on halide solutions. Uptake on H_2O exhibits a slight positive temperature dependence that is unusual for this type of uptake. In contrast, the rates of uptake of $BrNO_2$ on the halide solutions did not exhibit a measurable temperature dependence, similar to $ClNO_2$. The rate of $BrNO_2$ uptake increased with its gas-phase concentration, which is taken as evidence for the presence of fast secondary reactions involving nitrite ion, that itself is consumed by additional $BrNO_2$ according to reactions 78 and 79,

$$BrNO_2 + NO_2^- \rightarrow Br^- + N_2O_4 \quad (78)$$

$$N_2O_4 + H_2O \rightarrow HONO + HNO_3 \quad (79)$$

which may explain the incidence of nitrate. In fact, in this case the condensed-phase products Br^-, NO_2^-, and NO_3^- have been detected. The secondary chemistry is first and foremost a problem of uptake experiments on pure water, as uptake on halide solutions effectively prevents secondary chemistry by virtue of the enhanced rate. In fact, in the presence of bromide or iodide, the uptake rate of $BrNO_2$ is greatly enhanced, as shown in Table 7. No gas-phase products were detected for $BrNO_2$ interaction with pure water and chloride solutions. The main gas-phase products for bromide and iodide solutions were Br_2 and I_2.

Caloz et al.[249] performed uptake experiments with $BrNO_2$ in a Knudsen cell flow reactor at ambient

temperature, using a source reaction involving solid KBr. $BrNO_2$ was generated in situ using a small flow cell upstream of the Knudsen reactor using reaction 80, for which the uptake coefficient γ was 0.32 ± 0.05. Reaction 80 is the solid-state version of the inverse

$$Br_2 + KNO_2 \rightarrow BrNO_2 + KBr \qquad (80)$$

of reaction 72, and is only weakly exothermic according to Table 6 (reaction 66). The large uptake coefficient of Br_2 is somewhat of a surprise, but it is appropriate for the use of reaction 80 as a source for $BrNO_2$. A small amount of HONO has been observed that is attributed to the hydrolysis of $BrNO_2$ on the surface of KNO_2 according to reaction 74. The lifetime of $BrNO_2$ in the presence of solid KNO_2 is only 10 s in the low-pressure flow reactor, which is much shorter than the lifetime in a static quartz cell of 1 h, measured by Frenzel et al.[247] Under the experimental conditions used by Caloz et al.,[249] $BrNO_2$ apparently undergoes a heterogeneous decomposition according to reaction 81, where NO_2 has been detected using LIF in a yield twice that of Br_2.

$$BrNO_2 \rightarrow 0.5Br_2 + NO_2 \qquad (81)$$

However, $BrNO_2$ is not markedly reactive on a nonreactive salt substrate such as $NaNO_3$, as a γ value of 5×10^{-3} has been measured which indicates a slow reaction. Moreover, no decomposition products have been observed. In agreement with observations made by Frenzel et al.[247] and Schweitzer et al.,[172] reaction 73 is fast, with $\gamma \geq 0.3$ and Br_2 as the only detectable reaction product. The reactivity of $BrNO_2$ on chlorides was immeasurably slow, in agreement with the endothermic nature of reaction 76 or 77 (see Table 6), the latter of which is significantly more endothermic than the former because an interhalogen compound is formed. However, this observation is in disagreement with the claims for an equilibrium (reactions 76 and 65) in aqueous solution between $ClNO_2$ and $BrNO_2$, measured by Frenzel et al.,[172] who concede that $ClNO_2$ may have been formed by another route. In contrast to reaction 71, involving the formation of gas-phase NO_2, the analogous reaction of $BrNO_2$ with solid KNO_2 (reaction 73) is too slow to be observed under the molecular flow conditions of the Knudsen reactor, which is surprising in view of the large exothermicity displayed in Table 6. In summary, the interconversion kinetics of $BrNO_2$ and $ClNO_2$ on solid alkali halide salts as well as the associated product spectrum may provide useful guidance for the interpretation of multiphase reactions involving aqueous solutions.

Concluding Remarks. Nitryl bromide, $BrNO_2$, has a distinctly different chemistry than $ClNO_2$ because of the formal oxidation state of Br (+III) compared to Cl (−I). $BrNO_2$ readily reacts with bromide and iodide but not with chloride, despite claims to the contrary.[247] Akin to $ClNO_2$, its uptake onto aqueous halide solutions is dominated by S_N2-type displacement reactions, which is why the uptake coefficient depends on the halide concentration. Uptake into bromide and iodide solutions is accompanied by Br_2 and I_2 formation in the gas phase, in view of the limited solubility of molecular halogens in water, whereas uptake into pure water and chloride solutions does not lead to any volatile product formation. Similar to uptake into aqueous solution, the interaction of $BrNO_2$ with solid bromides is fast, whereas it is immeasurably slow for the interaction with chlorides and nitrites. In the former case the reaction is endothermic, whereas in the latter it is exothermic, as displayed in Table 6.

3.7. Reactions of HOCl

Huff and Abbatt[251] have studied the HOCl uptake on frozen aqueous bromide films in a low-pressure laminar flow coated-wall flow tube equipped with a differentially pumped mas spectrometer in order to study reactions 82 and 83.

$$HOCl + Br^- \rightarrow BrCl + OH^- \qquad (82)$$

$$BrCl + Br^- \rightarrow Br_2 + Cl^- \qquad (83)$$

Very similar to the case of Cl_2 interacting with the same substrate (see Table 12), a time-dependent rate of uptake was observed with the progress of the reaction, owing to depletion of bromide. The main reaction product was Br_2, along with minor amounts of BrCl. Unlike with Cl_2, the uptake coefficient γ for HOCl significantly increased below pH = 4 by a factor of 5, whereas it stayed constant in the range of pH = 4−10. The HOCl reaction rate does not increase with increasing bromide concentration in ice, as it is limited by pH, not bromide concentration, at pH values greater than 2. No interaction was noted on pure frozen chloride films at pH = 7, which is a surprise in view of the fact that the analogous reaction in solution readily occurs according to reaction 84.

$$HOCl + Cl^- \rightarrow Cl_2 + OH^- \qquad (84)$$

However, reaction 84 is slower by a factor of 100 compared to reaction 82 in solution.[252] It is also possible that the rate of reaction 84 is limited by the H^+ concentration at pH = 7.

On mixed chloride/bromide−ice substrates that were chosen to simulate reaction on Arctic sea ice, HOCl did not react at 233 K, presumably because of the large amount of unreactive chloride in the mixed-halide−ice film. The absence of reaction for HOCl is surprising, as the bromide concentration in the mixed-halide−ice film was equal to that in the pure bromide−ice film that gave rise to a reaction (Table 8). It is possible that the chloride that is present in 300-fold excess over bromide displaced the latter from the interface. Also, the absolute concentration of the halides in the sea salt surrogate prepared by Huff and Abbatt was a factor of 10 larger than that measured in natural seawater.

At 248 K, the above-mentioned halide−ice mixture gave rise to a reaction when exposed to HOCl. As in experiments with bromide films, a time-dependent loss rate of HOCl owing to the depeletion of bromide at the interface was observed to follow first-order kinetics. However, the γ value is smaller when we

Table 8. HOCl + M(Na,K)Br → Products

symbol	uptake coefficient	substrate	temp/K	reference
γ_{ss}	1.5×10^{-2}	0.1−1.0 wt % aqueous NaBr solution, pH = 4−10	233	Huff and Abbatt, 2000[251]
	5.1×10^{-2}	0.1 wt % aqueous NaBr solution, pH = 2		
	$<4.2 \times 10^{-3}$	20 wt % NaCl + 0.08 wt % NaBr, pH = 7	233	
	1.3×10^{-2}	20 wt % NaCl + 0.08 wt % NaBr, pH = 7	248	
γ_0	5×10^{-3}−1×10^{-2}	KBr grains	300	Santschi and Rossi, 2003[253]
	5×10^{-2}−0.2	ground KBr grains		
	2×10^{-2}	spray-deposited thin KBr film		

compare, for instance, the reaction probability for HOCl on a 0.1% bromide film at 248 K with a that on chloride/bromide film at the same conditions, the latter being a factor of 5 larger. The difference between the bromide−ice and the mixed chloride/bromide−ice films has to do with the freezing process and the associated composition of the substrate interface. The temperature of 248 K is between the eutectic temperature of NaCl/H_2O (252 K) and NaBr/H_2O (245 K), so the predicted composition of the halide−ice mixture would be ice, solid NaCl, and a concentrated solution of NaBr, onto which the reaction presumably takes place. It thus seems that the detailed surface composition of frozen substrates has a significant effect on the heterogeneous reaction kinetics. Absolute product yields in terms of the sum of Br_2 and BrCl were only 50% of the values expected on the basis of the quantity of HOCl lost. The balance was attributed to BrCl that was formed on the ice as a primary product, according to reaction 82, but remained adsorbed so as to avoid detection by MS. The relative yield was 97% Br_2 and 3% or less BrCl, making Br_2 the major reaction product under all conditions that were explored.

Santschi and Rossi[253] undertook a mechanistic study of HOCl uptake on solid KBr at ambient temperature in a Knudsen flow reactor in order to gauge the importance of chlorine in halogen activation events compared to the role of bromine. The solid KBr sample was presented as grains, ground powder, single crystals, and spray-deposited thin films. It turned out that the role of adsorbed reaction products was crucial in interpreting the kinetic results, which is the reason that a range of γ values has been given in Table 8. Initially, the main reaction product is Br_2, but smaller amounts of BrCl and HOBr, and even smaller amounts of BrOCl and Br_2O, have been observed as well. At later stages of the reaction, the bromine-containing products are replaced by the appearance of Cl_2 and Cl_2O. No surface regeneration has been observed for the HOCl reaction, in distinct contrast to Cl_2 uptake, whereas surface activation by adsorbed reaction products such as Br_2 and HOCl, and possibly BrCl, HBr, and HOBr, the presence of SAW, and the existence of surface defects are all important for both the kinetics and the product spectrum.

As a result of experiments with a concurrent Br_2 flow which deliberately introduces a surface-activating compound, it was concluded that two different reactions lead to release of Cl_2O and Cl_2 in long-term experiments of HOCl uptake on KBr, namely one in the presence of adsorbed Br_2 and the other in its absence. The main processes that are important in the initial stages of HOCl uptake are given in reactions 85 and the solid-state analogues of reactions 82 and 83.

$$KBr + H_2O \rightleftarrows HBr + KOH \quad (85)$$

$$HOCl + HBr \rightarrow BrCl + H_2O \quad (82)$$

$$BrCl + KBr \rightarrow Br_2 + KCl \quad (83)$$

Equilibrium G4 lies far to the left and serves to initiate the reaction by providing a reactive site in the form of HBr. The expected acid−base reaction between HOCl and KOH would not lead to molecular halogens, which are experimentally observed; instead, the reaction proceeds through reaction 82, which leads to the oxidation of bromide (Br(−I)) in HBr to hypobromide (Br(+I)) in BrCl. Once KCl has accumulated at the interface, reactions with chlorine are taking place that are analogous to the bromine reactions.

$$KCl + H_2O \rightleftarrows HCl + KOH \quad (86)$$

$$HOCl + HCl \rightarrow Cl_2 + H_2O \quad (87)$$

SAW assumes the usual catalytic role, as it is not consumed, and under special circumstances autocatalytic uptake of HOCl may be seen, which leads to a significant enhancement of the uptake coefficient. On the other hand, steady-state uptake rates are often found to be smaller by a factor of 10 relative to γ_0. Very importantly, neither uptake of HOCl nor formation of reaction products has been observed on solid NaCl substrates, in analogy to results obtained by Huff and Abbatt.[251]

3.8. Reactions of HOBr

It has been suggested that halogen species may participate in the release of sea salt halogens through autocatalytic processes,[78−80] in addition to members of the NO_y family. In particular, the effects that an autocatalytic release of Br_2, initiated by the uptake of HOBr by marine aerosol, may have upon the chemistry of the marine boundary layer have been modeled.[79] Once this mechanism is initiated, it has the potential to oxidize essentially all of the bromide within the marine boundary layer in a matter of a few days. This Br-based chemistry has been mentioned briefly in the Introduction in relation to the "bromine explosion" that has the characteristics of a degenerate chain-branching reaction, comparable to the snowball effect. Therefore, the heterogeneous chemistry of HOBr has been studied in some detail in order to understand both chain initiation and

Table 9. HOBr + NaCl, KBr → BrCl, Br_2 + NaOH, KOH

symbol	uptake coefficient	substrate	temp/K	reference
γ_{HOBrss}	$(1.24 \pm 0.47) \times 10^{-3}$	30% NaCl/H_2O	230−240	Kirchner, Benter, and Schindler, 1997[107]
	$(1.42 \pm 0.17) \times 10^{-3}$	30% NaCl/H_2O + 0.08% NaBr/H_2O		
γ_{HOBrss}	$(3.27 \pm 0.48) \times 10^{-3}$	30% NaBr/H_2O		
γ_0	$(6.5 \pm 2.5) \times 10^{-3}$	NaCl salt powder, grain	300	Mochida et al., 1998[254]
γ_{ss}	$(1.0 \pm 0.3) \times 10^{-3}$	NaCl salt powder, grain		
γ_0	(0.18 ± 0.04)	KBr salt powder, thin film		
γ_{ss}	$(3.0 \pm 0.5) \times 10^{-2}$	KBr salt powder, thin film		
γ_{ss}	$\leq 1.5 \times 10^{-3}$	NaCl aerosol, 75% rh, unbuffered	298	Abbatt and Waschewsky, 1998[225]
	≥ 0.2	NaCl aerosol, 75% rh, pH = 0.3, 7.2, buffered		
α_{HOBrss}	$\geq 10^{-2}$	aqueous NaCl salt solution	274	Fickert, Adams, and Crowley, 1999[164]
α_{HOBrss}	$\geq 10^{-2}$	aqueous KBr salt solution		
γ_{ss}	$\geq 10^{-2}$	aqueous NaCl, aqueous NaBr, aqueous NaCl/NaBr solution, pH = 2, 6 H_2SO_4	233, 248	Huff and Abbatt, 2002[257]
γ_0	$(3.2 \pm 0.9) \times 10^{-2}$	2 M NaCl + 3×10^{-3} M NaBr frozen salt solution	233	Adams, Holmes, and Crowley, 2002[256]
	$(1.2 \pm 0.5) \times 10^{-2}$	2 M NaCl + 3×10^{-3} M NaBr frozen salt solution	253	
	$> 10^{-2}$	0.1 M NaBr frozen salt solution	248	
	3.6×10^{-2}	3×10^{-3} M NaBr frozen salt solution	248	
α_{HOBr}	0.6 ± 0.2	100-nm NaBr aerosol at 37% rh, deliquescent	298	Wachsmuth et al., 2002[258]

chain propagation processes, the former of which is still essentially unexplained to this day.

Kirchner et al.[107] performed an uptake study using a laminar flow tube connected to an electron-impact ionization reflectron time-of-flight mass spectrometer (TOFMS) via a differential pumping stage for molecular beam sampling. The total pressure in the jacketed flow tube was in the range 5−20 mbar He at a carrier gas flow velocity of 8 ms^{-1}. Ice films were produced by spraying water or aqueous solutions of alkali halides onto the interior walls of the cold flow tube. Gaseous HOBr was entrained in carrier gas by bubbling He through a 0.2 M HOBr aqueous solution in 20 wt % H_2SO_4 and passed through a cold trap at 273 K in order to reduce the water content. The HOBr decays were first order in HOBr at concentrations of $(0.6-1.3) \times 10^{13}$ molecules cm^{-3} and led to the formation of BrCl and significant amounts of Br_2 in the case of samples spiked with NaBr, simulating model sea salt aerosol, according to eqs 88 and 89, with reaction 90 occurring concurrently as an efficient secondary reaction.

$$HOBr + NaCl \rightarrow BrCl + NaOH \qquad (88)$$

$$HOBr + NaBr \rightarrow Br_2 + NaOH \qquad (89)$$

$$BrCl + NaBr \rightarrow Br_2 + NaCl \qquad (90)$$

A typical product ratio is 42 ± 10% BrCl and 48 ± 9% Br_2, representing a factor of 500 enrichment in the gaseous products compared to the stoichiometry of the dopant, namely bromide. Reaction 89 is noteworthy as it selectively reacts with the bromide that is the minority species in the condensed phase. The uptake coefficients on ice doped with NaCl and on ice doped with NaCl/NaBr mixtures were found to be identical within experimental error. Interaction of HOBr with pure H_2O ice led to the formation of Br_2O, in addition to the uptake of HOBr on the ice. Br_2O is certainly formed following the interaction of two HOBr molecules and should not be important at the low atmospheric HOBr concentrations.

Mochida et al.[254] studied the uptake of HOBr in a Knudsen cell flow reactor equipped with a modulated molecular beam MS detector in both continuous-flow and real-time pulsed-dosing experiment using polycrystalline NaCl and KBr as well as spray-deposited samples. On both salts, a high initial value of γ_0 was observed that slowly converged to saturation of the uptake. The initial uptake probability, γ_0, increased with the mass of solid salt and was therefore corrected using the pore diffusion model, the result of which is displayed in Table 9. On NaCl, the reaction products were BrCl (delayed) and Br_2, the prompt formation of which was unexpected and which was shown to arise from the bimolecular self-reaction of HOBr on the solid salt surface at higher partial pressures of HOBr, according to reaction 91.

$$2HOBr \rightarrow Br_2 + H_2O + 0.5O_2 \qquad (91)$$

On KBr, molecular bromine was observed as a unique product. On solid $NaNO_3$ samples, HOBr spontaneously decomposed at a similar rate and with Br_2 yields of 50%, which is a strong indication for the occurrence of reaction 91. On both NaCl and KBr, the Br_2 yield tended toward 50% at limiting high concentration of HOBr. This may be taken as proof that, on both chloride and bromide salts, heterogeneous decomposition is dominant, whereas at low concentration, reactions 88 and 89 control the Br_2 yield of 100%. A strong decrease of the uptake coefficient with increasing HOBr concentration has been observed, which corresponds to a rate law for uptake different from first order as well as significant surface saturation that becomes increasingly apparent with increasing HOBr concentration. In reaction 89, on average 5−10% of the surface Br represents reactive sites for HOBr, with surface saturation taking place on the seconds time scale at the flow rates used.

To better quantify the rates at which key trace gases interact with sea salt aerosols, Abbatt and Waschewsky[225] studied the kinetics of uptake of HOBr on deliquescent NaCl aerosol at 75% relative humidity, the deliquescence point of NaCl, and ambient temperature using an aerosol kinetics flow tube technique. The gas phase has been probed using CIMS, and the polydisperse aerosol was character-

ized using an optical spectrometer. Pertinent details may be found in section 3.2, in relation to HNO_3 uptake on the same aerosol. The uptake coefficient of HOBr on unbuffered NaCl aerosol is low, whereas it increases by at least a factor of 1000 on aerosol acidified to pH = 0.3 or on aerosol buffered at pH = 7.2 using a phosphate buffer, and it could easily be as large as 1.0. Owing to the atmospheric pressure in the aerosol flow tube, uptake coefficients between 0.2 and 1.0 can no longer be distinguished, owing to gas diffusion limitations at the mode of the aerosol used. Apparently, reaction 88 proceeds only in neutral or acidic solution, so the reaction product NaOH must be effectively neutralized in order to prevent the increase in pH during HOBr uptake. With regard to HOBr uptake into buffered neutral solution, it is known[252] that reaction 88 may be general-acid-catalyzed according to reaction 92, where HA represents the general acid that transfers a proton during the halogen-exchange reaction.

$$HA + HOBr + Cl^- \rightarrow H_2O + A^- + BrCl \quad (92)$$

In the case of the phosphate buffer, HA has been shown to be the weak acid $H_2PO_4^-$ rather than its salt HPO_4^-. It is therefore possible that the efficiency of HOBr uptake into neutral buffered solution is due to the presence of HA, which is a constituent of the buffering system, rather than due to the presence of H_3O^+. This could mean that simply buffering the aerosol system would bias the outcome of the uptake experiment. In conclusion, the inefficient uptake of HOBr into unbuffered NaCl aqueous aerosol suggests that the loss of HOBr on acidified aerosol is driven by reactive processes and not by the solubility of HOBr in aqueous NaCl solution.

To better define the chemical processes that release and sustain the high concentrations of reactive bromine in the Arctic marine boundary layer in relation to the "bromine explosion" events, Fickert et al.[164] have studied the acid-catalyzed uptake of HOBr on bromide and mixed chloride/bromide solutions using a WWFT under conditions of laminar flow at 10−26 Torr of He or N_2 pressure. The uptake of HOBr on the aqueous solution was found to be limited by gas-phase diffusion, such that the authors effectively measured the diffusion coefficient of HOBr in He and N_2 at 274 K as well as a lower limit of the mass accommodation coefficient given in Table 9. Both Br_2 and BrCl products were observed in the gas phase, the relative yield of which was dependent on the ratio of Cl^- to Br^-. At typically 1 M Cl^- and 10^{-3} M Br^-, more than 90% of the HOBr taken up was released into the gas phase as Br_2, whereas BrCl was the dominant product at $[Br^-] \leq 10^{-5}$ M. The dependence of the relative yields of Br_2 and BrCl as a function of $[Br^-]$ could be explained by the aqueous-phase equilibria 93 and 94, which indicate the importance of secondary chemistry of the primary product BrCl in the presence of Br^-.

$$BrCl + Br^- \rightleftarrows Br_2Cl^- \quad (93)$$

$$Br_2 + Cl^- \rightleftarrows Br_2Cl^- \quad (94)$$

Most importantly, the ratio $[BrCl]/[Br_2]$ does not depend on the competing reactions 88 and 89 of HOBr for Cl^- and Br^-, as it is given entirely by eq 95, which is derived from the known solution equilibria 93 and 94,[255] where K_{93} and K_{94} are the equilibrium constants for the equilibria 93 and 94.

$$[BrCl]/[Br_2] = ([Cl^-]/[Br^-])(K_{94}/K_{93}) \quad (95)$$

Equation 95 predicts a decreasing ratio of $[BrCl]/[Br_2]$ with increasing Br^- concentration, in agreement with observations. Fickert et al.[164] found that the composition of the gas phase reflected the aqueous-phase equilibria 93 and 94, owing to the small solubility of both BrCl and Br_2 in aquoues solution, and confirmed the validity of aqueous-phase equilibria such as reactions 93 and 94 for the modeling of multiphase chemistry. The role of pH in the efficiency of bromine release from the aqueous phase was examined by carrying out HOBr uptake experiments using 1 M Cl^- and 10^{-3} M Br^- solutions at pH between 4 and 10. At pH of less than 6.5, at least 90% of the HOBr taken up onto the aqueous Cl^-/Br^- solution was released into the gas phase as Br_2, whereas no bromine was released in solutions of pH > 9. The authors provide strong support for the acid-catalyzed nature of reactions 88 and 89, studied by Wang and Margerum,[255] in that HOBr and not BrO^- is the reactive species in aqueous solution. The significant drop in the Br_2 yield at high pH was attributed to an as-yet unidentified side reaction that transforms Br_2 or BrCl into a species that is unobservable in the gas phase. The acidity requirement is a strong constraint on the physicochemical system in the atmosphere, ruling out neutral aerosols as the seat of the heterogeneous bromine cycling.

Adams et al.[256] studied the uptake of HOBr on frozen salt solutions, mimicking sea ice, using a laminar flow tube equipped with a quadrupole mass spectrometer. HOBr is efficiently taken up onto the frozen surfaces at temperatures between 233 and 253 K, where it reacts to from the primary products BrCl and Br_2. The relative concentration of BrCl and Br_2, formed by the fast secondary reaction 90, strongly depended on the ratio of Cl^- to Br^- in the solution used to generate the frozen salt solution. For a mixed-salt surface of composition similar to that of sea spray, the major product at low conversion of surface reactants was Br_2. The uptake coefficients are listed in Table 9, and show a slight negative temperature dependence. Variation of the pH of the NaCl/NaBr solution did not affect the γ values, which seem to scale with the Br^- concentration. The reaction mechanism implies the formation of BrCl as a primary reaction product, which goes on to react with Br^- on the frozen surface according to reactions 88−90. This latter point was checked in independent reference experiments and confirmed the hypothesis of the secondary reaction of BrCl. The uptake of HOBr on pure solid NaCl and NaBr substrates was similar to that observed with the frozen solutions.

Motivated by the potential significance of reactions occurring on sea ice, Huff and Abbatt[257] performed studies of the uptake of HOBr on ice surfaces

containing either chloride or bromide as well as a mixture of both ions at 233 and 248 K using a laminar flow coated-wall flow tube at 0.8−2 Torr that was equipped for MS detection. Compared to analogous reactions with HOCl, HOBr reactions were slower than expected, based on the relative rate constants for ambient temperature solution reactions such as HOCl + HBr. The γ values generally increased slightly with acidity, and they were larger for pure bromide compared to pure chloride frozen solutions. At 233 K, the uptake of HOBr definitely saturated, owing to the depletion of H_3O^+ and/or halide, whereas such was not the case at 248 K, where sustained uptake of HOBr and formation of BrCl and Br_2 was observed. This difference in the uptake kinetics is attributed to the presence and stability of different phases of the pure and mixed frozen alkali halide solutions, some of which are dependent on the eutectic point ($NaBr/H_2O$). The importance of the surface composition for interfacial kinetis has been discussed in section 3.7.

At both 233 and 248 K, Br_2 was formed exclusively from pure bromide films, and BrCl was exclusively generated from pure chloride films. In the bromide−chloride mixture of appropriate ratio mimicking the composition of seawater ($[Cl^-]/[Br^-] = 288:1$), BrCl was the only observed product at 233 K, whereas at 248 K a mixture of BrCl and Br_2 was observed. Thus, HOBr reacted only with Cl^- at 233 K, whereas it reacted with both Cl^- and Br^- at 248 K in mixtures of Cl^- and Br^-. It was established that the Br_2 formed at the latter conditions originated mainly from the primary reaction 89, rather than from the secondary reaction 90. The system behaved as if the ions were mobile within a liquid phase at 248 K, but not at 233 K. A qualitative model was proposed in which HOBr interacted with the dissolved halide by forming a complex of the type $HOBr{\cdot}X^-$ whose halogen exchange was assisted by the proximity of the H_3O^+ from the acid component of the frozen substrate. On the other hand, a configuration of similar energy, namely $BrOH{\cdot}X^-$, does not lead to halogen exchange, which is the reason for absolute product yields that are markedly smaller than 100%. For this reason, reaction probabilities for the formation of BrCl or Br_2 were higher on acidified films than on films formed from neutral frozen solutions. Without going into any details, the complexation of HOBr could qualitatively explain all major experimental results. The major obstacle to a quantitative understanding of the ternary condensed-phase system seems to be detailed knowledge about the halide-containing phases as a function of temperature in terms of the composition of the interface that is communicating with HOBr.

Wachsmuth et al.[258] adopted an unconventional approach in their study of the uptake of HOBr on NaBr aerosol of 100 nm average diameter at 37% relative humidity by using short-lived radioactively labeled HO*Br, resulting from the decay of Se atoms adsorbed on a quartz plate in the presence of adsorbed H_2O at 130 °C. The authors verified that the NaBr aerosol remained a supersaturated liquid (deliquescent) aerosol, as the efflorescence point of NaBr aqueous aerosol was found to be below 37% rh. The special feature of this study was that an extremely low HOBr concentration of approximately 300 cm^{-3} was used, in order to avoid the depletion of the aerosol in protons that ordinarily would stall reaction 89. Under these conditions, at maximum one HOBr molecule was taken up per particle. The authors thus avoided the problem of the proton control of the reaction, which other researchers circumvented by working with an acidified aerosol. The rate of uptake was clearly limited by the mass accommodation coefficient, which was calculated to be 0.6 ± 0.2. This value is a factor of 10 larger than estimates used in numerical models. Wachsmuth et al.[258] tried to validate their innovative but complex approach using uptake of HOBr on dry aerosol, especially since one may raise questions associated with the chemical speciation of the radioactively labeled bromine. On the bais of uptake experiments of HO*Br on solid NaBr aerosol, an uptake coefficient of at least 0.5 was estimated which is higher by a factor of 3 than that obtained in the uptake study done by Mochida et al.[254] Future experiments will have to show if the significantly larger value for γ may be due to the residual level of H_2O vapor in the aerosol flow tube, corresponding to 6% rh, or to some other factor affecting the uptake kinetics. This 6% rh may be sufficient to lead to an appreciable accumulation of SAW on the solid NaBr, thus increasing the reaction probability of reaction 89.

Concluding Remarks. HOBr readily reacts with salt aerosol and frozen aqueous salt solutions, as well as in solution, in what appears to be a general-acid-catalyzed halogen-exchange reaction. This indicates that HOBr, rather than BrO^-, is the reactive species. The reaction comes to a halt in unbuffered salt aerosols because of the increase in pH with the progress of reaction, in agreement with the mechanistic statement given above. The primary reaction product is BrCl, which is consumed in a fast secondary reaction by excess bromide to yield Br_2. This secondary chemistry is, in part, responsible for the enrichment in Br_2 that results from reaction of HOBr on frozen aqueous salt solutions, mimicking seawater. However, HOBr undergoes competitive heterogeneous decomposition on solid alkali salts, resulting from the bimolecular self-reaction, yielding Br_2O that is unstable and decomposes to O_2 and Br_2.

3.9. Reactions of HOI ($IONO_2$)

Mössinger and Cox[120] investigated the uptake of HOI generated in situ on solid NaCl, NaBr, and sea salt using a coated-wall flow tube equipped with a differentially pumped mass spectrometer. On exposure of HOI to NaCl and NaBr, prompt formation of ICl and IBr was observed, according to reactions 96 and 97.

$$HOI + NaCl \rightarrow ICl + NaOH \quad (96)$$

$$HOI + NaBr \rightarrow IBr + NaOH \quad (97)$$

When HOI was exposed to sea salt, IBr was observed to be the first product that appeared, followed by the formation of ICl in the gas phase. Apparently, reaction 97 takes place until complete exhaustion of the

Table 10. HOI + KBr, NaCl → Products

symbol	uptake coefficient	substrate	temp/K	reference
γ_{ss}	$(6 \pm 2) \times 10^{-2}$	solid KBr powder, thin solid film	300	Allanic and Rossi, 1999[264]
	$(4 \pm 2) \times 10^{-2}$	solid NaCl powder, thin solid film	300	
	$(5 \pm 2) \times 10^{-2}$	$NaNO_3$ grains	300	
γ_{ss}	$(3.4 \pm 0.9) \times 10^{-2}$	solid NaBr	278−298	Mössinger and Cox, 2001[120]
	$(1.6 \pm 0.4) \times 10^{-2}$	solid NaCl		
	$(6.1 \pm 2.1) \times 10^{-2}$	solid sea salt		
γ_{ss}	$>5 \times 10^{-2}$	frozen solution of 2 M NaCl + 3×10^{-3} M NaBr	243	Holmes, Adams, and Crowley, 2001[261]
	$>10^{-2}$	solid homogeneous mixture of 2 M NaCl + 3×10^{-3} M NaBr	298	

bromide supply, after which reaction 96 rises to importance, thus pointing toward a definite preference for bromine release upon HOI interaction. On a fresh surface of sea salt, the initial uptake was time-dependent and fell toward the steady-state value reported in Table 10. It, in turn, slowly decreased with time by a factor of between 2 (NaCl) and 4 (NaBr, sea salt) due to aging or passivation. In all cases, no dependence of γ on relative humidity could be measured, as water vapor up to 23% relative humidity had no effect on γ_{ss}. The authors explained this with the fact that the water background in most of their experiments was above the deliquescence point of 7% rh for NaOH. The initial product yields on pure NaCl and NaBr substrates were <100% and 100%, respectively, as ICl had a tendency to remain physically adsorbed on the NaCl surface once formed, such that it desorbed some time later. On sea salt substrates, initially about 80% of the HOI was converted to ICl and IBr, and on all substrates, the yield decreased with the exposure to HOI because of secondary reactions of the primary products with solid NaOH. The uptake coefficients of HOI, ICl, and IBr on the solid reaction product NaOH were significantly lower, such that the initial product yields faithfully represent the primary process. Quantitative estimates show that, in all cases, only a small fraction (that is, ≪1%) of all available Cl^- and Br^- ions present in the sample had reacted with HOI. To explain the prompt appearance of IBr, it is thought that part of this selectivity of HOI for bromine activation in solid sea salt stems from halide segregation processes, in which bromide is enriched on the substrate surface. This halide segregation process has been observed before on bromide-doped NaCl,[259,260] and may perhaps also take place on frozen solutions of chloride and bromide, mimicking frozen seawater.

Holmes et al.[261] performed uptake experiments of a mixture of HOI and $IONO_2$ on frozen aqueous solutions of NaCl and NaBr at 243 K, as well as on solid mixtures of NaCl and NaBr at 298 K, using a flow tube equipped with a differentially pumped mass spectrometer, operated under laminar flow conditions. Owing to a side reaction during the generation of HOI, which was synthesized from the reaction of atomic O with an alkyl iodide, $IONO_2$ always occurred together with HOI, both of which were monitored by mass spectrometry in what appear to be superb MS signals (ion counting) for both HOI at *m/e* 144 (HOI^+) and $IONO_2$ at *m/e* 46 (NO_2^+), with an excellent signal-to-noise ratio. Holmes et al.[261] present convincing arguments that the heterogeneous kinetics of both HOI and $IONO_2$ on the frozen salt solution and on the solid salt substrates are quite similar to each other. On a frozen salt solution containing 2 M NaCl and 2×10^{-3} M NaBr, HOI/$IONO_2$ were taken up efficiently in a first-order reaction, the γ value of which is listed in Table 10. Molecular IBr was instantaneously observed as a result, with ICl surging some time later at the expense of IBr, in agreement with results obtained by Mössinger and Cox.[120] Despite the different time profiles of IBr and ICl generation, the summed concentration is very close to the sum of HOI and $IONO_2$ taken up, thus leading to a 100% yield of reaction products. No evidence of other reaction products, such as I_2, BrCl, Br_2, or Cl_2, was obtained. The delayed formation of ICl on frozen salt substrates has also been observed in uptake experiments of HOI/$IONO_2$ on pure frozen NaCl solutions. The reaction mechanism initially involves the competition of both Cl^- and Br^- for HOI/$IONO_2$ according to reactions 96 and 97. The preference for release of Br-containing products is attributed to the preferred reaction rate constant for IBr compared to ICl formation, which was deduced from the analogous reaction in solution,[261−263] where the rate constant for reaction 97 was a factor of 114 larger than that for reaction 96. In addition, part of the preference for bromine release comes from the incidence of the fast halogen-exchange reaction 98, which has been verified in separate reference experiments (see Table 12).

$$ICl + Br^- \rightarrow ICl + Cl^- \qquad (98)$$

Moreover, the surface concentration of Br^- is not known with certainty, but it is believed that there is an enrichment of bromide at the interface, which will favor reaction 97 over reaction 96 at the beginning of the halogen exchange.[259,260] Once the Br^- supply at the interface is nearing exhaustion with the progress of reaction, desorption of ICl becomes competitive with reaction 98, which leads to the increase of the observed ICl gas-phase concentration with time. Repetitive exposure experiments revealed that the duration of IBr formation and the delay of the ICl appearance became smaller with increasing number of uptake experiments. However, there was also evidence that Br^- was resupplied to the interface during the intervals of two consecutive uptake experiments. Concerning the reaction mechanism for reaction of $IONO_2$ with frozen salt solutions, the authors were unable to determine whether a direct reaction of $IONO_2$ with the halide ions took place, or whether the process involved prior hydrolysis of $IONO_2$ to HOI, which subsequently generated the

observed reaction products IBr and ICl in a fast secondary reaction.

The value for γ listed in Table 10 was derived from linear decay plots of the relative HOI concentration. The decay for the marker of $IONO_2$, namely *m*/*e* 46, was not of single-exponential type, as it involved the nonreactive and therefore nondecaying component NO_2. Deconvolution of the observed decay rate into the two components led to a γ value that is identical to the one for HOI within experimental uncertainty. Moreover, this γ value is consistent with the mass accommodation coefficient derived from the measurement of the diffusion coefficient of HOI/$IONO_2$ in He at 243 K, which is part of the same study. Experiments performed to examine the uptake of HOI onto solid salt substrates that were generated from evaporation of the salt solutions used to generate the frozen salts discussed above resulted in $\gamma > 10^{-2}$ at 298 K. The solid salt mixtures apparently do not require a high gas-phase humidity or high surface water content to proceed, in agreement with the presence of SAW. The uptake experiments on solid salts showed the same characteristic time-dependent product formation of IBr and ICl as on frozen salt solutions at 243 K. In conclusion, the uptake of HOI/$IONO_2$ on both frozen (243 K) and solid (298 K) salt substrates is controlled by gas-phase diffusion rather than by surface processes in these flow reactor experiments.[261]

Allanic and Rossi[264] measured the uptake rates of HOI in a Teflon-coated Knudsen flow reactor on a variety of substrates, including solid NaCl and KBr, using MS detection. HOI was formed in situ in the reaction of atomic oxygen generated in a microwave discharge of pure O_2 with C_2H_5I. Owing to the low total pressures in the flow reactor, HOI underwent significant decomposition, both in the HOI source region and on the gold-plated parts of the flow reactor. The heterogeneous decomposition was accounted for in the measurement of the uptake coefficient displayed in Table 10. The interaction of HOI on solid NaCl only led to heterogeneous decomposition of HOI to I_2, at the exclusion of the expected reaction product ICl (reaction 96). On solid KBr, both I_2 and IBr have been recorded as reaction products, with a branching ratio between heterogeneous decomposition (I_2) and the halogen-exchange reaction 97 (IBr) of approximately 6:1. This trend toward decomposition of HOI taking place on salt surfaces was confirmed by studying the interaction on solid $NaNO_3$, which also led to the formation of I_2 and to identical values of γ for HOI within experimental error. This study clearly shows the limitation of the use of a flow reactor operating in the molecular flow regime in cases where the gas-phase species is prone to decomposition.

Concluding Remarks. HOI has a propensity for the formation of IBr when reacting on either sea salt or a solid mixed chloride/bromide salt substrate, as well as on mixed-halide frozen solutions, mimicking sea ice. The prompt appearance of IBr is followed by a delayed formation of ICl, which is also the case for pure chloride salts. Akin to HOBr, it reacts efficiently with the ambient and frozen salt substrates. At least three reasons may be cited for the preferential reaction of HOBr and HOI with bromide: (a) larger rate constant for bromide compared to chloride reaction, in analogy to the situation in solution at 300 K; (b) fast secondary reaction, converting ICl to IBr in the presence of excess bromide; and (c) surface segregation processes, leading to the enrichment of bromide on solid chloride/bromide substrates.

3.10. Reactions of Cl_2

Molecular chlorine is a form of active chlorine that has been directly observed in a convincing manner in the tropospheric marine environment[61] using sensitive atmospheric pressure ionization (API) mass spectrometry, although the origin and the chemical reactions responsible for the formation of Cl_2 have not been clearly elucidated as yet. Using a tandem mist chamber, active chlorine (Cl_2*), which includes Cl_2 and HOCl not trapped in the acidic mist chamber, has been measured in the range from <26 to 254 pptv Cl in the marine atmosphere.[63,207] Using a photoactive halogen detector with scavenger hydrocarbons, photolytically active species Cl_p, which include Cl_2, HOCl, ClNO, $ClNO_2$, and $ClONO_2$, have been detected in the range from <9 to 100 pptv as Cl_2 in the Canadian Arctic at Alert.[64,65] In addition, recent studies have revealed the possibility of Cl_2 formation, resulting from the heterogeneous reaction of O_3 with deliquesced salt aerosol,[265] and Br_2 formation from deliquesced NaBr aerosol.[19]

Frenzel et al.[247] have studied the uptake of Cl_2 on nitrite-containing aqueous solutions in a WWFT and have observed an essentially gas-diffusion-controlled rate of uptake that corresponded to $\gamma = 6.5 \times 10^{-5}$, measured at the lowest nitrite concentration of 1×10^{-3} M. The primary product is $ClNO_2$, formed at a maximum yield of 50%, which goes on to react with the remaining nitrite in a fast secondary reaction, as discussed in section 3.5. The reaction occurs according to eq 99.

$$Cl_2 + NO_2^- \rightarrow ClNO_2 + Cl^- \qquad (99)$$

Nitryl chloride is formally the anhydride of HCl and nitric acid, corresponding to chlorine in the −I and nitrogen in the +V oxidation states. Reaction K1, therefore, describes the oxidation of nitrite by molecular chlorine, resulting in chloride and nitryl chloride, whose Cl formal oxidation state is Cl(−I). It has been noted by Zetzsch and co-workers in the past that some experiments performed in aerosol chambers may be subject to heterogeneous formation of Cl_2 that apparently takes place at the walls of the chamber[22−26] and which they regard as an artifact. Owing to the photolytically unstable nature of Cl_2, special care is required to account for the presence of parasitic atomic chlorine in large static aerosol chambers that may lead to fast chain reactions.

Mochida et al.[266] performed uptake experiments of Cl_2 on both sea salt and pure bromide and chloride substrates, using a Knudsen flow reactor equipped with a mass spectrometer. Uptake coefficients of Cl_2 measured on powder samples were corrected using the pore diffusion model they fitted to the mass

Table 11. Cl_2 + 2MBr (M = Na,K) → Br_2 + 2MCl

symbol	uptake coefficient	substrate	temp/K	reference
γ_0	$(2.4 \pm 1.3) \times 10^{-2}$	thin film of NaBr	300	Mochida et al., 1998[266]
	$(2.1 \pm 0.4) \times 10^{-2}$	NaBr powder, 10−100 μm		
	$(3.1 \pm 1.1) \times 10^{-2}$	natural sea salt		
	$(2.2 \pm 1.1) \times 10^{-2}$	synthetic sea salt		
γ_0	$(2.7 \pm 0.3) \times 10^{-2}$	solid KBr	300	Aguzzi and Rossi, 1999[228]
γ_0	1.1×10^{-2}	0.01% NaBr ice film, pH = 7	233	Huff and Abbatt, 2000[251]
	2.5×10^{-2}	0.1% NaBr ice film, pH = 7		
	6.0×10^{-2}	1% NaBr ice film, pH = 7		
	9.8×10^{-2}	5% NaBr ice film, pH = 7		
	$<2.0 \times 10^{-3}$	mixed chloride/bromide−ice film, pH = 7	233	
	4.8×10^{-2}	mixed chloride/bromide−ice film, pH = 7	248	
γ_0	$<2.8 \times 10^{-2}$	2 M NaCl + 3×10^{-3} M NaBr frozen solution	233	Adams, Holmes and Crowley, 2002[256]

dependence of the observed initial value of the Cl_2 uptake coefficient and were independent of the Cl_2 concentration. The corrected γ values, obtained from Cl_2 uptake on salt powder and on bromide thin films, agreed within experimental uncertainty, which lends credence to the correction scheme applied. The expected primary product BrCl was observed only in small quantities, owing to the fast secondary reactions, 51 or 90, of BrCl on the bromide substrate, leading to a near-unity yield of 92 ± 8% of Br_2 for the overall reaction on all salt samples. Synthetic sea salt, natural sea salt, and bromide salt all led to essentially identical values of γ, within experimental uncertainty, regardless of the type of cation (Na^+ or K^+) and presentation (powder, thin salt film). In addition, the yields of Br_2 are identical, within experimental uncertainty, for both pure bromides (NaBr, KBr) and sea salt substrates, despite the disparity in the bulk abundance between chloride and bromide (667:1). As discussed above, this Br_2 enrichment may be due either to bromide surface segregation[259,260] and/or to a rate enhancement specific to bromide.[88,262,263] The corrected value of γ for the nonreactive interaction of Cl_2 on NaCl powder was an order of magnitude lower than that for the reactive case and was ascribed to physical adsorption.

Aguzzi and Rossi[228] performed real-time pulsed-dose experiments using a Knudsen flow reactor equipped with a mass spectrometer on solid KBr at ambient temperature in order to provide reference experiments for the interpretation of results that implied fast secondary reactions, such as is the case for $ClONO_2$ + KBr (reaction 50). In this case, the primary product of the reaction, namely BrCl, was not observable because it reacted away faster than it was formed, resulting in Br_2, as will be discussed below. The real-time technique is an ideal tool to visualize the reaction mechanism and the temporal sequence of the different reactions in a comlex mechanism.

$$Cl_2 + Br^- \rightarrow BrCl + Cl^- \qquad (100)$$

$$BrCl + Br^- \rightarrow Br_2 + Cl^- \qquad (101)$$

Molecular bromine, along with a very small amount of BrCl, was observed as reaction product. The γ value was independent of pH in the range 2−7, in contrast to the study of HOCl uptake on the same substrate and temperature. However, there is a direct relationship between higher reaction probability and larger amounts of bromide in the ice film up to a concentration of 3 wt %, at which point the ice surface is completely covered with bromide ions (see Table 11). At this point, the maximum reaction probability of 0.1 is reached, and any increase in bromide concentration in the ice film beyond 3 wt % does not lead to a higher reaction probability. The results of this study suggest that, within a factor of 5, all the bromide ions in the ice film were accessible to Cl_2. In addition, uptake of Cl_2 at 233 K is consistent with a surface reaction onto a solid according to an Ely−Rideal mechanism, rather than mass accommodation into a liquid atop the substrate surface. Owing to the weak interaction of Cl_2 with ice, the Eley−Rideal mechanism is preferred over the Langmuir−Hinshelwood model. Cl_2 is totally unreactive on a chloride−ice film at pH = 7 and in the range 0.1−1 wt %.

On mixed chloride/bromide−ice substrates that were chosen so as to simulate reaction on Arctic sea ice, Cl_2 did not react at 233 K, presumably because of the large amount of unreactive chloride in the mixed-halide−ice film. The absence of reaction for Cl_2 is surprising, as the bromide concentration in the mixed-halide−ice film was equal to that in the pure bromide−ice film that gave rise to a reaction (Table 11). It is possible that the chloride, which is present in 300-fold excess over bromide, displaced the latter from the interface. Also, the absolute concentrations of the halides in the sea salt surrogate prepared by Huff and Abbatt were a factor of 10 larger than those measured in natural seawater, such that the results of this laboratory study may, perhaps, not be directly transferable to the atmospheic situation.

At 248 K, the above-mentioned halide−ice mixture gave rise to a reaction when exposed to Cl_2, in contrast to experiments performed at 233 K. As in experiments with pure bromide films, a time-dependent loss rate of Cl_2, owing to the depeletion of bromide at the interface, was observed to follow first-order kinetics. However, γ scales with the bromide content and is, in general, larger for the mixed bromide/chloride frozen solution compared to the pure bromide at equal amounts of bromide, for instance, for a 0.1% bromide film at 248 K and pH = 7. The difference between the pure bromide and the mixed chloride/bromide films has to do with the freezing process and the associated composition of the substrate interface. The temperature of 248 K is between the eutectic temperatures of $NaCl/H_2O$ (252 K) and

Table 12. XY (Interhalogens, Br_2) + MZ (Alkali Halides) → Products

symbol	uptake coefficient	substrate	temp/K	reference
		BrCl + Na(K)Br → Br_2 + Na(K)Cl		
γ_0	1.8×10^{-2}	0.1% NaBr ice film, pH = 2, 7	233	Huff and Abbatt, 2000[251]
	4.2×10^{-2}	1% NaBr ice film, pH = 7		
γ_0	0.14	solid KBr	298	Aguzzi and Rossi, 1999[228]
	6×10^{-2}	solid NaCl		
γ_0	$>3.4 \times 10^{-2}$	2 M NaCl + 3×10^{-3} M NaBr frozen solution	233	Adams, Holmes, and Crowley, 2002[256]
		Br_2 + NaCl(KBr) → Products		
γ_0	4×10^{-3}	solid NaCl	298	Aguzzi and Rossi, 1999[228]
	3×10^{-3}	solid KBr		
γ_0	$>2.5 \times 10^{-2}$	2 M NaCl + 3×10^{-3} M NaBr frozen solution	233	Adams, Holmes, and Crowley, 2002[256]
	$>10^{-2}$	3×10^{-3} M NaBr frozen solution	233	
		ICl + NaBr → IBr + NaCl		
γ_{ss}	$(6.8 \pm 1.8) \times 10^{-3}$	solid NaBr	298	Mössinger and Cox, 2001[120]
	$(1.2 \pm 0.4) \times 10^{-3}$	solid sea salt	298	
γ_0	$>10^{-2}$	2 M NaCl + 3×10^{-3} M NaBr, frozen	243	Holmes, Adams, and Crowley, 2001[261]
		IBr + NaBr → IBr(ads)		
	$(6 \pm 2) \times 10^{-4}$	solid NaBr	298	Mössinger and Cox, 2001[120]

NaBr/H_2O (245 K), so the predicted composition of the halide−ice mixture would be ice, solid NaCl, and a concentrated solution of NaBr, onto which the reaction presumably takes place. It thus seems that the detailed surface composition of frozen substrates has a significant effect on the heterogeneous reaction kinetics. Absolute product yields in terms of the sum of Br_2 and BrCl were only 50% of the value expected on the basis of the quantity of HOCl lost. The balance was attributed to BrCl that was formed on the ice as a primary product, according to reaction 100, but remained adsorbed so as to avoid detection by MS. The relative yield was 98−99% Br_2 and 1−2% BrCl, making Br_2 the major reaction product under all conditions that were explored.

Adams et al.[256] studied the uptake of Cl_2 on mixed frozen salt solutions using a fast laminar flow tube equipped with a quadrupole mass spectrometer. Table 11 reveals an efficient uptake of Cl_2, resulting in Br_2 that was presumably formed in the secondary reaction 101 from the primary product BrCl. The uptake of Cl_2 as well as the formation of Br_2 decreased with time.

Concluding Remarks. Molecular chlorine is quite reactive toward bromide presented as a solid, as well as frozen aqueous solutions, down to temperatures of 248 K. At low temperatures, mixtures of chlorides and bromides seem to more reactive than bromides alone because the bromide is present as a salt brine that undergoes reaction with Cl_2, whereas the chloride is present as a frozen solid. This underlines the need to pay particular attention to phase diagrams in aqueous ternary salt systems when investigating heterogeneous reactions at low temperatures. Invariably, Br_2 has been detected as the major product, because the primary product BrCl undergoes a fast secondary reaction with bromide.

3.11. Reactions of BrCl, Br_2, ICl, and IBr

Molecular bromine is an active halogen compound that is easily photolyzed in the atmosphere and has so far not been detected in the environment, as is the case for the other interhalogens. Frenzel et al.[247] have performed an uptake study on dilute aqueous nitrite-containing solutions using a WWFT. Br_2 was found to be lost at a high rate on a 5×10^{-3} M nitrite solution, with the rate of uptake being near the gas-phase diffusion limit. The primary product, $BrNO_2$, appears instantaneously in essentially 100% yield according to reaction 102.

$$Br_2 + NO_2^- \rightarrow BrNO_2 + Br^- \qquad (102)$$

Nitryl bromide subsequently undergoes fast secondary reactions that have been discussed in section 3.6 in relation to $ClNO_2$.

To unravel the reaction mechanism of HOCl and HOBr uptake on halide-containing solutions or ice films, Huff and Abbatt[251] performed uptake experiments of BrCl in a low-pressure coated-wall laminar flow tube equipped with a differentially pumped mass spectrometer. Because the mentioned reaction mechanism is complex, owing to the fast secondary reaction of the primary product with bromide, reactions 90 and 83 have been investigated in some detail in relation to HOCl and HOBr uptake, respectively. The rate of uptake at 233 K decreased with time, in agreement with the decrease of the surface bromide concentration. The rate of uptake was first order in BrCl, independent of pH in the range 2−7, and increased with increasing surface bromide concentration in the range 0.1−1% NaBr, as displayed in Table 12. Experimentally, small signals of BrCl are observed in HOCl and HOBr uptake experiments on aqueous frozen halide solutions at 233 K.[251,257] This may be due to either the rate-limiting production of the BrCl primary product (reactions 82 and 88) or the slow desorption of BrCl off the halide/ice substrate (reaction 103).

$$BrCl(ads) \rightarrow BrCl(g) \qquad (103)$$

Huff and Abbatt[251] observed that the gas-phase concentration of BrCl increased at the end of the reaction (that is, as the bromide supply on the substrate decreased) and concluded that reaction 103 became competitive with reaction 83 or 90 for both HOCl and HOBr. They were thus able to show that most of the BrCl formed in the primary reaction stayed on the ice surface at 233 K. A comparison of γ values for the Cl_2 and HOCl halide/ice interaction

in Tables 11 and 8 reveals that BrCl reacts with bromide more slowly than Cl_2 at 233 K and at the same rate or slower than HOCl, depending on pH. This result is in stark contrast to the reactivity of BrCl on solid KBr, on which BrCl reacts significantly faster than Cl_2.[228] However, the result that γ increases with decreasing pH is unique to HOCl (Table 8), as no such dependence has been found for Cl_2 or BrCl.

Mössinger and Cox[120] investigated the uptake of ICl and IBr on solid NaCl, NaBr, and sea salt using a coated-wall flow tube equipped with a differentially pumped mass spectrometer. No interaction of ICl and IBr was found on NaCl, and IBr did not interact with NaBr, either. However, ICl reacted on NaBr according to reaction 104.

$$ICl + NaBr \rightarrow IBr + NaCl \qquad (104)$$

The fast initial uptake decreased to a steady-state value on the time scale of minutes. When NaBr was used as a reactive substrate, IBr was observed as a product at a yield of 100 ± 34% initially, later decreasing to 70 ± 34%, concomitantly with a loss of reactivity with exposure to ICl. On sea salt, initially only IBr was observed, similar to the heterogeneous reaction of HOI on sea salt; later the branching ratio was 30 ± 34% to 70 ± 34% of IBr to ICl, respectively, the latter of which was only physically adsorbed on the sea salt substrate.

On exposure of IBr to sea salt, adsorption was observed[120] without formation of gas-phase reaction products. However, after the IBr uptake was halted, all the initially adsorbed IBr desorbed, pointing to a nonreactive physical adsorption process of IBr on sea salt.

Holmes et al.[261] performed experiments on ICl vs IBr interaction on frozen salts by performing uptake experiments at 243 K in a laminar coated-wall flow tube equipped with a differentially pumped mass spectrometer, using a frozen solution of 2 M NaCl and 3×10^{-3} M NaBr, reflecting the concentration ratio in seawater. They observed efficient uptake of ICl, resulting in stoichiometric amounts of IBr according to reaction 104. The uptake of IBr on frozen salt solutions showed very different characteristics, in that no formation of reaction products and only physical adsorption were observed. After the inflow of IBr was halted, IBr quantitatively desorbed again at 243 K.

Aguzzi and Rossi[228] have studied the heterogeneous interaction of BrCl and Br_2 on both solid NaCl and KBr using real-time pulsed-valve experiments performed in a Knudsen flow reactor equipped with a mass spectrometer. This technique was ideally suited to investigate reactive and nonreactive systems that were affected by the occurrence of fast secondary reactions, such as in $ClONO_2$ + KBr (reaction 50). BrCl, the primary reaction product of reaction 50, reacts away so fast on solid KBr that its formation is not observable in continuous-flow experiments that reveal only Br_2 as its final reaction product, according to reaction 83.

However, in pulsed-valve experiments, BrCl is observable, such that the temporal sequence of the complex reaction system may be resolved. Tables 11 and 12 reveal that BrCl reacts away faster by a factor of 5 on solid KBr, according ro reaction 83, than it is formed in reaction 100. At ambient temperature, Br_2 physically adsorbs on adsorption sites of NaCl and KBr, as does BrCl, owing to the stability of the corresponding trihalide complex. However, the adsorption quickly saturates once a few percent of the surface area of the salt substrate are occupied. Another manifestation of the existence of the trihalide ionic complex precursor mechanism is the fact that the uptake coefficient for nonreactive BrCl adsorption on solid NaCl decreases with increasing gas residence time in the flow reactor: for instance, γ decreases from 6×10^{-2} to 1×10^{-2} when the gas-phase residence time increases from 0.35 to 2.50 s. The γ values for all nonreactive uptake experiments involving Br_2/KBr, Br_2/NaCl, and BrCl/NaCl are of the order of a few percent, which may correspond to the characteristic rate of interaction with the precursor site. Interestingly enough, no uptake of Cl_2 on NaCl has been observed in real time, which may have to do with the instability of the trihalide complex $Na^+Cl_3^-$ in this case.

Adams et al.[256] studied the uptake of BrCl and Br_2 on mixed frozen salt solutions using a fast laminar coated-wall flow tube equipped with a quadrupole mass spectrometer. Table 12 reveals that BrCl is taken up efficiently on the mixed chloride/bromide salt solution. The increase in gas-phase Br_2 is approximately equal to the summed loss of BrCl and Cl_2 (from an impurity in BrCl). If the initial Cl^--to-Br^- ratio is close to 660, as found in seawater, BrCl will react on the surface to form Br_2 according to reaction 101. Both the rate of uptake of BrCl and the formation of Br_2 decrease on the time scale of 500 s at 233 K. Br_2 also interacted strongly both with mixed frozen Cl^-/Br^- and with pure frozen Br^- substrates in halogen interconversion reactions. On pure bromide at 233 K, Br_2 is taken up to react with the substrate and released to form a different Br_2 molecule, which was arrived at by performing experiments with isotopically labeled NaBr, enabling the distinction between the reactant and product Br_2.

3.12. Reactions of O_3

Heterogeneous reactions of O_3 with natural sea salt components have been proposed to be responsible for halogen release in the marine boundary layer, where large amounts of sea salt aerosol exist on a global scale. Chemically speaking, the ozone interaction amounts to oxidation of bromide and possibly chloride, resulting in the release of photochemically active volatile halogen species. Both Cl_2[19] and Br_2[265,267] have been observed to be formed in laboratory experiments as a result of the interaction of O_3 with natural sea salt, but less so with pure alkali halides. In the environment, salt substrates may be found in sea salt aerosol that occurs most often in deliquesced form but also in the presence of seawater ice at high latitudes, where sea salt crystals are embedded in or located on the ice matrix. The heterogeneous reaction of O_3 with sea salt and concomitant Br_2 release is important to the mechanism of bromine

Table 13. O_3 + Substrates → Products

symbol	uptake coefficient	substrate	temp/K	reference
γ_{ss}	$(1.3 \pm 0.3) \times 10^{-6}$	NaCl, NH_4NO_3, $(NH_4)_2SO_4$	235−299	Il'in et al., 1991[269]
γ_{ss}	$<1 \times 10^{-4}$	NaCl aerosol, unbuffered, pH = 7.2	300	Abbatt and Waschewsky, 1998[225]
γ_0	10^{-2}−10^{-3}	synthetic sea salt, 10−100 μm	300	Mochida et al., 2000[266]
	$(9.7 \pm 4.6) \times 10^{-4}$	natural sea salt, 10−100 μm		
	$<10^{-5}$	NaBr, NaCl, KCl powder, 10−100 μm		
	1×10^{-3}	$MgBr_2$ hydrate		
	$(6.3 \pm 3.0) \times 10^{-4}$	$CaBr_2$ hydrate		
γ_0	$(3.6 \pm 1.0) \times 10^{-2}$	NaCl/$FeCl_3$ (1 wt %), 10−100-μm powder	298	Sadanaga et al., 2001[20]
	$(3.3 \pm 1.2) \times 10^{-2}$	NaCl/$FeCl_3$ (0.1 wt %), 10−100-μm powder		
	$(1.3 \pm 0.8) \times 10^{-3}$	NaCl/Fe_2O_3 (1 wt %), 10−100-μm powder		
	$(3.2 \pm 1.1) \times 10^{-2}$	SSS/$FeCl_3$ (1 wt %), 10−100-μm powder		

cycling in relation to the "bromine explosion" events taking place in the Arctic, because this reaction may represent the appropriate initiation step, even though the original source of atomic Br needed to initiate the chain destruction of ozone remains controversial.[268] The special significance of ozone oxidation of halides in halide-containing condensed phases lies in the absence of any participation of NO_x or NO_y that enables these processes in pristine unpolluted environments.

Il'in and co-workers[269] performed experiments under static conditions by observing the O_3 concentration decay in cylindrical coated-quartz reaction vessels using optical absorption at 254 nm in the presence of Ar in the temperature interval 223−305 K. Typical O_3 and Ar pressures were 30−125 mTorr and 2 Torr, respectively, and all decays were of single-exponential type, indicating first-order loss rate coefficients that were also found to be independent of ozone concentration. All salts investigated had identical uptake coefficients, and all were independent of temperature within experimental uncertainty. Repetitive exposure experiments led to γ values identical to the first uptake of O_3, and the reaction mechanism reportedly involves a precursor state prior to surface reaction. No reaction products are reported. The conclusion of this study is that the uptake coefficient of O_3 is quite small on the polar salt surface down to 223 K, a conclusion that is consistent with the results of another kinetic study performed by Alebić-Juretić on salt powders using a fluidized bed reactor.[269]

Abbatt and Washewsky[225] performed uptake experiments of O_3 on liquid NaCl aerosol flowing down across an aerosol flow tube at atmospheric pressure. The gases were analyzed using CIMS detection after passage through a pinhole into the detection chamber. The NaCl aerosol that formed in an ultrasonic nebulizer had a bimodal distribution (large average diameter, 2−4 μm; small, <1 μm), with typical surface areas and particle number densities in the range of $(1-6) \times 10^{-3}$ cm^2/cm^3 and $(1-4) \times 10^4$ particles/cm^3, respectively. No loss of ozone was detected in experiments performed on neutral pH aerosols; therefore, an upper limit for γ is given for unbuffered NaCl aerosol and NaCl aerosol buffered at pH = 7.2 using NaH_2PO_4/Na_2HPO_4. For the interaction of ozone with acidified aerosols at pH = 0.3, which had been generated by adding HCl to the NaCl nebulizing solution, a 5−10% decline in O_3 was detected for high aerosol surface areas of approximately 7×10^{-3} cm^2/cm^3 and long reaction times (~8 s). Coincident with the decline in the ozone signal, an increase of the Cl_2 signal occurred, which would correspond to an uptake coefficient of $(1-2) \times 10^{-4}$ if the reaction were taking place on the aerosol surface. However, it was judged more likely that this oxidation reaction of chloride took place at the walls of the flow tube or on wall-deposited aerosols, as has been noted before by Zetzsch and co-workers[22−26] in relation to work carried out using large static chambers.

Mochida et al.[270] studied the uptake of O_3 on both commercially available and natural sea salts, as well as on pure model compounds, using a low-pressure Knudsen flow reactor equipped with a differentially pumped mass spectrometer. The uptake was below the detection limit for pure NaBr, corresponding to $\gamma < 10^{-5}$ (see Table 13), whereas reactive uptake of O_3 on two types of commercial sea salts, as well as on natural sea salt, was in the 10^{-3} range. Yields of 50−100% of Br_2 were detected. These uptake coefficients were approximately 3 orders of magnitude larger than that on bulk bromide solution estimated from the known liquid-phase kinetics and uptake properties of O_3 on bulk liquids. The γ values displayed in Table 13 correspond to initial rates of ozone uptake and were corrected for penetration of O_3 into deeper layers using the pore diffusion model. The rate law for O_3 uptake was first order on the natural sea salt and on one synthetic sea salt, whereas it was not first order on the other type of synthetic sea salt. The initial γ value was reduced by 50% after the solid sample had taken up typically 4×10^{15} molecules, using the geometric surface area for the estimate. This resistance to saturation, as well as the preference for bromide oxidation, despite the small abundance of bromide compared to chloride in natural sea salt, makes this process a potentially important ozone sink in the MBL. The propensity of the gas-phase reactant, O_3 in this case, for specific reaction with bromide that is present as a minority species is well known and has been noted above for HOX (X = Cl, Br, I), the halogens, and the interhalogens. It has to do in part with the enrichment of bromide at the gas−substrate interface, as well as with the eutectic properties of bromide compared to chloride solutions in the case of frozen salt substrates. It seems that minor components of the sea salt, possibly Mg and Ca halides, may be responsible for enhanced uptake of ozone compared to that obtained with pure alkali halides that react at least 100 times slower with O_3 (see Table 13).

Several experiments addressing the halogen release from sea salt upon interaction with O_3 are noteworthy. Hirokawa et al.[267] studied the formation of Br_2 from solid poylcrystalline NaBr particles close to their deliquescence point in a slow-flowing gas experiment, where ozone was flowing by the crystalline sample at atmospheric pressure. No Cl_2 was observed, which indicated that the oxidation rate of chloride was too slow to be observed under those experimental conditions, and near-UV irradiation at $\lambda > 290$ essentially did not change the results. In addition, identical yields of Br_2 were obtained when ozone was allowed to interact with a mixture of NaCl and NaBr polycrystalline samples. Oum et al.[265] reported the formation of gaseous Br_2 from the reaction of seawater ice kept at $T < 272$ K with O_3 in the dark using a slow-flowing gas uptake experiment at atmospheric pressure on frozen panels of natural and synthetic seawater using atmospheric pressure chemical ionization mass spectrometry (API-CI). These observations suggest that this reaction is a potential source of tropospheric photolyzable bromine in high-latitude coastal regions in winter.[64] In addition, it may also be the source of the photolyzable bromine gas measured in the Arctic, believed to be responsible for the ozone destruction at polar sunrise in "bromine explosion" events discussed above. Specifically, this experiment again provided solid evidence for Br_2 formation at the exclusion of Cl_2, despite the large abundance of chloride compared to bromide in the sea salt sample, which may be due to the presence of a liquid brine enriched in bromide on top of the frozen ice matrix. Irradiation at 254 nm essentially left the conclusions unchanged, except, perhaps, for the occurrence of small amounts of BrCl and possibly HOBr, but no Cl_2 was detected. As expected, increasing concentrations of O_3 as well as bromide in the ice sample increased the rate of formation of Br_2. The results are consistent with known liquid-phase reaction kinetics and equilibria involving the oxidation of bromide to BrO^- as an initiation step.[272] Experiments performed by Oum et al.[19] showed that Cl_2 was generated from the photolysis of O_3 in the presence of sea salt particles above their deliquescence point. These researchers performed experiments in a large static aerosol chamber equipped with FTIR and UV/vis spectrometry, as well as API-CI mass spectrometry. Polydisperse sea salt or NaCl aerosol was irradiated at 254 nm at O_3 concentrations in the range 0.8−14 ppm and at 86−90% relative humidity. Depending on the ozone concentration, a rapid appearance of Cl_2 was detected, which was thought to arise from OH-initiated oxidation of Cl^- to atomic Cl occurring in the condensed phase. In summary, O_3, light, and aqueous particles containing Cl^-, either from sea salt or from NaCl, are necessary for the formation of Cl_2.

Sadanaga et al.[20] performed uptake experiments of O_3 on NaCl and synthetic sea salt powders that had been doped with water-soluble ferric ion (Fe^{3+}) using a Knudsen flow reactor equipped for phase-sensitive mass spectrometry. The uptake coefficients of O_3 on NaCl and synthetic sea salt (SSS) were found to be enhanced from $<10^{-5}$ to approximately 3.5×10^{-2} in the presence of water-soluble Fe^{3+} for Fe/Na weight ratios in excess of 0.1%. Cl_2 release in the dark was observed as a reaction product, that is, without the need to irradiate the reaction mixture. The chlorine yields were between 25 and 50% of the ozone taken up for an Fe/Na ratio of 1.0 and 0.5 wt %, respectively, under the condition of a sufficient quantity of SAW. On the combination SSS/$FeCl_3$, only Br_2 was observed, which supports the above conclusion that bromine release is favored over chlorine release. This also implies that Cl_2 will be generated from ferric ion-doped sea salt substrates if the bromide supply of an atmospheric particle is exhausted. However, the Fe^{3+} must be water soluble, as mixtures of NaCl and ferric oxide did not lead to Cl_2 formation, although the γ value was enhanced by at least 2 orders of magnitude, compared to that for O_3 interaction on NaCl, $\gamma < 10^{-5}$,[266] as given in Table 13. The authors infer that this reaction may be responsible for the "missing Cl_2 source" of 330 pptv per day found by Spicer and co-workers,[61] given the significant probability of finding internally mixed sea salt particles with water-soluble ferric ions.

Concluding Remarks. Ozone readily oxidizes bromide to Br_2 when it is interacting with frozen salt mixtures, mimicking sea ice, or aqueous salt aerosols that are surrogates for marine aerosols. This seems to be a dark reaction where no actinic light is required. The oxidation of chloride to Cl_2 requires the presence of light and aqueous aerosols and is thought to be due to oxidation of chloride in the liquid phase, owing to the presence of OH free radical. However, a possible catalytic influence of the reactor walls cannot be excluded at this time, although it may be that the same redox chemistry is occurring on the reactor walls as within the aqueous aerosols. In the presence of soluble ferric ions within the aqueous aerosol, Cl_2 formation has been observed in the absence of light. However, in this dark reaction, Br_2 is favored over Cl_2 formation, which is observed when the bromide source is exhausted.

3.13. Reactions of BrO

Abbatt[273] studied uptake rates of BrO using a coated-wall flow tube at 1.3 mbar total pressure of He, coupled to a Br resonance fluorescence (RF) detector, where BrO concentrations $<5 \times 10^{10}$ molecules cm^{-3} were generated from the reaction $Br + O_3 \rightarrow BrO + O_2$, by discharging Br_2/He in a microwave cavity and adding $(1-3) \times 10^{13}$ molecules cm^{-3} O_3 downstream. After BrO interacted with the active surface, it was converted to Br in the reaction $BrO + NO \rightarrow Br + NO_2$. The sulfite was dissolved in 23 wt % NaCl solution, and 1.3 mbar H_2O vapor was added to the carrier gas, to result in 2.7 mbar total pressure. The γ values for the uptake of BrO in the presence of SO_3^{2-} were corrected for the uptake on the 23 wt % NaCl solution alone ($\gamma = (1.5 \pm 0.3) \times 10^{-3}$). The uptake experiments involving bisulfite were performed in the presence of SO_2 in the pressure range $1 \times 10^{-3}-3.1 \times 10^{-2}$ mbar, resulting exclusively in bisulfite, as it is the dominant form of S(IV) in the covered pH range. The reactivity of BrO toward sulfite and bisulfite seems to be identical (Table 14).

Table 14. $BrO + HSO_3^-/SO_3^- \rightarrow HOBr/BrO^- + SO_3^-$

symbol	uptake coefficient	substrate	temp/K	reference
γ_{ss}	$(1.9 \pm 0.4) \times 10^{-3}$	0.1 M Na_2SO_3 frozen solution	213	Abbatt, 1996[271]
	$(2.0 \pm 0.4) \times 10^{-2}$	1.0 M Na_2SO_3 frozen solution		
γ_{ss}	$(1.3 \pm 0.3) \times 10^{-2}$	5 mM Na_2SO_3 in 23 wt % NaCl	253	Abbatt, 1996[271]
	$(1.5 \pm 0.3) \times 10^{-3}$	10 mM Na_2SO_3 in 23 wt % NaCl		
	7.4×10^{-3}	4×10^{-4} M HSO_3^- in 23 wt % NaCl		
	1.23×10^{-2}	1.6×10^{-3} M HSO_3^- in 23 wt % NaCl		

Table 15. $NO_3 + X^- \rightarrow$ Products

symbol	uptake coefficient	substrate	temp/K	reference
γ_{ss}	$(1.14 \pm 0.12) \times 10^{-3}$	aqueous NaCl, 0.01 M	273 ± 1	Rudich et al., 1996[274]
	$(2.73 \pm 0.40) \times 10^{-3}$	aqueous NaCl, 0.1 M	273 ± 1	
	$(6.0 \pm 1.5) \times 10^{-3}$	aqueous NaCl, 0.5 mM	273 ± 1	
	$(1.56 \pm 0.26) \times 10^{-3}$	1 mM aqueous NaBr solution	273 ± 1	
	$(5.5 \pm 1.3) \times 10^{-3}$	10 mM aqueous NaBr solution	273 ± 1	
	$(2.75 \pm 0.53) \times 10^{-3}$	1 mM aqueous $NaNO_2$ solution	273 ± 1	
γ_{ss}	$(1.3 \pm 0.2) \times 10^{-3}$	aqueous KI, 1×10^{-5} M	273 ± 1	Rudich et al., 1996[275]
	$(3.24 \pm 0.53) \times 10^{-3}$	aqueous KI, 8×10^{-5} M	273 ± 1	
γ_{ss}	$(4.6 \pm 3.0) \times 10^{-2}$	NaCl powder, grain, thin solid film	298	Seisel et al., 1997[277]; 1999[278]
	$(2.0 \pm 1.0) \times 10^{-1}$	KBr powder, grain, thin solid film	298	
	$(3.3 \pm 0.1) \times 10^{-1}$	KI, NaI powder, thin solid film	298	
γ_{ss}	$>2.0 \times 10^{-3}$	0.1 M NaCl solution	293	Thomas et al., 1998[279]
γ_{ss}	$(1.7 \pm 1.2) \times 10^{-2}$	NaCl thin film	258−301	Gratpanche and Sawerysyn, 1999[280]
	0.11 ± 0.06	NaBr thin films	293	
γ_{ss}	2×10^{-3}−4×10^{-2}	NaCl thin film	300	Gershenzon et al., 1999[281]
	0.1−0.3	NaBr thin films	300	
γ_{ss}	2.9×10^{-4}	$a_{HCOO^-} = 10^{-2}$ M	273 ± 1	Imamura et al., 1997[282]
	7.5×10^{-4}	$a_{OH^-} = 10^{-2}$ M		
	2.4×10^{-3}	$a_{SO_3^{2-}} = 10^{-2}$ M		

In conclusion, neither BrO nor ClO is lost efficiently on surfaces such as sulfuric acid, Pyrex, or ice at 213 K. At higher concentrations, BrO self-reaction, leading to Br_2, was observed. For BrO, it was observed that the utpake coefficient on an aqueous NaCl solution at 253 K was small (that is, $\gamma < 3 \times 10^{-3}$) but that it is significantly enhanced upon addition of S(IV) to the solution, either by adding SO_2 in the gas phase or by dissolving solid Na_2SO_3. The products have not been studied but are thought to result in a free radical, although there are no reported studies which show that the reaction does, in fact, proceed. These results imply that the heterogeneous interaction of BrO and ClO will probably be insignificant under atmospheric conditions.

3.14. Reactions of NO_3

Rudich et al.[274,275] studied the uptake of NO_3 free radical in a vertically mounted wetted-wall laminar flow tube connected to a long-path absorption cell of 12.6-m optical path. Uptake coefficients were measured from the decrease of the NO_3 concentration in the lowest 25 cm (interaction region) after a 60-cm-long equilibration section, leading to an interaction time of 18−26 ms at a total pressure made up of 6 mbar H_2O and 6.7−13.3 mbar He. NO_3 was generated through thermal decomposition of N_2O_5 at 400 K, resulting in concentrations in the range 2×10^{11}−1×10^{12} molecules cm^{-3}. NO_3 was detected using radiation from a stabilized single-mode diode laser emitting near 662 nm and recording its absorption in the long-path absorption cell, thus affording a detection sensitivity for NO_3 of 5×10^9 molecules cm^{-3}. The uptake coefficient was calculated from measured first-order rate constants for NO_3 loss and was in the range 1.5×10^{-4}−6×10^{-3}, depending on the aqueous salt concentration (see Table 15). The uptake is thought to be reactive and is proposed to occur according to reactions 105 and 106, which corresponds to a charge-exchange reaction in solution.

$$NO_3 + X^- \rightarrow NO_3^- + X \qquad \text{with X = Cl, Br, I} \tag{105}$$

$$NO_3 + NO_2^- \rightarrow NO_3^- + NO_2 \tag{106}$$

$$NO_3 + H_2O \rightarrow HNO_3 + OH \tag{107}$$

In order to extract the Henry's law solubility of NO_3 in aqueous solution, the reaction rate constant for the solution reaction 106 has to be known. Henry's law solubility of NO_3 has been measured to be $H = 0.6 \pm 0.3$ M atm^{-1}, assuming a rate constant for reaction 106 from Exner et al.[276] and using an estimated diffusion coefficient for NO_3 in liquid water of 13−17 $cm^2\ s^{-1}$ at the total pressure used. Of note is the small solubility of NO_3 in aqueous solution, as well as the H abstraction from H_2O (reaction 107) that occurs in pure water, despite the large difference in bond dissociation energy between H_2O and HNO_3. The authors could rule out reaction 108

$$NO_3 + OH^- \rightarrow NO_3^- + OH \tag{108}$$

because the rate of uptake of NO_3 was independent of pH and the solution rate constant measured by Exner et al.[276] could not account for the measured value of γ. A similar uptake study, using the same equipment, has been performed for NO_3 on iodide-containing aqueous solution.[275] The uptake was

entirely given by liquid-phase reactivity at the given [KI], and γ_{ss} increased with increasing solute concentration. The conclusion was that NO_3 uptake was controlled by the electron-transfer reaction 105.

Seisel et al.[277,278] studied the uptake kinetics of NO_3 free radical in a Knudsen flow reactor equipped with dual diagnostics, namely molecular-beam-modulated electron-impact mass spectrometry (MS) and laser-excited fluorescence (LIF) detection of NO_3 and NO_2 free radical, excited at approximately 662 and 440 nm, respectively, and detected at wavelengths in excess of 700 nm in the presence of solid NaCl, KBr, and KI(NaI) powder, salt grains, or thin spray-coated salt films. NO_3 is generated from thermal decomposition of N_2O_5 in a small Knudsen cell upstream of the main reactor that is connected through a capillary and that is heated to approximately 530 K. The NO_3 densities inside the Knudsen reactor, typically between 3×10^{10} and 1×10^{12} molecules cm^{-3}, were determined in titration experiments according to the fast gas-phase reaction $NO_3 + NO \rightarrow 2NO_2$, thus enabling the recording of the mass spectrum of NO_3. The heterogeneous reaction rate constants, measured using MS and LIF, were first order in $[NO_3]$ and agreed with one another within experimental error. In addition, the measured uptake coefficients were independent of sample mass, and thus of sample presentation as a powder or thin solid salt film, and indicated a significant surface residence time of NO_3 on the substrates of interest, thus making any correction using the pore diffusion model unnecessary. Thus, γ values on spray-coated thin salt films were identical, within experimental error, to results obtained on powder substrates. The uptake of NO_3 on solid alkali halide salt substrates is reactive and proceeds according to the exothermic reaction 105, with X = Cl, Br, I. It is noteworthy that it leads to a direct nonphotolytic generation of atomic halogen. The primary atomic reaction product has been observed for bromide and iodide substrates, whereas HCl was the only detected gas-phase reaction product for NaCl. In reference experiments with authentic atomic Cl, it was established that the primary product Cl stayed adsorbed on the salt surface. At short gas residence times, the HCl yield was 100% of the NO_3 taken up and increased to 300%, owing to side reactions also resulting in HCl. For bromide and iodide substrates, atomic Br and I have been directly observed, together with molecular bromine and iodine, whose yield increased from 20% to 50% with increasing gas residence time, owing to heterogeneous recombination of atomic Br and I on the Teflon-coated internal walls of the flow reactor. Minor amounts of HBr and HI were also observed.

Thomas et al.[279] performed uptake experiments at atmospheric pressure and 293 K using a continuous flow of NO_3 generated by oxidation of NO in excess ozone on a dilute aquoues NaCl solution flowing across a series of wetted denuders. Matrix-isolated EPR spectroscopy was used to monitor the purity of the NO_3 flow that was detected after heterogeneous reaction, as it provides a spectroscopic measurement of NO_2, NO_3, and peroxy free radicals. The NO_3 taken up by the aqueous solution was converted to nitrate anion following reaction 105. Nitrate, in turn, was reduced to NO_2^-, which was monitored by a sensitive spectrophotometric method using the Saltzman reaction. The nitrogen mass balance for the experimental setup was close within experimental error, and the measured value of $\gamma_{ss} = 2 \times 10^{-3}$ given in Table 15 represents a lower limit. The authors critically compare their results with the work by Rudich et al.[274,275] and point out the acceptable agreement of the Henry's law solubility for NO_3 in pure water of $H = 1.8 \pm 1.5$ M atm^{-1}, obtained by Thomas et al.,[279] with the value of 0.6 M atm^{-1}, obtained by Rudich.[274] However, Thomas et al. found much lower values for the rate of removal of NO_3 by pure water according to reaction 107 than Rudich et al.,[274] in agreement with the expectation that it is endothermic or at least close to thermoneutral, despite the possible incidence of significant solvent effects. As a consequence, NO_3 solubility in pure water could be much lower, in order to accommodate both data sets if experimental artifacts were to be excluded, such as reactive organic impurities in the aqueous solution. In conclusion, there is no obvious reason, based on thermodynamic grounds, why the solubility of NO_3 in aqueous solution should be much larger than that for NO_2, which was determined to be in the range 0.007−0.012 M atm^{-1}. The experimental methodology used by the two groups, consisting of measuring the rate of uptake of NO_3, critically depends on a number of parameters that are associated with significant experimental uncertainties: D_g, the gas-phase diffusion constant of NO_3 in the carrier gas; D_l, the diffusion constant for liquid diffusion; and k_1, the rate constant of the trapping reaction 105. Therefore, no definite conclusion as to the solubility of NO_3 in aqueous solution may be given at this time, except to say that it may potentially be much lower than measured by either groups.

Gratpanche et al.[280] performed uptake experiments of NO_3 in a coated-wall fast-flow reactor coupled to gas-phase EPR detection of OH free radical using spray-coated NaCl films. NO_3 was generated from the thermal decomposition of N_2O_5, present at a concentration of 10^{11} molecules cm^{-3}, and led to NO_3 concentrations in the range $1 \times 10^{10}-5 \times 10^{11}$ molecules cm^{-3}. NO_3 was titrated in excess H atoms, generated in a microwave discharge of He/H_2 mixtures, according to the reaction $NO_3 + H \rightarrow NO_2 + OH$. NO_2 went on to react with excess H to generate additional OH according to $NO_2 + H \rightarrow NO + OH$. Starting from N_2O_5, the nitrogen mass balance indicates that, for every mole of NO_3 converted, one obtains 3 mol of OH, two from NO_3 and one from NO_2, generated in the thermal decomposition of N_2O_5, that are subsequently detected by EPR. The NO_3/NaCl interaction led to a temperature-independent value of γ_{ss} over the temperature range 258−301 K (see Table 15), whereas NO_3/NaBr showed a slight negative T dependence, amounting to a factor of 2 over the range 243−293 K. No NO_3 uptake was observed on thin solid films which were spray-coated using pure methanol, presumably because of the absence of SAW on the salt substrate.

Gershenzon et al.[281] performed NO_3 uptake experiments using a coated-wall fast-flow reactor equipped with either molecular beam sampling MS or matrix-isolation EPR detection of NO_3. NO_3 was generated from thermal decomposition of N_2O_5 at 470 K. The uptake coefficient γ has been found to be independent of the NO_3 concentration in the range $3 \times 10^9-10^{11}$ molecules cm^{-3}. Beyond $[NO_3] = 10^{12}$ molecules cm^{-3}, γ is inversely proportional to $[NO_3]$. At temperatures in excess of 373 K, γ becomes temperature independent over a wide range of concentrations. The initial rate of uptake partially saturates with time and converges toward a steady-state value that is given in Table 15. In agreement with literature results, the rate of uptake on solid bromide substrates is faster than that on chloride. The authors propose a precursor mechanism in order to interpret their kinetic data.

Imamura et al.[282] performed an uptake experiment of NO_3 on aqueous solutions containing anions X^- that maybe found in cloudwater droplets, namely $X^- = HSO_3^-$, SO_3^{2-}, $HCOO^-$, CH_3COO^-, and OH^-. They used a wetted-wall flow reactor coupled to long-path absorption detection of NO_3 whose initial concentration was $(2-20) \times 10^{11}$ molecules cm^{-3}, with the total pressure being mostly H_2O vapor in the range 10−16 Torr. The uptake was determined as a function of liquid-phase reactant concentration and was entirely given by the liquid-phase reactivity. The γ_{ss} value increased with increasing solute activity and is given in Table 15 for the midrange of the used solute activities. The results are presented in terms of the product $H^2D_l k$, where H is the Henry's law constant for NO_3 solubility in aquoues solution, D_l the diffusion coefficient of NO_3 in solution, and k the pseudo-first-order rate constant for the reaction $NO_3 + X^-$. The linear correlation between the measured rate coefficients and those for the corresponding SO_4^- free radical reactions, and the dependence of the measured rate coefficients on the redox potential of the X/X^- pair, both suggest that the $NO_3 + X^-$ reactions proceed by electron transfer, in agreement with previous results obtained with similar solute anions.

Concluding Remarks. NO_3 free radical undergoes a rapid electron transfer reaction both with solid alkali halide substrates and with aqueous halide solutions, resulting in atomic halogen. For solid bromides and iodides, the atomic halogens have been directly detected in the gas phase, whereas for solid chlorides, the secondary product HCl has been monitored. Linear correlations between the measured rate coefficients and the redox potentials of a variety of anionic solutes lead to indirect evidence for an electron-transfer reaction in solution. The solubility determinations of NO_3 in aqueous solution certainly represent an upper limit, owing to uncertainties in kinetic and transport parameters used to interpret the uptake experiments of NO_3. Two sets of independent experiments result in Henry's law solubilities that are approximately 2 orders of magnitude larger than the corresponding values for NO_2. Moreover, both sets of experiments show a large disagreement regarding the reactivity of NO_3 with H_2O. The proposed H abstraction of H_2O by NO_3 in aqueous solution must await independent confirmation before any firm conclusions may be drawn.

3.15. Reactions of NO_2

Vogt and Finlayson-Pitts[140,283] investigated the heterogeneous reaction of NO_2 with polycrystalline NaCl that occurs according to reactions 109 and 110. The reactant is monomeric NO_2 in reaction 109, whereas it is the dimer that reacts in reaction 110, monomer and dimer being connected through the rapidly established equilibrium 111.

$$2NO_2 + NaCl \rightarrow NOCl + NaNO_3 \quad (109)$$

$$N_2O_4 + NaCl \rightarrow NOCl + NaNO_3 \quad (110)$$

$$2NO_2 \rightleftarrows N_2O_4 \quad (111)$$

The reaction resulted in the formation of NOCl and solid $NaNO_3$ and was followed by monitoring the formation of nitrate on the surface of the ground NaCl sample as a function of time using diffuse reflectance FTIR spectroscopy (DRIFTS) in mostly He but also air as carrier gas. The rate of nitrate formation was obtained from the integrated area of all absorptions in the region of the antisymmetric NO_3^- stretch (ν_3 at 1390 cm^{-1} band), namely at 1333 and 1460 cm^{-1}, as well as at 1380 cm^{-1} at larger extents of reaction. While IR absorptions in the regions associated with the ν_1, ν_2, and ν_3 modes of the nitrate ion are recorded, they are not identical to those typically observed for a dilute mixture of $NaNO_3$ in NaCl. At low extents of reaction, thereby ensuring constant choride supply, the IR absorption bands are attributed to the formation of isolated $NaNO_3$ formula units, whereas at later stages $NaNO_3$ microcrystallites that are comparable to bulk $NaNO_3$ are formed. This results from the fact that, early on in the reaction, only a few percent of the surface chloride are replaced by nitrate, which should support the formation of isolated $NaNO_3$ units. In addition, the conversion of the isolated nitrate species to the microcrystalline modification, species 2, may be accelerated by the action of SAW and heat that will promote the nitrate crystallization. Thus, the formation of the SAW layer on treatment with water would mobilize both nitrate species. Subsequent heating results in recrystallization, forming separate regions of $NaNO_3$ and NaCl. Bands due to both of the formerly distinguishable species are then no longer observed, at the expense of the isolated nitrate species.

Junkermann and Ibusuki[47] studied the reaction of 10 ppm NO_2 with solid NaCl in the presence of water and/or O_3 using DRIFTS. They also observed several bands in the 1400 cm^{-1} region, which they assigned to NO_2^-, nitrite, rather than NO_3^-. However, neither their spectra nor the ones obtained by Vogt and Finlayson-Pitts[140,283] showed the strong peak at ~1270 cm^{-1} which is characteristic of $NaNO_2$. Given the facile formation of HNO_3 in NO_x−water mixtures, it is likely that HNO_3 was an important reactant in the

Table 16. NO_2 + Substrate (NaCl, KBr, SSS,[a] NH_4Cl) → Products

symbol	uptake coefficient	substrate	temp/K	reference
γ_0	$(1.3 \pm 0.6) \times 10^{-4}$	N_2O_4+ solid NaCl	298	Vogt and Finlayson-Pitts, 1994,[140] 1995[283]
γ_0	$(4.0 \pm 1.6) \times 10^{-4}$	N_2O_4 + solid NaCl, He	298	Langer, Pemberton, and Finlayson-Pitts, 1997[141]
	$(0.9 \pm 0.5) \times 10^{-4}$	N_2O_4 + synthetic sea salt, He		
	$(3.0 \pm 2.9) \times 10^{-4}$	N_2O_4 + solid NaCl, air		
	$(1.0 \pm 0.5) \times 10^{-8}$	NO_2 + synthetic sea salt, air		
γ_{ss}	$\leq 1 \times 10^{-7}$	NO_2 + solid NaCl	300	Caloz et al., 1997[166]
	2×10^{-7}	NO_2 + solid KBr		
γ_{ss}	$<1.0 \times 10^{-4}$	NaCl aerosol, unbuffered, pH = 0.3, 7.2	300	Abbatt and Washewsky, 1998[225]
γ_0	$(7 \pm 2) \times 10^{-5}$	solid polycrystalline NH_4Cl	298	Takenaka and Rossi, 2003[287]
	$(1 \pm 0.3) \times 10^{-5}$	deposited NH_4Cl aerosol	298	
	$(2.1 \pm 0.4) \times 10^{-4}$	solid polycrystalline NH_4Cl	323	

[a] Synthetic sea salt.

Junkermann and Ibusuki study, ultimately leading to the formation of nitrate bands, as discussed above.

The reactor residence time in the Vogt and Finlayson-Pitts investigation[140,283] was on the order of 3 s, the NO_2 concentration ranged from 1.8×10^{14} to 29×10^{14} molecules cm^{-3} at 30 mbar total pressure, and the extent of reaction was kept small. The rate law was checked using the integrated absorbance of the ν_3 band at 1333 cm^{-1} and others and resulted in a second-order dependence of the rate of nitrate formation on NO_2 concentration ($n = 1.6 \pm 0.2$). Nitrate accumulation on the salt samples was measured using the azo dye method. The heterogeneous reaction was interpreted using a mechanism wherein N_2O_4 directly reacted with NaCl, following reaction 110, after prior dimerization in equilibrium 111, resulting in NOCl (not routinely observed) and $NaNO_3$. The γ_0 value displayed in Table 16 therefore refers to the uptake of N_2O_4 in equilibrium with NO_2, as the dimer seems to be the active species under the given pressure and temperature conditions of the experiment. However, the overall heterogeneous reaction mechanism seems to be complex, as γ seemed to decrease with increasing NO_2/N_2O_4 concentration. Previous work on this reaction by Finlayson-Pitts[43] led to the conclusion that γ_0 for reaction 109 was $>5 \times 10^{-8}$ at a partial pressure of NO_2 in the Torr range based on the study of the rate of formation of NOCl. Complicating factors found in this DRIFTS study were uncertainties regarding the penetration depth of the IR radiation, nitrate concentration gradients and H_2O adsorption. In addition, it was complicated to assess the absolute concentration of formed nitrate on the NaCl sample.

Langer et al.[141] reinvestigated the heterogeneous reaction of NO_2 with NaCl and extended their study to synthetic sea salt using the same experimental technique as that used by Vogt and Finlayson-Pitts.[140,283] The heterogeneous reaction kinetics has been measured by monitoring the integrated absorbance in the ν_3 region of surface nitrate (1312 and1538 cm^{-1}) using DRIFTS, with NO_2 concentrations ranging from 1.5×10^{14} to 24.4×10^{14} molecules cm^{-3}. The IR absorbance of the observed solid nitrate product was independently calibrated using a wet technique that implied reduction of the nitrate to nitrite and subsequent spectrophotometric measurement of the azo dye after azo coupling. Both NaCl and synthetic sea salt were ground to monodisperse nonporous cubes with average size of 2.4 μm. The IR bands due to surface nitrate, formed during the reaction of NO_2, are shown to be similar to those from the reaction of $MgCl_2 \cdot 6H_2O$, a major hydrate in the mixture which was used as a surrogate for all of the crystalline hydrates. Significant amounts of surface-adsorbed water are generated in the reaction of synthetic sea salt with NO_2 in air, which appears at least in part to be due to liberation of strongly bound water of hydration in the crystalline hydrates. This result was obtained by observing the nonlinear increase of the IR absorption band at 1635 cm^{-1}, which together with the 3370 cm^{-1} band was identified as adsorbed water by comparison to a spectrum of the synthetic sea salt that had been exposed to gas-phase H_2O. It is noteworthy that the 1635 cm^{-1} band is not observed on NaCl substrates under identical experimental conditions. The reaction of NO_2 with the hydrates present in synthetic sea salt may disrupt the crystal lattice because the chloride evaporates as NOCl according to reactions 109 and 110. It thereby frees up H_2O that was formerly locked up as a crystal hydrate, thereby making it available to the pool of SAW, which is a different type of strongly bound water. The lower than linear increase of the band at 1635 cm^{-1} at the later stages of the NO_2−salt reaction is probably caused by desorption into the gas stream of the carrier gas.

The observed rate law corresponds to a pseudo-first-order reaction based on the formation of the solid nitrate product. However, it is noted that the rate coefficient decreases with increasing NO_2 concentration, which suggests a complex reaction mechanism. The reaction order in the rate law with respect to NO_2 that interacts with ground synthetic sea salt is 1.8 ± 0.3 when the reaction is carried out in He as a carrier gas but only 1.2 ± 0.2 when air is used as the carrier gas. For comparison, the reaction order for the N_2O_4−ground NaCl reactions was re-examined and found to be 1.8 ± 0.3 in He and 1.6 ± 0.3 in synthetic air, essentially in agreement with previous work using the same experimental technique.[140,283] Langer et al.[141] assumed that N_2O_4 is the reacting species for the purpose of expressing the kinetics in the form of uptake coefficients listed in Table 16. For the N_2O_4−NaCl reactions in He and air, and for the N_2O_4−synthetic sea salt reaction in He, the reaction probabilities are similar, as they lie in the range of 10^{-4}. The reaction of synthetic sea salt with NO_2 in the presence of air is treated in terms of a first-order reaction by attributing the rate-limiting step to the

monomeric NO_2 that interacts with the salt substrate, because the order of the reaction of synthetic sea salt with NO_2 in air approaching unity is smaller than that in He. Although the mechanistic reason for this weaker dependence on $[NO_2]$ is by no means clear at the moment, the uptake probability has been coined on the basis of monomeric NO_2. This leads to γ values in the range of approximately 10^{-8}. This may be compared to the results obtained by Sverdrup and Kuhlman,[284] who measured γ values on the basis of the loss of NO_2 on an artificial sea salt substrate in the range $10^{-7}-10^{-8}$ over a range of relative humidities of 44−88%. However, the nature of the intermediate containing one molecule of NO_2 has not been fully elucidated yet, but ancillary EPR experiments are hinting toward a radical ion complex between Cl^- and NO_2, $[Cl\cdots NO_2]^-$, as is also the case for the bromide system.[285] The atmospheric significance of this reaction is necessarily rather limited because the partial pressure of N_2O_4 in the atmosphere is exceedingly small, owing to the low concentrations of atmospheric NO_2.

This work highlights the significant sensitivity of the reaction kinetics expressed as uptake coefficient as a function of the properties of the salt substrate. Using the same DRIFTS technique, the γ value obtained by Vogt and Finlayson-Pitts[140,283] is a factor of 3 smaller than the one obtained by Langer et al.[141] (see Table 15), who attribute this difference to the quantity of surface defects on the salt substrate, which controls the ability to form pools of SAW, enabling the halogen-exchange reaction. This difference in the amount of surface-adsorbed water has been shown by Peters and Ewing,[50] who have studied the reaction of NO_2 with the (100) face of NaCl and also find that this reaction is second order in NO_2. They report a reaction probability for N_2O_4 of approximately 1×10^{-6} for dry NaCl but approximately 1×10^{-4} for NaCl in the presence of water vapor at a pressure of 9.5 mbar. This observation on the effect of water vapor on the kinetics is consistent with the observation that strongly bound water, adsorbed to the surface of NaCl powders, plays a critical role in its chemistry. However, this strongly bound adsorbed water (SAW) is not to be confused with hydrate water, which is part of the coordination sphere of cations making up the highly ordered structure of ionic crystals. A last remark concerns the differential reactivity of the synthetic sea salt substrate vs its surrogate, such as NaCl toward NO_2, which is in marked contrast to the situation concerning O_3 reactivity with respect to the same pair of substrates. In the case of the former, no significant difference in reactivity has been found compared to the latter, where ozone has a markedly higher reactivity toward natural and synthetic sea salt compared to NaCl as far as the γ value is concerned. In addition, in the case of ozone, the nature of the reaction products is also significantly different (see section 3.12),

Caloz et al.[166] performed a kinetic study of the rate of uptake of NO_2 on NaCl and KBr ground powder using a Knudsen flow reactor coupled to a mass spectrometric (MS) detector. The goal of the study was to measure the uptake rate of NO_2 at low partial pressure so that one could exclude significant amounts of the dimer N_2O_4 in the gas phase, whose reactivity with salt substrates had been determined by Finlayson-Pitts and co-workers.[140,141,283] The rate of uptake, measured from the decay of NO_2 in the gas phase, was in fact so slow that the Knudsen flow reactor had to be used as a static reactor, because the longest achievable gas residence time with the smallest escape aperture in place was insufficient to obtain a measurable decay. The decay of NO_2 in the presence of dry NaCl or KBr was measured by monitoring the remaining quantity of NO_2 after a given amount of time in the range 0−5000 s by monitoring the quantity of remaining NO_2. This was achieved by taking the calibrated integral of the MS signal at *m/e* 46, due to NO_2 effusing out of the static reactor, and converting it to absolute yields. The NO_2 decays were first order and independent of the initial NO_2 concentration, the range $10^{12}-10^{13}$ molecules cm^{-3}, which is smaller by approximately 2 orders of magnitude compared to the values obtained by the DRIFTS studies.[140,141,283] For the NaCl substrate, the first-order reaction rate to constant k was 4.2×10^{-4} s^{-1}, compared to a rate constant for NO_2 decay in the empty sample compartment of 2.6×10^{-4} s^{-1}. The observed products were HCl and HONO, but no NOCl was detected. NOCl was investigated in a separate reference experiment, interacting with NaCl, and decayed on a similar time scale, yielding the same products, namely HCl and HONO. For the KBr substrate, the NO_2 decays were first order and independent of the initial NO_2 concentration in the range $2 \times 10^{12}-1 \times 10^{13}$ molecules cm^{-3}. The first-order reaction rate constant k was $(1.15 \pm 0.15) \times 10^{-3}$ s^{-1}, compared to a rate constant for NO_2 decay in the empty sample compartment of 2×10^{-4} s^{-1}. No products were observed. Both salt substrates contained sufficient adsorbed H_2O, despite prolonged pumping at 1.3×10^{-5} mbar at ambient temperature. Owing to the similarity of the NO_2 decay with and without NaCl sample, the authors preferred to give an upper limit for γ in the case of NaCl, namely $\gamma < 10^{-7}$, whereas the γ value for the KBr substrate could be established within experimental uncertainty, given that the decay rate constant in the presence compared to the one in the absence of KBr was different by a factor of 5 or so. For polycrystalline NaCl, the γ value measured by Caloz et al.[166] agrees with the measurement by Sverdrup and Kuhlman.[284]

Abbatt and Washewsky[225] performed an uptake experiment on liquid NaCl aerosol flowing down across an aerosol flow tube at atmospheric pressure using CIMS detection. The NaCl aerosol formed in an ultrasonic nebulizer had a bimodal distribution (large average diameter, 2−4 μm; small, <1 μm), with typical surface areas and particle number densities in the range of $(1-6) \times 10^{-3}$ cm^2/cm^3 and $(1-4) \times 10^4$ particles/cm^3, respectively. No statistically significant decay of the NO_2 signal was observed when NO_2 was given a long reaction time of approximately 8 s in the presence of high total surface areas of unbuffered NaCl aerosols. The value of γ displayed in Table 16 is an upper limit to the uptake coefficient and refers to unbuffered aerosol, pH = 0.3 and pH =

Table 17. HO_2 + Substrate (NH_4HSO_4, NH_4NO_3, NaCl)

symbol	uptake coefficient	condensed phase	temp/K	reference
γ_0	0.53 ± 0.45	0.055 μm NH_4HSO_4, aerosol	300	Mozurkewich et al., 1987[288]
	0.34 ± 0.10	0.081 μm NH_4HSO_4 aerosol	300	
γ_{ss}	$(1.5 \pm 0.25) \times 10^{-2}$ [a]	solid films of KCl, NaCl, NH_4NO_3, $(NH_4)_2SO_4$	295	Gershenzon et al., 1995[289]
γ_{ss}	$(3.0 \pm 0.3) \times 10^{-2}$	solid NaCl	243	Remorov et al., 2002[290]
	$(1.2 \pm 0.2) \times 10^{-2}$		295	
	$(2.6 \pm 0.5) \times 10^{-3}$		345	

[a] Value has been corrected to 1.33×10^{-2} for the interaction of HO_2/NaCl at 295 K.[290]

7.2, for NO_2 concentrations ranging from 3×10^{12} to 2×10^{14} molecules cm^{-3}.

An interesting question arises if one considers ammonium salts occurring in the troposphere, such as $(NH_4)_2SO_4$ or NH_4HSO_4, as a storage compound of nitrogen in reduced form, namely in the formal −III oxidation state that could potentially react with nitrogen in its oxidized form, such as NO_2 (+IV formal oxidation state), in a reverse disproportionation reaction, to result in molecular nitrogen or at least nitrogen in a low oxidation state. Taking as an example the reaction of NO_2 with NH_4Cl that was taken as a proxy for tropospheric ammonium salts for its ease of experimental handling, two possible reactions consisting of an ion-exchange mechanism may be formulated:

$$NH_4Cl + 2NO_2 \rightarrow NH_4NO_2 + ClNO_2 \quad (112)$$

$$NH_4Cl + 2NO_2 \rightarrow NH_4NO_3 + ClNO \quad (113)$$

The ammonium nitrite resulting from reaction 112 is unstable and decomposes spontaneously into N_2 and H_2O,[286] whereas NH_4NO_3 is stable to a certain extent under ambient conditions. The atmospheric implications of reaction 112 would be a decrease of NH_3 per mole of reacted NO_2, whereas $ClNO_2$ would undergo rapid photolysis into atomic chlorine and NO_2 under atmospheric conditions, as discussed above. Reaction 113 would leave NH_3 untouched but would nevertheless lead to chlorine activation. Takenaka and Rossi[287] measured the heterogeneous interaction of NO_2 on a solid polycrystalline film of NH_4Cl as a function of temperature over the limited range 295−335 K, using the diffusion tube technique, and came to the conclusion that reaction 112 indeed takes place exclusively, but that NH_4NO_2 undergoes competitive hydrolysis to HONO + NH_3 at a branching ratio of 95%, favoring HONO formation, at ambient temperature. Only 5% of NH_4NO_2 undergoes decomposition to N_2 and $2H_2O$. In this way, NH_3 is an effective catalyst in the destruction of NO_2 in the presence of solar photons ($h\nu$) and atmospheric acidity, such as HCl, HNO_3, or H_2SO_4, as the net may be expressed as in reaction 114:

$$NO_2 + HCl + h\nu \rightarrow Cl + HONO \quad (114)$$

The results, therefore, do not support an efficient reverse disproportionation reaction between reduced and oxidized forms of nitrogen on solid ammonium salts. From a kinetic point of view, reaction 112 is interesting, as both the uptake coefficient γ and the surface residence time τ_s of NO_2 adsorbed on NH_4Cl first increase and subsequently decrease with temperature. This unusual behavior has been explained by invoking a complex reaction mechanism wherein activated adsorption of both a nonreactive and a reactive adsorption intermediate takes place in the temperature range of interest.

Concluding Remarks. NO_2 is essentially unreactive on salt substrates at ambient temperature. Because much of the older work has been performed at higher partial pressure of NO_2, where the equilibrium fraction of N_2O_4 cannot be neglected, the measurement of γ has, in fact, addressed the reactivity of N_2O_4 on salt, which is of the order of 10^{-4}, in contrast to γ of monomeric NO_2, whose upper limit has been given as 10^{-7}. It seems that the reactivity on bromide is somewhat enhanced compared to that on chloride. In addition, NO_2 is unreactive on deliquescent NaCl aerosol. It may be concluded that the title reaction is unimportant in the marine boundary layer at atmospheric NO_2 concentrations. However, the interaction of NO_2 with solid salt gives rise to a persistent free radical whose nature has not been elucidated in detail.

3.16. Reactions of HO_2, OH

Mozurkewich et al.[288] performed HO_2 uptake experiments using an atmospheric-pressure flow tube with chemical detection of HO_2 using a fast chain chemical amplification of HO_2, coupled to NO_2 chemiluminescence detection. The HO_2 was generated by thermal dissociation of H_2/H_2O over a hot NiCr wire, with estimated densities of 10^8-10^9 molecules cm^{-3}. The aerosol was produced from atomizing salt solutions and was size-selected by a differential mobility analyzer. The fraction selected was monodisperse (particle radii within ±14%) and contained typically $(2-3) \times 10^5$ particles cm^{-3}. A Cu(II) salt was added to the solution in order to oxidize HO_2 to H_2O_2 in solution, thus preventing re-evaporation of HO_2. The uptake coefficient may therefore be interpreted as corresponding to the kinetics of HO_2 accommodation on the surface of fine aqueous aerosol particles. The pseudo-first-order rate constant for loss of HO_2, k_I, was interpreted in terms of HO_2 wall loss (k_w) and a second-order rate constant (k_{II}) for the loss of HO_2 on the surface of the aerosol: $k_I = k_w + k_{II}N$ (N = number of particles). The authors conclude that the Cu(II) concentration used in their experiments (up to 0.0063 mole/kg solution) may have been only marginally sufficient to trap the HO_2. The uptake coefficient of HO_2 on aqueous $LiNO_3$ aerosol (r = 0.054 mm) was 0.57 ± 0.16. It thus appears that HO_2 accommodation on a liquid aerosol droplet is fast, as indicated in Table 17.

Gershenzon et al. [289] equipped a fast laminar flow reactor with off-axis matrix isolation electron paramagnetic resonance (EPR) detection in H_2O vapor. Owing to a large volumetric flow, the cold finger collector located in the EPR cavity was moved off-axis in order to avoid excessive heating by the gas flow. In this arrangement, the radicals were deposited on the off-axis collector rod by gas-phase diffusion, and a solid-state EPR spectrum was recorded after suitable collection times. This technique was applied at low $[HO_2]$ of typically $(3-5) \times 10^9$ cm^{-3}. An additional real-time detection method was used at high $[HO_2]$ of typically $(1-3) \times 10^{11}$ cm^{-3}, where OH was generated from an added excess of NO, followed by gas-phase EPR detection. HO_2 was generated by a microwave discharge of an H_2 impurity in He, followed by addition to O_2. The solid sample was coated on a central movable rod that was mounted coaxially to the cylindrical reaction vessel. The external cylinder walls were passivated using halocarbon wax, which led to a first-order wall deactivation of HO_2 on the order of $\gamma_w = (7 \pm 2) \times 10^{-4}$ at 295 K. The decrease of the wall temperature to 245 K led to a 3-fold increase in γ_w; a further decrease of the wall temperature made kinetic studies impractical, owing to a sharp increase of γ_w below $T < 240$ K. For solid NaCl, KCl, NH_4NO_3, and $(NH_4)_2SO_4$, the γ value was in the range $(1-2) \times 10^{-2}$ at 295 K. The kinetic results remained the same for solid NaCl, in the range $4 \times 10^9-3 \times 10^{11}$ cm^{-3}, thus pointing to a rate law for uptake that is first order in $[HO_2]$. However, in later work, Gershenzon and coworkers[290] corrected the γ value for NaCl from the original 1.5×10^{-2} (high $[HO_2]$) and 1.65×10^{-2} (low $[HO_2]$) to 1.33×10^{-2}.

Using the same coupled laminar flow reactor−matrix isolation EPR technique, Gershenzon and coworkers[290] investigated the negative temperature dependence of the uptake rate constant for HO_2 interacting with solid NaCl in more detail. On one hand, matrix isolation detection of HO_2 was used for $[HO_2] = 4 \times 10^{10}$ cm^{-3}, whereas gas-phase EPR detection was used for $[HO_2] = 5 \times 10^{11}$ cm^{-3} over a combined temperature range 243−345 K. Both detection techniques result in identical γ values within experimental error. In the range 243−300 K, the following Arrhenius-type relation for γ was obtained, incorporating a small negative temperature dependence, albeit smaller than that used in previous studies:[289] $\gamma = (5.66 \pm 3.62) \times 10^{-5} \exp[(1560 \pm 140)/T]$. However, the γ value sharply decreases in the range 300−345 K. The heterogeneous interaction probably does not lead to chlorine activation when HO_2 interacts with NaCl, despite a favorable overall thermochemistry for the reaction $HO_2 + NaCl \rightarrow NaOH + 0.5(Cl_2 + O_2)$; instead, the authors believe that the heterogeneous reaction leads to products that are identical to the ones observed in the gas phase, namely $H_2O_2 + O_2$. Remorov et al.[290] go on to interpret the temperature dependence of γ using a combined Ely−Rideal and Langmuir−Hinshelwood mechanism and come to the conclusion that the present temperature range is too narrow to allow unambiguous classification of the heterogeneous reaction mechanism. This detailed and careful study underlines the need to detect reaction products of heterogeneous reactions of free radicals and possibly their branching ratios in view of the paucity of reliable results in the literature.

Table 18. HO + Substrate (NH_4HSO_4, NH_4NO_3, NaCl)

symbol	uptake coefficient	condensed phase	temp/K	reference
γ_{ss}	$<3.0 \times 10^{-2}$	dry $(NH_4)_2SO_4$	296	Cooper and Abbatt, 1996[290]
γ_{ss}	$<2.0 \times 10^{-3}$	dry $(NH_4)_2SO_4$	296	
γ_{ss}	1.5×10^{-2}	solid NaCl	245	Ivanov et al., 1996[292]
	4.1×10^{-3}		300	
	8.3×10^{-3}	solid NH_4NO_3	245	
	3.9×10^{-3}		300	

Cooper and Abbatt[291] performed an uptake study of OH free radical using a coated-wall laminar flow tube coupled to OH resonance fluorescence detection of OH by measuring the first-order loss rate of OH in the presence of various types of substrates at different temperatures. The results are displayed in Table 18. The residence time of OH in the doubly jacketed radical injector was 10 ms, and OH was generated using both $F + H_2O \rightarrow HF + OH$ and $H + NO_2 \rightarrow OH + NO$. The latter was used when dry substrates were required. F and H atoms were produced in a microwave discharge of CF_4 in He and H_2 in He, respectively. The OH concentration was $<5 \times 10^{10}$ molecules cm^{-3}, and the total pressure in the flow tube was 1.33 mbar. A Pyrex reaction tube was coated with an aqueous solution of $(NH_4)_2SO_4$ (ammonium sulfate) and NH_4HSO_4 (ammonium bisulfate) and subsequently inserted into the thermostated flow tube. The sample may therefore be regarded as a solid nonporous polycrystalline solid. The interaction of OH with ammonium bisulfate is apparently reactive, as the rate of OH uptake does not saturate, whereas the analogous interaction of OH with ammonium sulfate first leads to a large rate of uptake but saturates completely within 400 s at the given [OH] and some 41 cm^2 of active substrate. The γ values given in Table 18 both address upper limits for the steady-state uptake and do not correspond to the observed rapid initial "conditioning" or passivation of ammonium sulfate. The ability to passivate ammonium sulfate toward OH has been observed before. However, the root cause for the reactivity of OH toward ammonium bisulfate is not known with certainty. The ion HSO_4^- may perhaps react with OH in the liquid phase in the presence of SAW.

Ivanov et al. [292] studied the uptake of OH on salt substrates using a laminar flow reactor equipped for EPR detection of gas-phase OH. The solid substrate was supported on a variable-length metal rod, mounted coaxially within the laminar flow tube, and OH free radicals were generated using the fast reaction $H + NO_2$. The uptake coefficients γ for OH interacting with solid NaCl and NH_4NO_3 are found to have a negative temperature dependence; nevertheless, γ is identical within the uncertainties for both substrates at 300 K (Table 18). The temperature dependence of γ may be expressed by the following expressions in the range 245−340 K: $\gamma = (1.2 \pm 0.7) \times 10^{-5} \exp[(1750 \pm 200)/T]$ for solid NaCl, and $\gamma = (1.4 \pm 0.5) \times 10^{-4} \exp[(1000 \pm 100)/T]$ for solid NH_4-

Table 19. CH_3O_2 + Substrate (Quartz, NaCl)

symbol	uptake coefficient	condensed phase	temp/K	reference
γ_{ss}	4×10^{-3}	solid NaCl	296	Gershenzon et al., 1995[289]

NO_3. Owing to the high reactivity of OH in the gas phase, it was concluded that the heterogeneous reactions of OH on solid salts should be of minor importance in the troposphere.

Concluding Remarks. Despite earlier reports to the contrary, it now appears that the reactivity of OH toward "inert" salt substrates, such as nitrates, sulfates, and alkali halides, is low and corresponds to an upper limit of $\gamma < 4 \times 10^{-3}$, with the exception of ammonium bisulfate, which seems to be reactive toward OH, with γ being at least an order of magnitude larger. However, in the presence of organic coatings on solid salts, γ increases to large values approaching 1.0.[291] The reactivity of HO_2 toward solid salts seems to be at least an order of magnitdue larger, with γ being on the order of a few percent. Several studies have confirmed the negative temperature dependence of the rate of uptake below ambient temperature, despite some significant quantitative differences. The study cited in the text[290] presents a credible (low) value of −3.1 kcal/mol and also points out a precipitous drop of γ at T > 300 K. Remorov et al.[290] make a strong case for the type of reaction products that are identical to the ones observed for the gas-phase reaction, namely $H_2O_2 + O_2$.

3.17. Reactions of CH_3O_2

Gershenzon et al.[289] performed an uptake study in a fast laminar flow coaxial reactor using a mobile free radical source for the admission of CH_3O_2 free radical, the results of which are displayed in Table 19. The polycrystalline NaCl was supported on the external reactor walls. The CH_3O_2 free radical, at a typical concentration of $<(1-2) \times 10^{11}$ cm^{-3}, was detected downstream in an EPR cavity after matrix isolation in a H_2O matrix at $T = 77$ K and at concentrations of $[H_2O] = (0.3-1) \times 10^{14}$ cm^{-3}, which was adjusted between the reaction and detection region so as not to affect the uptake measurement, which was performed according to the "added flow" or additional flux technique. For this purpose, an additional flux of He carrier gas is passed across the reactor, which shortens the free radical residence time in the flow tube or increases the flow velocity, thus enabling the measurement of the uptake coefficient. The CH_3O_2 free radicals were generated in the addition reaction $CH_3 + O_2 \rightarrow CH_3O_2$ at several Torr total pressure of pure oxygen. The CH_3 radicals have been generated in the reaction $F + CH_4 \rightarrow HF + CH_3$, where F atoms were generated in the mobile microwave discharge of F_2/He. The total pressure in the fast-flow reactor was in the range 2.4−2.8 mbar.

3.18. Reactions of HCl, HBr

Fenter et al.[211] performed uptake experiments involving HCl on solid polycrystalline (ground) NaCl

Table 20. HCl, HBr + Salt (NaCl)

symbol	uptake coefficient	condensed phase	temp/K	reference
γ_0	3.0×10^{-3}	solid NaCl, rh ≤ 1%	300	Fenter, Caloz, and Rossi, 1994[211]

Table 21. Cl + Salt ($(NH_4)_2SO_4$)

symbol	uptake coefficient	condensed phase	temp/K	reference
γ_{ss}	5.0×10^{-4}	solid $(NH_4)_2SO_4$	300	Martin, Judeikis, and Wun, 1980[293]

in a low-pressure Knudsen flow reactor, equipped for molecular-beam sampling and phase-sensitive detection using an electron-impact quadrupole mass spectrometer. The initial uptake at a flow of 5×10^{14} molecules s^{-1} depends only on the external (geometric) sample surface and is independent of the mass and grain size of the salt sample, unlike the number of adsorption sites that are distributed throughout the bulk of the salt substrate (Table 20). These uptake experiments were performed in order to help interpret uptake experiments of HNO_3 on ground salts substrates using a simple numerical chemical kinetic model. One of the surprising features of the HNO_3/HCl system on polycrystalline NaCl is the fact that HNO_3 displaces HCl into the gas phase and that ground NaCl apparently represents a reservoir for HCl. The role of SAW is thought to be critical, as no adsorption of HCl or HBr on single-crystal NaCl has been observed.

3.19. Reactions of Atomic Cl

Martin et al.[293] measured the uptake kinetics in a fast-flow tube equipped with EPR detection of Cl. A 1% Cl_2-in-He mixture at 2.0−2.7 mbar, or pure Cl_2 at 0.33 mbar, was discharged in a microwave cavity at 20 W in order to generate atomic Cl. The discharge tube was coated with solid B_2O_3 in order to minimize wall losses of Cl. The inside of the reactive part of the flow tube was coated with ammonium sulfate ($(NH_4)_2SO_4$), whereas the remainder was passivated using halocarbon wax. All kinetic results were obtained from the full numerical integration of the parabolic flow system and the chemical mechanism, including axial diffusion. It resulted in a value of γ displayed in Table 21.

3.20. Reactions of SO_2

Gebel and Finlayson-Pitts[294] studied the uptake of SO_2 on synthetic sea salt (SSS) and two of its components, NaCl and $MgCl_2 \cdot 6H_2O$, at 298 K using a Knudsen flow reactor equipped with mass spectrometric detection. Significant uptake on dried salts was not observed, placing upper limits on the γ value of $<1 \times 10^{-4}$ for NaCl, $<5 \times 10^{-4}$ for $MgCl_2 \cdot 6H_2O$, and $<8 \times 10^{-5}$ for SSS (Table 22). However, SSS and $MgCl_2 \cdot 6H_2O$ that had not been dried before use showed significant uptake of SO_2. The magnitude of the uptake depended heavily on the exposure time and the amount of desorbed water. Initially, the measured uptake coefficients for SO_2 on SSS were as high as 0.09, but they rapidly decreased below 10^{-2}

Table 22. SO_2 + Salt (NaCl, SSS,[a] $MgCl_2 \cdot 6H_2O$)

symbol	uptake coefficient	condensed phase	temp/K	reference
γ_{ss}	$<1 \times 10^{-4}$	dried solid NaCl	298	Gebel and Finlayson-Pitts, 2000[294]
	$<5 \times 10^{-4}$	dried solid $MgCl_2 \cdot 6H_2O$		
	$<8 \times 10^{-5}$	dried solid SSS[a]		
γ_0	9×10^{-2}	humid SSS[a]		

[a] Synthetic sea salt.

with a $t^{-1/2}$ dependence as expected for approach to the equilibrium saturation concentration in an aqueous solution. The decreasing uptake coefficient slowly approaches zero over hours, consistent with reaction in a water layer with species such as $CaCO_3$. The products of the reaction were shown by DRIFTS to include low-solubility metal sulfites. These studies show that uptake of SO_2 on sea salt particles, even below their deliquescence/efflorescence points, can be treated as if it is into an aqueous salt solution.

4. Acknowledgments

Since my venue to EPFL, I had, and continue to have, the great pleasure to work on the subject of heterogeneous chemistry with the following talented persons, to whom I am very grateful for their contributions: A. Aguzzi, C. Alcala-Jornod, A. Allanic, T. Brown, F. Caloz, A. Clericetti, L. Chaix, Ch. Delval, B. Demirdjian, F. Fenter, B. Flückiger, A. Gerecke, L. Gutzwiller, F. Karagulian, O. Le Bihan, Th. Koch, M. Klingler, M. Mochida, N. Ngouabé, R. Oppliger, P. Pratte, D. Razanodranorosoa, M. Rodriguez-Pires, M. S. Salgado-Muñoz, Ch. Santschi, S. Seisel, D. Stadler, K. Tabor, N. Takenaka, A. Thielmann, A. Thöny, B. Toth, and M. Wolf. Special thanks go to our mechanical technician "wizard" F. Comino and to professor H. van den Bergh for continued support.

The following agencies have provided the critically needed funding: Fonds National Suisse de la recherche scientifique, Office Fédéral de l'enseignement et de la recherche, AVINA Foundation, and Office Fédéral de l'environnement, forêt et paysage. In addition, I thank the EPFL for the generous start-up funds and continued support over the years that has been administered by the Service de Prospective et Recherche.

5. References

(1) Global Ozone Research and Monitoring Project. *Scientific Assessment of the Ozone Depletion: 2002*; Report No. 47; World Meteorological Organization: Geneva, Switzerland, 2003.
(2) *Aviation and the Global Atmosphere: IPCC Special Report*; Cambridge University Press: Cambridge, U.K., 1999.
(3) Molina, M. J.; Molina, L. T.; Kolb, C. E. *Annu. Rev. Phys. Chem.* **1996**, *47*, 327.
(4) Ravishankara, A. R. *Science* **1997**, *276*, 1058.
(5) DeHaan, D. O.; Brauers, T.; Oum, K.; Stutz, J.; Nordmeyer, T.; Finlayson-Pitts, B. J. *Int. Rev. Phys. Chem.* **1999**, *18*, 343.
(6) Hemminger, J. C. *Int. Rev. Phys. Chem.* **1999**, *18*, 387.
(7) Jacob, D. *Atmos. Environ.* **2000**, *34*, 2131.
(8) Warneck, P. *Chemistry of the Natural Atmosphere*; Academic Press Inc.: San Diego, CA, 1988.
(9) Finlayson-Pitts, B. J.; Pitts, J. N., Jr. *Chemistry of the Upper and Lower Atmosphere: Theory, Experiments and Applications*; Academic Press: San Diego, CA, 2000.
(10) Seinfeld, J. H.; Pandis, S. N. *Atmospheric Chemistry and Physics, from Air Pollution to Climate Change*; John Wiley and Sons: New York, 1998.
(11) Dentener, F. J.; Crutzen, P. J. *J. Geophys. Res.* **1993**, *98*, 7149.
(12) Dentener, F. J.; Carmichael, G. R.; Zhang, Y.; Leliveld, J.; Crutzen, P. J. *J. Geophys. Res.* **1996**, *101*, 22869.
(13) Thompson, A. *Science* **1992**, *256*, 1157.
(14) Crutzen, P. J. *Faraday Discuss.* **1995**, *100*, 1.
(15) Buseck, P. R.; Posfai, M. *Proc. Natl. Acad. Sci. U.S.A.* **1999**, *96*, 3372.
(16) O'Dowd, C.; Smith, M. H. *J. Geophys. Res.* **1993**, *98*, 1137.
(17) Gong, S. L.; Barrie, L. A.; Prospero, J. M.; Savoie, D. L.; Ayers, G. P.; Blanchet, J. P.; Spacek, L. J. *Geophys. Res.* **1997**, *102*, 3819.
(18) O'Dowd, C.; Smith, M. H.; Consterdine, I. E., Lowe, J. A. *Atmos. Environ.* **1997**, *31*, 73.
(19) Oum, K. W.; Lakin, M. J.; De Haan, D. O.; Brauers, T.; Finlayson-Pitts, B. J. *Science* **1998**, *279*, 74.
(20) Sadanaga, Y.; Hirokawa, J.; Akimoto, H. *Geophys. Res. Lett.* **2001**, *28*, 4433.
(21) Langer, S.; Pemberton, R. S.; Finlayson-Pitts, B. J. *J. Phys. Chem.* **1997**, *101A*, 1277.
(22) Zetzsch, C.; Pfahler G.; Behnke, W. *J. Aerosol Sci.* **1988**, *19*, 1203.
(23) Behnke, W.; Zetzsch, C. Halogenierte Organische Verbindungen in der Umwelt (VDI Verlag: Düsseldorf, Germany). *VDI−Ber.* **1989**, *745*, 153.
(24) Behnke, W.; Zetzsch, C. *J. Aerosol. Sci.* **1990**, *21*, S229.
(25) Zetzsch, C.; Behnke, W. *In The Tropospheric Chemistry of Ozone in the Polar Regions*; Niki, H., Becker, K. H., Eds.; NATO ASI Series 17; Springer-Verlag: New York, 1993.
(26) Behnke, W.; Scheer, V.; Zetzsch, C. Production of a Photolytic Precursor of Atomic Cl from Aerosols and Cl^- in the Presence of O_3. In *Naturally-Produced Organohalogens*; Grimvall, A., de Leer, E. W. B., Eds.; Kluwer Academic Publishers: Dordrecht, The Netherlands, 1995; pp 375−384.
(27) Nalbandian, A. B. In *Problems in Chemical Kinetics*; Emanuel, N., Ed.; MIR Publishers: Moscow, 1981; Chapter 16, p 183.
(28) Andreae, M. O. Future Climates of the World: A Modeling Perspective. In *World Survey of Climatology*; Henderson-Sellers, A., Ed.; Elsevier: Amsterdam, 1995; Vol. 16, p 341.
(29) Woods, D. C.; Chuan, R. L.; Rose, W. I. *Science* **1985**, *230*, 170.
(30) Mankin, W. G.; Coffey, M. T. *Science* **1984**, *226*, 170.
(31) Michelangeli, D. V.; Allen, M.; Yung, Y. L. *J. Geophys. Res.* **1989**, *94*, 18429.
(32) Michelangeli, D. V.; Allen, M.; Yung, Y. L. *Geophys. Res. Lett.* **1991**, *18*, 673.
(33) Cahill, T. A.; Wilkinson, K.; Schnell, R. *J. Geophys. Res.* **1992**, *97*, 14513.
(34) Parungo, F.; Kopcewicz, B.; Nagamoto, C.; Schnell, R.; Sheridan, P.; Zhu, C.; Harris, J. *J. Geopyhs. Res.* **1992**, *97*, 15867.
(35) Lowenthal, D. H.; Borys, R. D.; Rogers, C. F.; Chow, J. C.; Stevens, R. K.; Pinto, J. P.; Ondov, J. M. *Geophys. Res. Lett.***1993**, *20*, 693.
(36) *IPCC Climate Change 2001: The Scientific Basis*; Contribution of Working Group I to the Third Assessment Report of the Intergovernmental Panel on Climate Change; Cambridge University Press: Cambridge, U.K., 2001.
(37) Posfai, M.; Xu, H.; Anderson, J. R.; Buseck, P. R. *Geophys. Res. Lett.* **1998**, *25*, 1907.
(38) Murphy, D. M.; Thomson, D. S.; Middlebrook, A. M.; Schein, M. E. *J. Geophys. Res.* **1998**, *103*, 16485.
(39) O'Dowd, C. D.; Smith, M. H.; Consterdine E. I.; Lowe, J. A. *Atmos. Environ.* **1997**, *31*, 73.
(40) Robbins, R. C.; Cadle, R. D.; Eckhardt, D. L. *J. Meterorol.* **1959**, *16*, 53.
(41) Cadle, R. C.; Robbins, R. C. *Discuss. Faraday Soc.* **1960**, *30*, 155.
(42) Schröder, W. H.; Urone, P. *Environ. Sci. Technol.* **1974**, *8*, 756.
(43) Finlayson-Pitts, B. J. *Nature* **1983**, *306*, 676.
(44) Finlayson-Pitts, B. J.; Ezell, M. J.; Pitts, J. N., Jr. *Nature* **1989**, *337*, 241.
(45) Behnke, W.; Krüger, H.-U.; Scheer, V.; Zetzsch, C. *J. Aerosol Sci.* **1991**, *22*, S609.
(46) Winkler, T.; Goschnick, J.; Ache, H. J. *J. Aerosol Sci.* **1991**, *22*, S605.
(47) Junkermann, W.; Ibusuki, T. *Atmos. Environ.* **1992**, *26A*, 3099.
(48) Behnke, W.; Scheer, V.; Zetzsch, C. *J. Aerosol Sci.* **1993**, *24*, S115.
(49) Weis, D. D.; Ewing, G. E. *J. Phys. Chem.* **1999**, *103*, 4865.
(50) Peters, S. J.; Ewing, G. E. *J. Phys. Chem.* **1996**, *100*, 14093.
(51) Ravishankara, A. R. *Science* **1997**, *276*, 1058.
(52) Andreae, M. O.; Crutzen, P. J. *Science* **1997**, *276*, 1052.
(53) Finlayson-Pitts, B. J.; Pitts, J. N., Jr. *Science* **1997**, *276*, 1045.
(54) Hemminger, J. C. *Int. Rev. Phys. Chem.* **1999**, *18*, 387.
(55) Finlayson-Pitts, B. J.; Hemminger, J. C. *J. Phys. Chem. A* **2000**, *104*, 11463.
(56) Sporleder, D.; Ewing, G. E. *J. Phys. Chem. A* **2001**, *105*, 1838.
(57) *IUPAC-Evaluated Kinetic, Photochemical and Heterogeneous Data for Atmospheric Chemistry* (http://www.iupac-kinetic.ch-.cam.ac.uk/). The last cumulative collection of data is the following: Atkinson, R.; Baulch, D. L.; Cox, R. A.; Hampson, R. F.; Kerr, J. A.; Rossi M. J.; Troe, J. Evaluated Kinetic, Photochemical and Heterogeneous Data for Atmospheric Chemistry, Supplement V, IUPAC Subcommittee on Gas Kinetic Data

Evaluation for Atmospheric Chemistry. *J. Phys. Chem. Ref. Data* **1997**, *26*, 521.
(58) *NASA-Evaluated Kinetic, Photochemical and Heterogeneous Data for Atmospheric Chemistry* (http://jpldataeval.jpl.nasa.gov/). For an older printed version, see: DeMore, W.; Sander, S. P.; Golden, D. M.; Hampson, R. F.; Kurylo, M. J.; Howard, C. J.; Ravishankara, A. R.; Kolb C. E.; Molina, M. J. *Chemical Kinetics and Photochemical Data for Use in Stratospheric Modeling*, Evaluation No. 12; JPL Publication 97-4; NASA Jet Propulsion Laboratory: Pasadena, CA, 1997.
(59) Singh H. B.; Kasting, J. F. *J. Atmos. Chem*. **1988**, *7*, 261.
(60) Keene, W. C.; Jacob D. J.; Fan, S.-M. *Atmos. Environ*. **1996**, *30*, R1.
(61) Spicer, C. W.; Chapman, E. G.; Finlayson-Pitts, B. J.; Plastridge, R. A.; Hubble, J. M.; Fast, J. D.; Berkowitz, C. M. *Nature* **1998**, *394*, 353.
(62) Pszenny, A. A. P.; Keene, W. C.; Jacob, D. J.; Fan, S.-M.; Maben, J. R.; Zetwo, M. P.; Springer-Young, M.; Galloway, J. N. *Geophys. Res. Lett*. **1993**, *20*, 699.
(63) Keene, W. C.; Maben, J. R.; Pszenny, A. A. P.; Galloway, J. N. *Environ. Sci. Technol*. **1993**, *27*, 866.
(64) Impey, G. A.; Shepson, P. B.; Hastie, D. R.; Barrie, L. A.; Anlauf, K. *J. Geophys. Res*. **1997**, *102*, 16005.
(65) Impey, G. A.; Shepson, P. B.; Hastie, D. R.; Barrie, L. A. *J. Geophys. Res*. **1997**, *102*, 15999.
(66) Jobson, B. T.; Niki, H.; Yokouchi, Y.; Bottenheim, J.; Hopper F.; Leaitch, R. *J. Geophys. Res*. **1994**, *99*, 25355.
(67) Wingenter, O. W.; Kubo, M. K.; Blake, N. J.; Smith, T. W., Jr.; Blake, D. R.; Rowland, F. S. *J. Geophys. Res*. **1996**, *101*, 4331.
(68) Singh, H. B.; Gregory, G. L.; Anderson, B.; Browell, E.; Sachse, G. W.; Davis, D. D.; Crawford, J.; Bradshaw, J. D.; Talbot, R.; Blake, D. R.; Thornton, D.; Newell R.; Merrill, J. *J. Geophys. Res*. **1996**, *101*, 1907.
(69) Singh, H. B.; Thakur, A. N.; Chen, Y. E.; Kanakidou, M. *Geophys. Res. Lett*. **1996**, *23*, 1529.
(70) Rudolph, J.; Koppmann, R.; Plass-Dulmer, Ch. *Atmos. Environ*. **1996**, *30*, 1887.
(71) Barrie, L. A.; den Hartog, G.; Bottenheim, J. W.; Landsberger, S. J. *Atmos. Chem*. **1989**, *9*, 101.
(72) Bottenheim, J. W.; Barrie, L. A.; Atlas, E.; Heidt, L. E.; Niki, H.; Rasmussen, R. A.; Shepson, P. B. *J. Geophys. Res*. **1990**, *95*, 18555.
(73) Oltmans, S. J.; Schnell, R. C.; Sheridan, P. J. *Atmos. Environ*. **1989**, *23*, 2431.
(74) Barrie, L. A.; Bottenheim, J. W.; Schnell, R. C.; Crutzen, P. J.; Rasmussen, R. A. *Nature* **1988**, *334*, 138.
(75) Wagner, T.; Platt, U. *Nature* **1998**, *395*, 486.
(76) McElroy, C. T.; McLinden, C. A.; McConnell, J. C. *Nature* **1992**, *355*, 150.
(77) Hebestreit, K.; Stutz, J.; Rosen, D.; Matviev, V.; Peleg, M.; Luria, M.; Platt, U. *Science* **1999**, *283*, 55.
(78) Mozurkewich, M. *J. Geophys. Res*. **1995**, *100*, 14199.
(79) Vogt, R.; Crutzen, P. J. *Nature* **1996**, *383*, 327.
(80) Sander, R.; Crutzen, P. J. *J. Geophys. Res*. **1996**, *101*, 9121.
(81) Chameides, W. L.; Davis, D. D. *J. Geophys. Res*. **1980**, *85*, 7383.
(82) Jenkin, M. E.; Cox, R. A.; Candeland, D. E. *J. Atmos. Chem*. **1985**, *2*, 359.
(83) Chatfield, R. B.; Crutzen, P. J. *J. Geophys. Res*. **1990**, *95*, 22319.
(84) Alicke, B.; Hebestreit, K.; Stutz, J.; Platt, U. *Nature* **1999**, *397*, 572.
(85) Allan, B. J.; McFiggans, G.; Plane, J. M. C. *J. Geophys. Res*. **2000**, *105*, 14363.
(86) McFiggans, G.; Plane, J. M. C.; Carpenter, L. J.; Coe, H.; O'Dowd, C. *J. Geophys. Res*. **2000**, *105*, 14371.
(87) Cox, R. A.; Bloss, W. J.; Jones, R. L.; Rowley, D. M. *Geophys. Res. Lett* **1999**, *26*, 1857.
(88) Vogt, R.; Sander, R.; von Glasow, R.; Crutzen, P. *J. Atmos. Chem*. **1999**, *32*, 375.
(89) McFiggans, G.; Cox, R. A.; Mossinger, J. C.; Allan, B. J.; Plane, J. M. C. *J. Geophys. Res*. **2002**, *107* (D15), art. no. 4271 (doi: 10.1029/2001JD000383).
(90) Adams, J. W.; Cox R. A. *J. Phys. IV* **2002**, *12* (PR10), 105.
(91) Junge, C. E. *Tellus* **1956**, *8*, 127.
(92) Cicerone, R. J. *Rev. Geophys. Res*. **1972**, *77*, 5330.
(93) Moyers, J. L.; Duce, R. A. *J. Geophys. Res*. **1972**, *77*, 5330.
(94) Martens, S.; Wesolowski, J. J.; Harris, R. C.; Kaifer, R. *J. Geophys. Res*. **1973**, *78*, 8778.
(95) Hitchcock, D. R.; Spiller, L. L.; Wilson, W. E. *Atmos. Environ*. **1980**, *14*, 165.
(96) Keene, W. C.; Pszenny, A. A. P.; Jacob, D. J.; Duce, R. A.; Galloway, J. N.; Schultz-Tokos, J. J.; Sievering, H.; Boatman, J. F. *Global Biochem. Cycles* **1990**, *4*, 407.
(97) Mouri, H.; Okada, K. *Geophys. Res. Lett*. **1993**, *20*, 49.
(98) McInnes, L. M.; Covert, D. S.; Quinn P. K.; Germani, M. S. *J. Geophys. Res*. **1994**, *99*, 8257.
(99) Graedel, T. E.; Keene, W. C. *Global Biogeochem. Cycles* **1995**, *9*, 47.
(100) Finlayson-Pitts, B. J.; Johnson, S. *Atmos. Environ*. **1988**, *22*, 1107.
(101) Finlayson-Pitts, B. J.; Livingston, F. E.; Berko, H. N. *J. Phys. Chem*. **1989**, *93*, 4397.
(102) Behnke, W.; Scheer, V.; Zetzsch, C. *J. Aerosol Sci*. **1994**, *25*, 277.
(103) McConnell, J.; Henderson, G.; Barrie, L.; Bottenheim, J. W.; Niki, H.; Langford, C.; Templeton, E. *Nature* **1992**, *355*, 150.
(104) Vogt, R.; Crutzen, P. J.; Sander, R. *Nature* **1996**, *383*, 327.
(105) Behnke, W.; Elend, M.; Krüger, H.-U.; Scheer, V.; Zetzsch, C. Br^- Catalyzed Production of Atomic Cl in the Presence of Seaspray Aerosol, Light and Ozone. In *The Proceedings of EUROTRAC Symposium 96*; Borrell, P., et al., Eds.; SPB Academic Publishing BV: The Hague, The Netherlands, 1996.
(106) Fan, S.-M.; Jacob, D. J. *Nature* **1992**, *359*, 522.
(107) Kirchner, U.; Benter, Th.; Schindler, R. N. *Ber. Bunsen-Ges. Phys. Chem*. **1997**, *101*, 975.
(108) Mozurkewich, M. *J. Geophys. Res*. **1995**, *100*, 14199.
(109) Tang, T.; McConnell, J. C. *Geophys. Res. Lett*. **1996**, *23*, 2633.
(110) Ramacher, B.; Rudolph, J.; Koppmann, R. *Tellus* **1997**, *49B*, 466.
(111) Jobson, B. T.; Niki, H.; Yokouchi, Y.; Bottenheim, J. W.; Hopper, F.; Leaitch, R. *J. Geophys. Res*. **1994**, *99*, 25355.
(112) Hausamann, M.; Platt, U. *J. Geophys. Res*. **1994**, *99*, 25399.
(113) Tuckermann, M.; Ackermann, R.; Gölz, C.; Lorenzen-Schmidt, H.; Senne, T.; Stutz, J.; Trost, B.; Unold, W.; Platt, U. *Tellus* **1997**, *49B*, 533.
(114) Martinez, M.; Arnold, T.; Seuwen, R.; Perner, D. *Ann. Geophys*. **1999**, *17*, 941.
(115) Foster, K. L.; Plastridge, R. A.; Bottenheim, J. W.; Shepson, P. B.; Finlayson-Pitts, B. J.; Spicer, C. W. *Science* **2001**, *291*, 471.
(116) Pilinis, C.; Pandis, S. N.; Seinfeld, J. H. *J. Geophys. Res*. **1995**, *100*, 18739.
(117) Tang, I. *J. Geophys. Res*. **1997**, *102*, 1883.
(118) Haywood, J. M.; Shine, K. P. *Geophys. Res. Lett*. **1995**, *22*, 603.
(119) Haywood, J. M.; Roberts, D. L.; Slingo, A.; Edwards, J. M.; Shine, K. P. *J. Clim*. **1997**, *10*, 1562.
(120) Mössinger, J. C.; Cox, R. A. *J. Phys. Chem*. **2001**, *105A*, 5165.
(121) De Haan, D. O.; Finlayson-Pitts, B. J. *J. Phys. Chem*. **1997**, *101A*, 9993.
(122) Martin, S. T. *Chem. Rev*. **2000**, *100*, 3403.
(123) Cantrell, W.; McCrory, C.; Ewing G. E. *J. Chem. Phys*. **2002**, *116*, 2116.
(124) Tang, I. N. *Atmos. Environ*. **1980**, *14*, 819.
(125) Tang, I. N.; Munkelwitz, H. R. *J. Aerosol Sci*. **1977**, *8*, 321.
(126) Mozurkewich, M.; Calvert, J. G. *J. Geophys. Res*. **1988**, *93*, 15889.
(127) Mentel, T. F.; Sohn, M.; Wahner, A. *Phys. Chem. Chem. Phys*. **1999**, *1*, 5451.
(128) Weingartner, E.; Gysel, M.; Baltensperger, U. *Environ. Sci. Technol*. **2002**, *36*, 55.
(129) Matta, E.; Facchini, M. C.; Decesari, S. *Atmos. Chem. Phys*. **2003**, *3*, 623.
(130) Gill, S. P.; Graedel, T. E.; Weschler, C. J. *Rev. Geophys. Space Phys*. **1983**, *21*, 903.
(131) Mazurek, M.; Masonjones, M. C.; Masonjones, H. D.; Salmon, L. G.; Cass, G. R.; Hallock, K. A.; Leach, M. *J. Geophys. Res*. **1997**, *102*, 3779.
(132) Fuzzi, S.; Facchini, M. C.; Matta, E. *Atmos. Res*. **2002**, *64*, 89.
(133) Winiwarter, W.; Fierlinger, H.; Puxbaum, H.; Facchini, M. C.; Arends, B. G.; Fuzzi, S.; Schell, D.; Kaminski, U.; Pahl, S.; Schneider, T.; Berner, A.; Solly, I.; Kruisz, C. *J. Atmos. Chem*. **1994**, *19*, 173.
(134) Andrews, E.; Larson, S. M. *Environ. Sci. Technol*. **1993**, *27*, 857.
(135) Saxena, P.; Hildemann, L. M.; McMurry, P. H.; Seinfeld, J. H. *J. Geophys. Res*. **1995**, *100*, 18755.
(136) Hochella, M. F. *Mineral. Mag*. **2002**, *66*, 627.
(137) Hochella, M. F. *Earth Planet. Sci. Lett*. **2002**, *203*, 593.
(138) Stipp, S. L. S.; Hansen, M.; Kristensen, R.; Hochella, M. F.; Bennedsen, L.; Dideriksen, K.; Balic-Zunic, T.; Leonard, D.; Mathieu, H. J. *Chem. Geol*. **2002**, *190*, 321.
(139) Rosso, K. M.; Becker, U.; Hochella, M. F. *Am. Mineral*. **1999**, *84*, 1549.
(140) Vogt, R.; Finlayson-Pitts, B. J. *J. Phys. Chem*. **1994**, *98*, 3747.
(141) Langer, S.; Pemberton, R. S.; Finlayson-Pitts, B. J. *J. Phys. Chem*. **1997**, *101*, 1277.
(142) Hallquist, M.; Petrucci, N. B.; Kreuzer, C.; Ostanin V. P.; Cox, R. A. *Phys. Chem. Chem. Phys*. **2002**, *2*, 4373.
(143) Foster, M. C.; Ewing, G. E. *J. Chem. Phys*. **2000**, *112*, 6817.
(144) Wheeler, A. *Adv. Catal*. **1951**, *3*, 249.
(145) Aris, R. *The Mathematical Theory of Diffusion and Reaction in Permeable Catalysts*; Clarendon: Oxford, U.K., 1975; Vol. 1.
(146) Friedman, S. P.; Seaton, N. A. *Chem. Eng. Sci*. **1995**, *50*, 897.
(147) Timonen, R.; Chu, L. T.; Leu, M.-T.; Keyser, L. F. *J. Phys. Chem*. **1994**, *98*, 9509.
(148) Leu, M.-T.; Timonen, R.; Keyser, L. F.; Yung, Y. L. *J. Phys. Chem*. **1995**, *99*, 13203.
(149) Chu, L. T.; Leu, M.-T.; Keyser, L. F. *J. Phys. Chem*. **1993**, *97*, 12798.
(150) Hanson, D. R.; Ravishankara, A. R. *J. Phys. Chem*. **1993**, *97*, 2802.
(151) Chu, L. T.; Leu, M.-T.; Keyser, L. F. *J. Phys. Chem*. **1993**, *97*, 7779.

(152) Keyser, L. F.; Leu, M.-T.; Moore, S. B. *J. Phys. Chem.* **1993**, *97*, 2800.
(153) Sahimi, M.; Gavalas, G. R. *Chem. Eng. Sci.* **1990**, *45*, 1443.
(154) Kim, J. H.; Ochoa, J. A. *Transp. Porous Media* **1987**, *2*, 327.
(155) Friedman, S. P.; Seaton, N. A. *Chem. Eng. Sci.* **1995**, *50*, 897.
(156) Kolb, C. E.; Worsnop, D. R.; Zahniser, M. S.; Davidovits, P.; Hanson, D. R.; Ravishankara, A. R.; Keyser, L. F.; Leu, M.-T.; Williams, R.; Molina, M. J.; Tolbert, M. A. Laboratory Studies of Atmospheric Heterogeneous Chemistry. In *Progress and Problems in Atmospheric Chemistry*; Barker, J. R., Ed.; Advanced Series in Physical Chemistry 3; World Scientific Publishing Co.: River Edge, NJ, 1995; p 771.
(157) Zondlo, M. A.; Hudson, P. K.; Prenni, A. J.; Tolbert, M. A. *Annu. Rev. Phys. Chem.* **2000**, *51*, 473.
(158) Delval, C.; Flückiger, B.; Rossi, M. J. *Atmos. Chem. Phys.* **2003**, *3*, 1131.
(159) Kaufman, F. *Annu. Rev. Phys. Chem.* **1979**, *30*, 411.
(160) Howard, C. J. *J. Phys. Chem.* **1979**, *83*, 3.
(161) Leu, M. T. *Geophys. Res. Lett.* **1988**, *15*, 17.
(162) Hanson, D. R.; Ravishankara A. R. *J. Geophys. Res.* **1991**, *96*, 5081.
(163) Utter, R. G.; Burkholder, J. B.; Howard, C. J.; Ravishankara A. R. *J. Phys. Chem.* **1992**, *96*, 4973.
(164) Fickert, S.; Adams, J. W.; Crowley, J. N. *J. Geophys. Res.* **1999**, *104*, 23719.
(165) Behnke, W.; George, C.; Scheer, V.; Zetzsch, C. *J. Geophys. Res.* **1997**, *102*, 3795.
(166) Caloz, F.; Fenter, F. F.; Tabor, K. D.; Rossi, M. J. *Rev. Sci. Instrum.* **1997**, *68*, 3172.
(167) Beichert, P.; Finlayson-Pitts, B. J. *J. Phys. Chem.* **1996**, *100*, 15218.
(168) Hu, J. H.; Abbatt, J. P. D. *J. Phys. Chem. A* **1997**, *101*, 871.
(169) Kane, S. M.; Caloz, F.; Leu, M.-T. *J. Phys. Chem. A* **2001**, *105*, 6465.
(170) Worsnop, D. R.; Zahniser, M. S.; Kolb, C. E.; Gardner, J. A.; Watson, L. R.; Van Doren J. M.; Jayne, J. T.; Davidovits, P. *J. Phys. Chem.* **1989**, *93*, 1159.
(171) George, C.; Ponche, J. L.; Mirabel, P.; Behnke, W.; Scheer, V.; Zetzsch, C. *J. Phys. Chem.* **1994**, *98*, 8780.
(172) Schweitzer, F.; Mirabel, Ph.; George, C. *J. Phys. Chem. A* **1998**, *102*, 3942.
(173) Behnke, W.; Holländer, W.; Koch, W.; Nolting, F.; Zetzsch, C. *Atmos. Environ.* **1988**, *22*, 1113.
(174) Saathoff, H.; Naumann, K.-H.; Riemer, N.; Kamm, S.; Möhler, O.; Schurath, U.; Vogel, H.; Vogel, B. *Geophys. Res. Lett.* **2001**, *28*, 1957.
(175) Wahner, A.; Mentel, T. F.; Sohn, M.; Stier, J. *J. Geophys. Res.* **1998**, *103*, 31103.
(176) Gershenzon, Y. M. Personal communication.
(177) Livingston, F. E.; Finlayson-Pitts, B. J. *Geophys. Res. Lett.* **1991**, *18*, 17.
(178) Tuazon, E. C.; Atkinson, R.; Plum, C. N.; Winer, A. M.; Pitts, J. N. *Geophys. Res. Lett.* **1983**, *10*, 953.
(179) Atkinson, R.; Tuazon, E. C.; MacLeod, H.; Aschmann, S. M.; Winer, A. M. *Geophys. Res. Lett.* **1986**, *13*, 117.
(180) Hjorth, J.; Ottobrini, G.; Cappellani, F.; Restelli, G. *J. Phys. Chem.* **1987**, *91*, 1565.
(181) Hatakeyama, S.; Leu, M.-T. *J. Phys. Chem.* **1989**, *93*, 5784.
(182) Sverdrup, G. M.; Spicer, C. W.; Ward, G. F. *Int. J. Chem. Kinet.* **1987**, *19*, 191.
(183) Platt, U.; Perner, D.; Winer, A. M.; Biermann, H. W.; Atkinson, R.; Pitts, J. N., Jr. *Environ. Sci. Technol.* **1984**, *18*, 365.
(184) Russell, A. G.; McRae, G. J.; Cass, G. R. *Atmos. Environ.* **1985**, *19*, 893.
(185) Chameides, W. L.; Davis, D. D.; Bradshaw, J.; Sandholm, S.; Rodgers, M.; Baum, B.; Madronich, S.; Carroll, M. A.; Gregory, G.; Schiff, H. I.; Hastie, D. R.; Torres, A.; Condon, E. *J. Geophys. Res.* **1990**, *95*, 10235.
(186) Chameides, W. L.; Stelson, A. W. *J. Geophys. Res.* **1992**, *97*, 20565.
(187) Keyser, L. F.; Moore, S. B.; Leu, M.-T. *J. Phys. Chem.* **1991**, *95*, 5496.
(188) Fenter, F. F.; Caloz, F.; Rossi, M. J. *J. Phys. Chem.* **1996**, *100*, 1013.
(189) Finlayson-Pitts, B. J.; Livingston, F. E.; Berko, H. N. *J. Phys. Chem.* **1989**, *93*, 4397.
(190) Hoffman, R. C.; Gebel, M. E.; Fox, B. S.; Finlayson-Pitts, B. J. *Phys. Chem. Chem. Phys.* **2003**, *5*, 1780.
(191) Zetzsch, C.; Behnke, W. *Ber. Bunsen-Ges. Phys. Chem.* **1992**, *96*, 488.
(192) Behnke, W.; Krüger, H.-U.; Scheer, V.; Zetzsch, C. *J. Aerosol Sci.* **1992**, *S23*, S933.
(193) Taylor, R. *Electrophilic Aromatic Substitution*; John Wiley and Sons: New York, 1990.
(194) van Doren, J. M.; Watson, L. R.; Davidovits, P.; Worsnop, D. R.; Zahniser, M. S.; Kolb, C. E. *J. Phys. Chem.* **1990**, *94*, 3265.
(195) Msibi, I. M.; Li, Y.; Schi, J. P.; Harrison, R. M. *J. Atmos. Chem.* **1994**, *18*, 291.
(196) Tang, I. N.; Fung, K. H.; Imre, D. G.; Munkelwitz, H. R. *Aerosol Sci. Technol.* **1995**, *23*, 443.
(197) Fried, A.; Henry, B.; Calvert, J. G.; Mozurkewich, M. *J. Geophys. Res.* **1994**, *99*, 3517.
(198) Robinson, G. N.; Worsnop, D. R.; Jayne, J. T.; Kolb, C. E.; Davidovits, P. *J. Geophys. Res.* **1997**, *102*, 3583.
(199) Koch, T. G.; van den Bergh, H.; Rossi, M. J. *Phys. Chem. Chem. Phys.* **1999**, *1*, 2687.
(200) Colburn, C. B. *Developments in Inorganic Nitrogen Chemistry*; Elsevier: New York, 1973; Vol. 2.
(201) Koch, T. G.; Banham, S. F.; Sodeau, J. R.; Horn, A. B.; McCoustra, M. R. S.; Chesters, M. A. *J. Geophys. Res.* **1997**, *102*, 1513.
(202) Hanson, D. R. *Geophys. Res. Lett.* **1997**, *24*, 1087.
(203) Johnson, D. W.; Margerum, D. W. *Inorg. Chem.* **1991**, *30*, 4845.
(204) Clegg, S. L.; Brimblecombe, P. *Atmos. Environ.* **1985**, *19*, 465.
(205) Brimblecombe, P.; Clegg, S. L. J. *Atmos. Chem.* **1988**, *7*, 1.
(206) Mamane, Y.; Mehler, M. *Atmos. Environ.* **1987**, *9*, 1989.
(207) Mamane, Y.; Gottlieb, J. *J. Aerosol Sci.* **1990**, *S21*, S225.
(208) Mamane, Y.; Gottlieb, J. *Atmos. Environ.* **1992**, *26A*, 1763.
(209) Woods, D. C.; Chuan, R. L.; Rose, W. I. *Science* **1985**, *230*, 170.
(210) Mankin, W. G.; Coffey, M. T. *Science* **1984**, *226*, 170.
(211) Fenter, F. F.; Caloz, F.; Rossi, M. J. *J. Phys. Chem.* **1994**, *98*, 9801.
(212) Davies, J. A.; Cox, R. A. *J. Phys. Chem. A* **1998**, *102*, 7631.
(213) Leu, M.-T.; Timonen, R. S.; Keyser, L. F.; Yung, Y. L. *J. Phys. Chem.* **1995**, *99*, 13203.
(214) Leu, M.-T.; Timonen, R. S.; Keyser, L. F. *J. Phys. Chem.* **1997**, *101*, 278.
(215) Clegg, S. L.; Brimblecombe P. *J. Phys. Chem.* **1990**, *94*, 5369.
(216) Tang, I.; Munkelwitz, H. R.; Lee, J. H. *Atmos. Environ.* **1988**, *22*, 2579.
(217) Hoffman, R. C.; Kaleuati, M. A.; Finlayson-Pitts, B. J. Personal communication.
(218) Laux, J. M.; Hemminger, J. C.; Finlayson-Pitts, B. J. *Geophys. Res. Lett.* **1994**, *21*, 1623.
(219) Ghosal, S.; Hemminger, J. C. *J. Phys. Chem. A* **1999**, *103*, 4777.
(220) Ghosal, S.; Hemminger, J. C. *J. Phys. Chem. A* **2003** (submitted).
(221) Zangmeister, C. D.; Pemberton, J. E. *J. Phys. Chem.* **2001**, *105A*, 3788.
(222) Barraclough, P. B.; Hall, P. G. *Surf. Sci.* **1974**, *46*, 393.
(223) Allen, H. C.; Laux, J. M.; Vogt, R.; Finlayson-Pitts, B. J.; Hemminger, J. C. *J. Phys. Chem.* **1996**, *100*, 6371.
(224) Laux, J. M.; Fister, T. F.; Finlayson-Pitts, B. J. *J. Phys. Chem.* **1996**, *100*, 19891.
(225) Abbatt, J. P. D.; Waschewsky, G. C. G. *J. Phys. Chem. A* **1998**, *102*, 3719.
(226) Guimbaud, C.; Arens, F.; Gutzwiller, L.; Gäggeler, H. W.; Ammann, M. *Atmos. Chem. Phys.* **2002**, *2*, 249.
(227) ten-Brink, H. M. *J. Aerosol Sci.* **1998**, *29*, 57.
(228) Aguzzi, A.; Rossi, M. J. *Phys. Chem. Chem. Phys.* **1999**, *1*, 4337.
(229) Gebel, M. E.; Finlayson-Pitts, B. J. *J. Phys. Chem. A* **2001**, *105*, 5178.
(230) Smart, R. S. C.; Sheppard, N. *J. Chem. Soc., Faraday Trans.* **1976**, *272*, 707.
(231) Estel, J.; Hoinkes, H.; Kaarmann, H.; Nahr, H.; Wilsch, H. *Surf. Sci.* **1976**, *54*, 393.
(232) Wassermann, B.; Mirbt, S.; Reif, J.; Zink, J.; Matthias, *J. Chem. Phys.* **1993**, *98*, 10049.
(233) Fölsch, S.; Henzler, M. *Surf. Sci.* **1991**, *247*, 269.
(234) Bruch, L. W.; Glebov, A.; Toennies, J. P.; Weiss, H. *J. Chem. Phys.* **1995**, *103*, 5109.
(235) Dai, D. J.; Peters, S. J.; Ewing, G. E. *J. Phys. Chem.* **1995**, *99*, 10299.
(236) Kittel, C. *Introduction to Solid State Physics*, 6th ed.; John Wiley and Sons: New York, 1986.
(237) Peters, S. J.; Ewing, G. E. *Langmuir* **1997**, *13*, 14093.
(238) Walter, H. U. *Z. Phys. Chem. NF* **1971**, *75*, 287.
(239) Kaiko, M.; Chikazawa, M.; Kanazawa, T. *Nippon Kagaku Kaishi* **1972**, *8*, 1386.
(240) Fölsch, S.; Stock, A.; Henzler, M. *Surf. Sci.* **1992**, *264*, 65.
(241) Lad, R. A. *Surf. Sci.* **1968**, *12*, 37.
(242) Koch, T. G.; Rossi, M. J. *J. Phys. Chem. A* **1998**, *102*, 9193.
(243) Caloz, F.; Fenter, F. F.; Rossi, M. J. *J. Phys. Chem.* **1996**, *100*, 7494.
(244) George, C.; Behnke, W.; Scheer, V.; Zetzsch, C.; Magi, L.; Ponche, J. L.; Mirabel, Ph. *Geophys. Res. Lett.* **1995**, *22*, 1505.
(245) Jayne, J.; Davidovits, P.; Worsnop, D. R.; Zahniser, M. S.; Kolb, C. E. *J. Phys. Chem.* **1990**, *94*, 6041.
(246) Hanson, D. R.; Ravishankara, A. R. *J. Phys. Chem.* **1994**, *98*, 5728.
(247) Frenzel, A.; Scheer, V.; Sikorski, R.; George, C.; Behnke, W.; Zetzsch, C. *J. Phys. Chem. A* **1998**, *102*, 1329.
(248) Fickert, S.; Helleis, F.; Adams, J.; Moortgat, G. K.; Crowley, J. N. *J. Phys. Chem. A* **1998**, *102*, 10689.
(249) Caloz, F.; Seisel, S.; Fenter, F.; Rossi, M. J. *J. Phys. Chem. A* **1998**, *102*, 7470.
(250) Lee, T. J. *J. Phys. Chem.* **1996**, *100*, 19847.
(251) Huff, A. K.; Abbatt, J. P. D. *J. Phys. Chem. A* **2000**, *104*, 7284.

(252) Kumar, K.; Margerum, D. W. *Inorg. Chem.* **1987**, *26*, 2706.
(253) Santschi, K: Rossi, M. J. 2003 (in press).
(254) Mochida, M.; Akimoto, H.; van den Bergh, H.; Rossi, M. J. *J. Phys. Chem. A* **1998**, *102*, 4819.
(255) Wang, T. X.; Margerum, D. W. *Inorg. Chem.* **1994**, *33*, 1050.
(256) Adams, J. W.; Holmes, N. S.; Crowley, J. N. *Atmos. Chem. Phys.* **2002**, *2*, 79.
(257) Huff, A. K.; Abbatt, J. P. D. *J. Phys. Chem.* **2002**, *106A*, 5279.
(258) Wachsmuth, M.; Gäggeler, H. W.; von Glasow, R.; Ammann, M. *Atmos. Chem. Phys.* **2002**, *2*, 121.
(259) Ghosal, S.; Shbeeb, A.; Hemminger, J. C. *Geophys. Res. Lett.* **2000**, *27*, 1879.
(260) Zangmeister, C. D.; Turner, J. A.; Pemberton, J. E. *Geophys. Res. Lett.* **2001**, *28*, 995.
(261) Holmes, N. S.; Adams, J. W.; Crowley, J. N. *Phys. Chem. Chem. Phys.* **2001**, *3*, 1679.
(262) Troy, R. C.; Kelley, M. D.; Nagy, J. C.; Margerum, D. W. *Inorg. Chem.* **1991**, *30*, 4838.
(263) Wang, Y. L.; Nagy, J. C.; Margerum, D. W. *J. Am. Chem. Soc.* **1989**, *111*, 7838.
(264) Allanic, A.; Rossi, M. J. *J. Geophys. Res.* **1999**, *104*, 18689.
(265) Oum, K. W.; Lakin, M. J.; DeHaan, D. O.; Finlayson-Pitts, B. J. *Geophys. Res. Lett.* **1998**, *25*, 3923.
(266) Mochida, M.; Hirokawa, J.; Kajii, Y.; Akimoto, H. *Geophys. Res. Lett.* **1998**, *25*, 3927.
(267) Hirokawa, J.; Onaka, K.; Kajii, Y.; Akimoto, H. *Geophys. Res. Lett.* **1998**, *25*, 2449.
(268) Niki, H., Becker, K. H., Eds. *The Tropospheric Chemistry of Ozone in the Polar Regions*; NATO ASI Series 1; Springer-Verlag: Berlin, 1993; Vol. 7, p 425.
(269) Il'in, S. D.; Selikhanovich, V. V.; Gershenzon, Y. M.; Rozenshtein, V. B. *Sov. J. Chem. Phys.* **1991**, *8*, 1858.
(270) Mochida, M.; Hirokawa, J.; Akimoto, H. *Geophys. Res. Lett.* **2000**, *27*, 2629.
(271) Alebic-Juretic, A.; Cvitas, T.; Klasinc, L. *Ber. Bunsen-Ges. Phys. Chem.* **1992**, *96*, 470.
(272) Taube, H. *J. Am. Chem. Soc.* **1942**, *64*, 2468.
(273) Abbatt, J. P. D. *Geophys. Res. Lett.* **1996**, *23*, 1681.
(274) Rudich, Y.; Talukdar, R. K.; Ravishankara, A. R.; Fox, R. W. *J. Geophys. Res.* **1996**, *101*, 21023.
(275) Rudich, Y.; Talukdar, R. K.; Imamura, R. W.; Fox, R. W.; Ravishankara, A. R. *Chem. Phys. Lett.* **1996**, *261*, 467.
(276) Exner, M.; Herrmann, H.; Zellner, R. *Ber. Bunsen-Ges. Phys. Chem.* **1992**, *96*, 470.
(277) Seisel, S.; Caloz, F.; Fenter, F. F.; van den Bergh, H.; Rossi, M. J. *Geophys. Res. Lett.* **1997**, *24*, 2757.
(278) Seisel, S.; Flückiger, B.; Caloz, F.; Rossi, M. J. *Phys. Chem. Chem. Phys.* **1999**, *1*, 2257.
(279) Thomas, K.; Volz-Thomas, A.; Mihelcic, D.; Smit, H. G. H.; Kley, D. *J. Atmos. Chem.* **1998**, *29*, 17.
(280) Gratpanche, F.; Sawerysyn, J.-P. *J. Chim. Phys.* **1999**, *96*, 213.
(281) Gershenzon, M. Y.; Il'in, S. D.; Fedotov, N. G.; Gershenzon, Y. M.; Aparina, E.; Zelenov, V. V. *J. Atmos. Chem.* **1999**, *34*, 119.
(282) Imamura, T.; Rudich, Y.; Talukdar, R. K.; Fox, R. W.; Ravishankara, A. R. *J. Phys. Chem. A* **1997**, *101*, 2316.
(283) Vogt, R.; Finlayson-Pitts, B. J. *J. Phys. Chem.* **1995**, *99*, 13052.
(284) Sverdrup, G. M.; Kuhlman, M. R. *Stud. Environ. Sci.* **1980**, *8*, 245.
(285) Wan, J. K. S.; Pitts, J. N., Jr.; Beichert, P.; Finlayson-Pitts, B. J. *Atmos. Environ.* **1994**, *28*, 3225.
(286) Rubin, M. B.; Noyes, R. M.; Smith, K. W. *J. Phys. Chem.* **1987**, *91*, 1618.
(287) Takenaka, N.; Rossi, M. J. *Atmos. Environ.* **2003** (submitted).
(288) Mozurkewich, M.; McMurry, P. H.; Gupta, A.; Calvert, J. G. *J. Geophys. Res.* **1987**, *92*, 4163.
(289) Gershenzon, Y. M.; Grigorieva, V. M.; Ivanov, A. V.; Remorov, R. G. *Faraday Discuss.* **1995**, *100*, 83.
(290) Remorov, R. G.; Gershenzon, Y. M.; Molina, L. T.; Molina, M. J. *J. Phys. Chem. A* **2002**, *106*, 4558.
(291) Cooper, P. L.; Abbatt, J. P. D. *J. Phys. Chem.* **1996**, *100*, 2249.
(292) Ivanov, A. V.; Gershenzon, Y. M.; Gratpanche, F.; Devolder, P.; Sawerysyn, J.-P. *Ann. Geophys.* **1996**, *14*, 659.
(293) Martin, L. R.; Judeikis, H. S.; Wun, M. *J. Geophys. Res.* **1980**, *85*, 5511.
(294) Gebel, M. E.; Finlayson-Pitts, B. J. *Geophys. Res. Lett.* **2000**, *27*, 887.

CR020507N